STRATIFICATION PREDICTION AND BOTTOM BOUNDARY LAYER DYNAMICS OVER THE TEXAS-LOUISIANA CONTINENTAL SHELF

A Dissertation

by

WENXIA ZHANG

Submitted to the Office of Graduate and Professional Studies of
Texas A&M University
in partial fulfillment of the requirements for the degree of

DOCTOR OF PHILOSOPHY

Chair of Committee,	Robert D. Hetland
Co-Chair of Committee,	Xiaopei Lin
Committee Members,	Steven F. DiMarco
	Scott A. Socolofsky
Head of Department,	Debbie Thomas

May 2015

Major Subject: Oceanography

ABSTRACT

The bottom boundary layer is an unstratified thin layer above the sea floor, separated from the more strongly stratified interior. Formation of a thin bottom boundary layer in the presence of stratification and a sloping bottom is common, and well characterized by theory. This thin layer is an important source of mixing over the continental shelf, and it plays a fundamental role in several continental shelf physical and biogeochemical processes, such as buoyancy advection, bottom material transport and hypoxia formation.

In this research, Both observations and numerical models are used to study models' ability of reproducing observed stratification and bottom boundary layer dynamics over the Texas-Louisiana shelf. Simulated vertical stratification, which is also representing the vertical density structure, was first evaluated since it directly controls the bottom boundary layer structure itself and is important for other bottom boundary layer dynamics. A new metric, the histogram of vertical stratification, is introduced in this research to evaluate the models' ability of reproducing observed stratification in a bulk sense. The improvement in model performance is attributed to the finer horizontal and temporal resolutions of a model, while factors like open boundary conditions and vertical resolutions are modified without any improvement in the ability of the model to simulate observed stratification. Towed, undulating CTD profiles collected during Mechanisms Controlling Hypoxia (MCH) program also detected mid-water oxygen minima in many transects. These intrusions are connected with the bottom boundary layer and follows the pycnocline seaward as a mid-water column tongue of low oxygen. We calculate convergence within the bottom boundary layer relative to density surfaces using the simulated results; there is

a convergence in the bottom boundary layer at the location where the pycnocline intercepts the bottom, creating an injection of bottom boundary layer water into the pycnocline. Convergent flow at the bottom, relative to isopycnal surfaces, is strongest in the density classes associated with the oxygen minimum layer. We believe these mid-water oxygen minima are actually intrusions of low oxygen protruding from the bottom boundary layer via buoyancy advection driven convergence, following the main pycnocline.

ACKNOWLEDGEMENTS

I would like to express my sincere thanks to my committee members: Dr. Robert D. Hetland, for his valuable suggestions and review of the manuscript; Dr. Steven F. DiMarco for carefully following my work, for sharing his scientific knowledge and ideas, and for his suggestions and comments; and Drs. Xiaopei Lin and Scott A. Socolofsky for being excellent professors. I would like also to thank Dr. Katja Fennel for her guidance, suggestions, and editorial comments. I am also thankful to her for encouraging me and being so supportive to my work. Thanks also go to China Scholarship Council for financial support.

Observational data presented here were obtained aboard the *R/Vs Gyre* and *Pelican* during MCH (Mechanisms Controlling Hypoxia) cruises. Thanks go to the Captain and crew of the R/V *Gyre* during our cruises in the Gulf of Mexico, as well as the help received from colleagues at Texas A&M University who participated on these cruises.

Last, but not least, my heartfelt thanks go to my family and friends during the entire study and always. Special thanks go to my family for their love and encouragement and for taking care of all my needs.

TABLE OF CONTENTS

Page

LIST OF FIGURES

FIGURE Page

LIST OF TABLES

TABLE Page

1. INTRODUCTION

The domain of interest in this study is the Texas-Louisiana shelf which is located in the northern Gulf of Mexico (Figure1.1). The Mississippi River system is the major source of fresh water, sediment, nutrients and pollutants for this region. It drains 42% of the continental watershed of the United States. The outflow usually peaks in spring and is at a minimum in early fall. The river enters the Gulf of Mexico through the Mississippi River birdfoot delta and the Atchafalaya River, which is a distributary of the Mississippi River diverted from the main channel at Old River. The Mississippi and Atchafalaya River system delivers about 5.3×10^2 km^3 of fresh water, 2.1 $\times10^8$ tons of sediment and 0.95 $\times10^6$ tons of nitrogen to this region every year (Milliman and Meade, 1983; Meade, 1996; Bianchi et al., 2010). The large flux of nutrients results in eutrophication within the Mississippi/Atchafalaya plume (Lohrenz et al., 1990; Turner and Rabalais, 1994; Fennel et al., 2011).

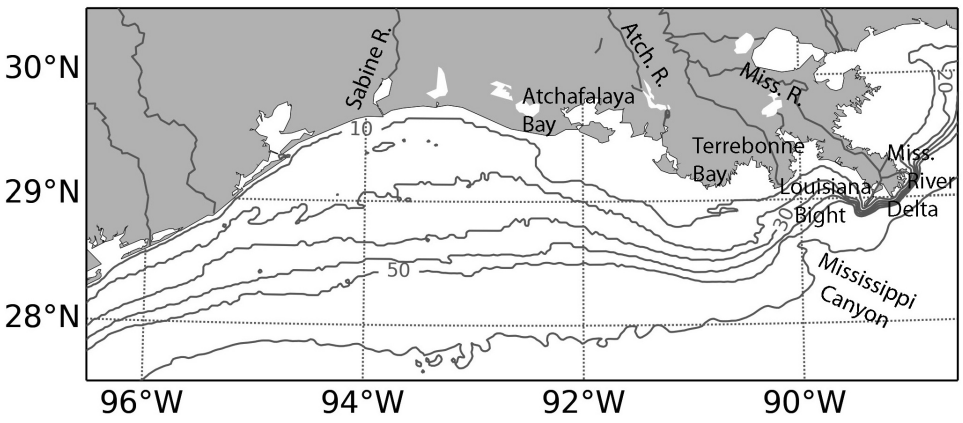

Figure 1.1: The study domain of this dissertation, which covers much of the Texas-Louisiana continental shelf. Bathymetric contours of 10, 20, 30, 40, 50, 200 m depth are shown on the map.

The wind over the Texas-Louisiana shelf is weak and upwelling favorable (from west to east) in summer (June through August), however during the other time of the year (September through May), the wind becomes stronger and downwelling favorable (from east to west) (Cochrane and Kelly, 1986; Cho et al., 1998; Nowlin et al., 2005, 1998). The freshwater introduced by the Mississippi/Atchafalaya River intensifies the stratification of the shelf under the weak and upwelling favorable wind condition in summer, and the strong stratification will be reduced by the strong and downwelling favorable wind during the other time of the year. The low-frequency circulation on the Texas-Louisiana shelf is mainly driven by this seasonal wind with a strong contribution from buoyancy forcing near the Mississippi and Atchafalaya Rivers. It flows westward along the Louisiana coast and then southward along the Texas coast in fall, winter and spring; while in summer, the flow reverses and moves upcoast. Currents over the outer shelf are variable, but predominantly upcoast throughout the year, probably resulting from the integrated effects of anticyclonic eddies impinging on the shelf edge (Cochrane and Kelly, 1986; Cho et al., 1998). The seasonal pattern of the circulation impacts the transport of harmful algae blooms, nutrient cycling, and seasonal hypoxia (Hetland and DiMarco, 2008; DiMarco et al., 2010).

Over the Texas-Louisiana shelf, hypoxia is a recurrent phenomenon that is primarily driven by the combined effects of nutrient loading and stratification introduced onto the continental shelf mainly from effluents derived from the Mississippi and Atchafalaya Rivers. Hypoxia is defined as water of dissolved oxygen concentration less than 1.4 mL L^{-1} (equivalent to 63 μM L^{-1} or 2 mg L^{-1}), and it is the threshold at which most oceanic animals evacuate (Renaud, 1986; Rabalais et al., 2002b). The freshwater discharge from the Mississippi River system intensifies the stratification of the Louisiana shelf under the weak and upwelling favorable wind

condition, facilitating hypoxia formation by inhibiting the exchange of atmospheric oxygen to subpycnocline waters (Wiseman et al., 1997; Hetland and DiMarco, 2008). The hypoxic area in the Gulf of Mexico is the second largest in the world, it occurs as early as late February and can last to early October, but is most severe, continuous and widely distributed during JuneAugust.

Stratification has been proved to be essential for seasonal hypoxia formation and destruction over the Texas-Louisiana shelf (Belabbassi, 2006; Hetland and DiMarco, 2008; Fennel et al., 2013). There are both vertical and horizontal stratification in the real ocean, stratification in this study will be representing vertical stratification if not specified. Stratification refers to the strength of the vertical density gradient. The higher the stratification the more the water column resists vertical mixing. The Brunt-Väisälä, N, is often used to express the degree of stratification, or more precisely, the natural frequency of oscillation for a water parcel displaced adiabatically from its rest position. The force causing the oscillation is the buoyant force. High values of N are found where the vertical density gradient is large and *vice versa*.

Two critical values of Brunt-Väisälä frequency, 40 cycles/h (0.035 s^{-1}) and 100 cycles/h (0.087 s^{-1}), were used in Belabbassi (2006) to define high vertical stability of water column. Six-years comprehensive data set obtained over the northern continental shelf and upper slope of the Gulf of Mexico during the LATEX-A (Nowlin et al., 1998) and NEGOM-COH (Jochens et al., 2002) programs suggest that regions of water column Brunt-Väisälä maxima less than 40 cycles/h were associated with poorly stratified water column and high oxygen concentrations near the bottom. While water column maximum Brunt-Väisälä frequencies are between 0 and 40 cycles/h, low-oxygen (<2.4 mL L^{-1}) or hypoxic waters do not occur at the bottom because of an ample supply of oxygen through vertical mixing. When maximum Brunt-Väisälä frequency values are between 40 and 100 cycles/h, low or hypoxic

conditions may develop near the bottom if oxygen removal exceeds oxygen supply. Dissolved oxygen concentrations near the bottom had only low or hypoxic conditions while maximum Brunt-Väisälä frequency values exceed 100 cycles/h, indicating that vertical mixing was reduced considerably.

Fennel et al. (2013) used a coupled biological model to investigate hypoxic area and prove that the predicted hypoxic area is highly related to stratification strength over the Texas-Louisiana shelf. The extent of physical stratification creates a physical bound – stratification envelope – on the regions where hypoxia may occur. This requires a hydrodynamic model to be able to reproduce observed stratification to predict bottom hypoxic area reasonably. However, there are horizontal processes that can alter stratification structures and make point-by-point comparisons difficult, especially for maximum values of water column stratification. Unpredictable, nonlieaner noise associated with baroclinic instabilities along the river plume fronts is significant (Marta-Almeida et al., 2013; Mattern et al., 2013). The noise reaches its strongest state during summer and weaker during the other time of the year; and this noise limits the maximum possible skill for model prediction. Mattern et al. (2013) showed that small perturbations in physical forcing lead to large uncertainties in model-simulated hypoxic area estimates, which is consistent with Marta-Almeida et al. (2013)'s arguments. DiMarco et al. (2010) observed a wave-like structure of vertical density as well as dissolved oxygen concentration distributions. Thus, when comparing model results to observations, the amplitude of stratification can be temporarily changed or the maximum value be displaced. Such that a direct model/data comparison may indicate poor model performance, even in cases where the model correctly predicts stratification in a mean or bulk sense.

Bottom boundary layer dynamics over the Texas-Louisiana shelf has also been proved to be essential for hypoxia formation and maintenance citedwiseman.ea:97,

hetland.dimarco:08, fennel.ea:13, also it is of importance for buoyancy advection and bottom material transports in other regions (Chapman and Lentz, 1994; Trowbridge and Lentz, 1998; Brink and Lentz, 2010a). The bottom boundary layer is an unstratified thin layer above the sea floor, and the top of the bottom boundary layer is the interface of itself and the more strongly stratified interior. The bottom boundary layer is thought of as the region in which the flow is directly modified by the presence of the bottom. In the ocean, the bottom boundary layer is expected to scale roughly as the Ekman scale for regions where rotation is important. Formation of a thin bottom boundary layer in the presence of stratification and a sloping bottom is common (Trowbridge and Lentz, 1991), and well characterized by theory (MacCready and Rhines, 1993; Brink and Lentz, 2010a,b). Although much thinner than the entire water column depth, it is an important source of mixing over a sloping continental shelf. The bottom boundary layer thickness varies with factors such as ambient stratification condition, the magnitude as well as direction of wind-driven along-shore current, freshwater discharge and topography (Trowbridge and Lentz, 1991; Lentz and Trowbridge, 1991; MacCready and Rhines, 1993; Chapman and Lentz, 1997; Trowbridge and Lentz, 1998; Brink and Lentz, 2010a,b). The alongshore current, freshwater discharge and topography influence the bottom boundary layer via altering the stratification structure of water column.

The bottom boundary layer is crucial for the formation of low dissolved oxygen concentration in bottom waters; a well-developed, thin bottom boundary layer is correlated with low bottom oxygen (Wiseman et al., 1997; Nowlin et al., 1998; Hetland and DiMarco, 2008; Fennel et al., 2013). In the ocean, the concentration of oxygen dissolved in the water has to be above a minimum value to support the normal metabolism of oceanic organisms. Wiseman et al. (1997) used ten years of mid-summer survey cruise data to investigate seasonal and interannual variability of

bottom hypoxia within the west Louisiana inner shelf. The measurements indicated that the depth of the main pycnocline represents only a lower bound on the depth of the hypoxic layer, while the bottom boundary layer (a weak secondary pycnocline which develops during strong water column stratification) is closely associated with the structure of the hypoxic layer. Nowlin et al. (1998) showed cross-sections of observed dissolved oxygen and salinity collected during the LATEX program, which indicating that hypoxic water was only found near the bottom within the bottom boundary layer.

Hetland and DiMarco (2008) used a realistic hydrodynamical model to investigate hypoxia dynamics over the Texas-Louisiana shelf. Rather than using a complex biogeochemical model, three simple parameterizations of biological respiration are compared. Simulated results indicated that hypoxic conditions caused by benthic respiration are only found inshore of the 50 m isobath. In agreement with observations (e.g., Nowlin et al., 1998), hypoxia is also only found near the bottom within the bottom boundary layer. Fennel et al. (2013) examined the sensitivity of hypoxia simulations to model resolution, variations in sediment oxygen consumption, and choice of physical horizontal boundary conditions over Texas-Louisiana shelf. All the hypoxia simulations from different scenarios are evaluated against monitoring observations, and the simulated hypoxic area takes a variety of values depends on the size of the sediment oxygen sink. Unlike the Chesapeake Bay where hypoxic condition occurs in the bottom waters of a relatively deep channel with restricted circulation and extend tens of meters above the bottom up to the main pycnocline, on the Texas-Louisiana shelf, hypoxic condition is restricted to a relatively thin layer above the sediment.

Bottom boundary layer responds asymmetrically to the direction of along-shore current over a stratified sloping shelf. Ekman transport of buoyancy over a slop-

ing bottom within the bottom boundary layer is driven by bottom stress associated with along-shore currents (Yankovsky and Chapman, 1997; Brink and Lentz, 2010a), and the direction as well as the magnitude of bottom Ekman transport alters bottom boundary layer structures. In the ocean, for along-shore flows of comparable strength, the bottom boundary layer is thicker during downwelling-favorable flow than that during upwelling-favorable flow (Trowbridge and Lentz, 1991; Lentz and Trowbridge, 1991). During upwelling-favorable flows, the excited Ekman transport within the bottom boundary layer advects denser water upslope underneath the lighter inner-shelf water, enhancing the density difference between the bottom boundary layer and the interior. So the vertical turbulent transport near the top of the bottom boundary layer is suppressed and the growth of the layer is inhibited. During downwelling-favorable flows, the Ekman transport advects lighter water downslope, reducing the density difference between the boundary layer and the interior, and the unstabilized near-bottom water causes vertical mixing and upward erosion of the top of the bottom boundary layer. So the growth of the layer is enhanced and the thickness is relatively thicker. Furthermore, a stronger along-shore current can enhance the above influence it has on bottom boundary layer structure and *vice versa* (Lentz and Trowbridge, 1991). Over the Texas-Louisiana shelf, bottom boundary layer thickness varies seasonally resulting from the variable stratification established from the combined contribution of seasonal wind patterns and large fresh water discharge.

The bottom boundary layer dynamics, along-shore current excited bottom Ekman transport within the bottom boundary layer, is essential for the entire water column dynamics (e.g., Trowbridge and Lentz, 1998). The bottom Ekman transport within the bottom boundary layer alters near bottom density field, momentum balance and even the entire water column current velocity field (Chapman and Lentz, 1994; Trowbridge and Lentz, 1998; Brink and Lentz, 2010a). Trowbridge and Lentz (1998)

examined observationally a concise set of vertically integrated, subinertial momentum balance which is provided by theoretical works. They presented this observational test based on time-series measurements collected on the northern California shelf during two winter seasons. The sloping bottom permits the cross-shore bottom Ekman transport to modify the density field, and the distortion of isopycnal surfaces and the sloping bottom combine together through mixing and advection generates cross-shore buoyancy forces. The measurements suggested that a buoyancy force resulting from the distortion of isopycnal surfaces within the bottom boundary layer is dynamically significant in the cross-shore momentum equation. Typically during downwelling-favorable flows the bottom boundary layer is thick, resulting in the buoyancy force being a dominant term in cross-shore momentum balance. Also, the mean along-shore momentum balance is significantly affected by a buoyancy force generated by an along-shore temperature gradient, which makes a only moderate success of Ekman balance in describing along-shore momentum equation.

The bottom Ekman transport driven by buoyancy advection in turn eventually brings the along-shore bottom velocity, hence bottom stress, to rest via thermal wind balance (Chapman and Lentz, 1994; Lentz and Chapman, 2004; Brink and Lentz, 2010a,b). During downwelling-favorable flows, the downslope bottom Ekman transport advects buoyant fluid offshore, pushing isopycnals migrating offshore. Near the bottom within the bottom boundary layer, isopycnals are concentrated and a front separating freshwater and salty water generates. The enhanced pressure gradient within the front adjusts through thermal wind balance and produces an along-shore current which is in the opposite direction of the interior along-shore flow, leading to a reduction of the interior along-shore current within the front. The velocity field across the base of the front is altered and the downslope Ekman transport at the foot of the front is inhibited.

Over the Texas-Louisiana shelf, bottom boundary layer dynamics is extremely active. At latitudes of 30°NS, the diurnal period of sea-breeze forcing coincides with the Coriolis frequency of planetary rotation, resulting in a resonant effect that leads to a maximum ocean diurnalinertial band response. The Texas-Louisiana shelf is located at $\sim$ 30°N, and in summer the land-sea breeze excites strong near-inertial flows with 24-h periodicity over the entire Texas-Louisiana shelf (Zhang et al., 2009). The combination of the strong inertial oscillation signals and the variations of freshwater discharge and wind stress modified freshwater distribution rise high variations of buoyancy advection in direction as well as amplitude along the bottom within the bottom boundary layer. Thus the active bottom boundary layer dynamics in turn will influence the other geophysical and biological processes over the shelf, which is the main topic of this dissertation.

In this dissertation, both observations and numerical modelings are used to investigate processes related to bottom boundary layer dynamics over the Texas-Louisiana shelf, and it is organized into 5 sections. Section 1 provides an introduction to general Texas-Louisiana shelf dynamics and bottom boundary layer dynamics and previous research activities. In Section 2, the ability of several comprehensive models to reproduce observed stratification is evaluated and the influence of bottom boundary layer dynamics on bottom hypoxia formation is investigated. The bottom boundary layer, considered as a secondary pycnocline, is proved to be essential for low oxygen formation and maintenance; and rather than using only the maximum values of stratification, histograms of vertical stratification is also introduced as a new metric to evaluate model skills in a bulk sense. In Section 3, a hydrodynamic model and towed, undulating CTD profiles are used to identify the dynamical mechanisms of the formation of a mid-water column oxygen minima. Buoyancy advection within the bottom boundary layer is of importance and discussed in detail in this section;

by computing the convergent flow along the bottom layer, the mid-water oxygen minima is proved to be an bottom low-oxygen water intrusion along frontal isopycnals driven by buoyancy advection within the bottom boundary layer. Following Section 3, convergent flow and the corresponding intrusion is further studied in Section 4. A simple two-dimensional model is set up to investigate the relationship between convergent flow and the upward flux of bottom material and identify how slope parameter influences the convergent flows at the foot of isopycnal fronts.

Results from this dissertation are expected to help us better understand the stratification distribution and the importance of the stratification to other shelf processes; as a thin layer compared to the whole water column, dynamics within the bottom boundary layer is essential for the entire water column, such as buoyancy transport across density surfaces and bottom material transports; and provide useful and efficient methods to study coastal dynamics over the Texas-Louisiana shelf and other regions.

2. PREDICTING STRATIFICATION OVER THE TEXAS-LOUISIANA CONTINENTAL SHELF

2.1 Overview

The Mississippi and Atchafalaya Rivers discharge 5.3×10^2 km^3 of fresh water and 0.95×10^6 tons of nitrogen into the northern Gulf of Mexico every year. The Texas-Louisiana shelf is affected by these discharges, which lead to seasonal bottom hypoxia due to the combined effects of stratification from the fresh water and eutrophication caused by the excess nitrogen load. Hypoxia is most severe in late summer, but has also been observed in both spring and fall. Since vertical stratification is a critical factor in the formation of bottom hypoxia, skill in reproducing observed stratification is important for an accurate simulation of seasonal hypoxia in numerical models. However, stratification can be influenced by a number of processes at many spatial and temporal scales, such as internal waves, making direct point-to-point comparisons between observations and their corresponding model counterparts difficult. Here, we introduce a new method for comparing histograms of stratification to assess the model skill at reproducing the character of stratification. We compare observations with two hydrodynamic models and evaluate their skill at reproducing stratification. The models' ability to reproduce observed stratification is dependent on model temporal and horizontal resolutions, while the vertical resolution and horizontal boundary treatment have a smaller impact on model skill. The main pycnocline and the bottom boundary layer play different roles but are both crucial for the formation of low dissolved oxygen concentration in bottom waters in this region.

2.2 Introduction

The Texas-Louisiana continental shelf is located in the northern Gulf of Mexico (Figure 2.1). Every year the Mississippi and Atchafalaya River system delivers about 5.3×10^2 km^3 of fresh water, 2.1 $\times10^8$ tons of sediment and 0.95 $\times10^6$ tons of nitrogen to this region (Milliman and Meade, 1983; Meade, 1996; Bianchi et al., 2010). The large flux of nutrients leads to eutrophication within the Mississippi/Atchafalaya plume (Lohrenz et al., 1990; Turner and Rabalais, 1994; Fennel et al., 2011), and hypoxic conditions form in the near-bottom waters over the mid-shelf (Rabalais et al., 2002a; Bianchi et al., 2010), at depths ranging from roughly 10 to 50 m. Hypoxia is defined as dissolved oxygen concentrations less than 1.4 mL L^{-1} (equivalent to 63 μM L^{-1} or 2 mg L^{-1}), and it is the threshold at which most oceanic animals evacuate (Renaud, 1986; Rabalais et al., 2002b). A significant portion of the freshwater discharge is trapped on the Louisiana shelf and transported downcoast (westward) by a coastal current (Cochrane and Kelly, 1986; Nowlin et al., 2005; Zhang and Hetland, 2012). During summer, when winds tend to be upweling-favorable, stratification intensifies and inhibits the exchange of oxygen-rich surface water to subpycnocline waters (Wiseman et al., 1997; Hetland and DiMarco, 2008; Bianchi et al., 2010). Bottom hypoxia is closely linked with stratification (Belabbassi, 2006; Wiseman et al., 1997), and even small-scale variations in stratification can influence bottom oxygen concentrations (DiMarco et al., 2010).

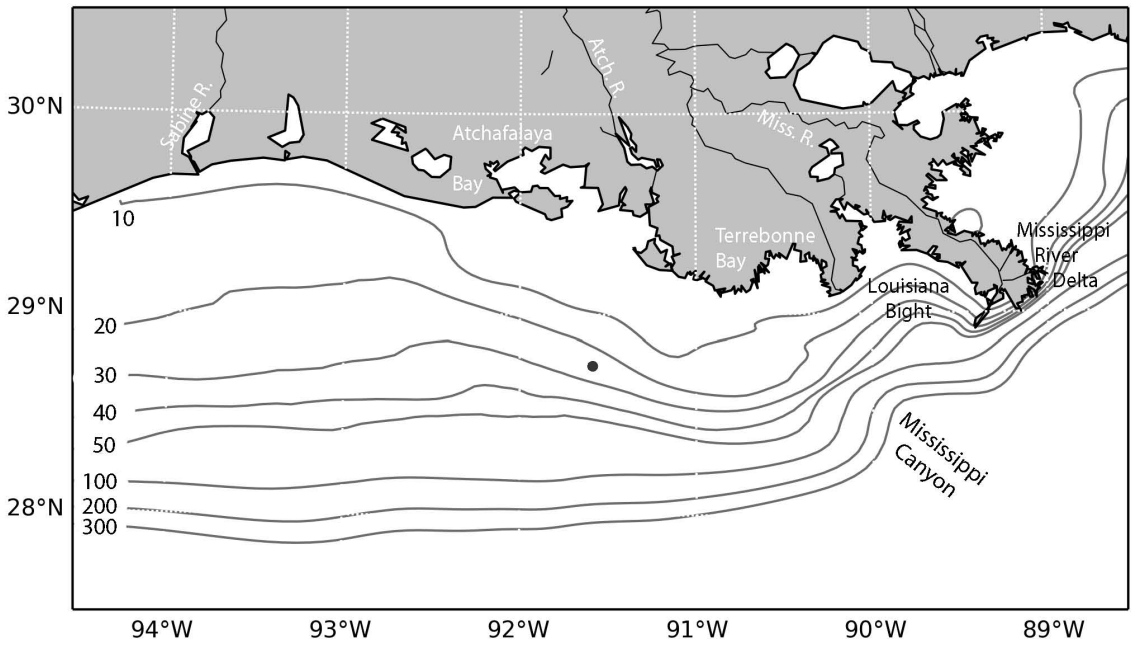

Figure 2.1: The study domain, which is covered by the MCH cruises, covers much of the Texas-Louisiana continental shelf. Bathymetric contours are also labeled in other maps, but only focus on regions within the 50 m isobath. The seasonal variation of vertical stratification of a station (black point) offshore of Atchafalaya Bay is examined, see Figure 2.5.

Belabbassi (2006) used a six-years comprehensive data set obtained over the northern continental shelf and upper slope of the Gulf of Mexico during the LATEX-A (Nowlin et al., 1998) and NEGOM-COH (Jochens et al., 2002) programs to investigate bottom oxygen. Her results indicate that low-oxygen waters (<2.4 mL L^{-1}) are found primarily in spring and summer and only in water depths between 10 and 60 m. Low-oxygen occurs only when the water column has a maximum Brunt-Väisälä frequency (N_{max}) greater than 40 cycles/h (0.035 s^{-1}); bottom water is always hypoxic when N_{max} exceeds 100 cycles/h (0.087 s^{-1}). Thus, there is a clear correlation between the strength of stratification in the pycnocline and bottom oxygen concentrations. However, Wiseman et al. (1997) note that the top of the hypoxic layer is

often significantly below the main pycnocline; rather the top of the hypoxic layer is more generally associated with the top of the bottom boundary layer. The bottom boundary layer is an unstratified thin layer above the sea floor, separated from the more strongly stratified interior. Formation of a thin bottom boundary layer in the presence of stratification and a sloping bottom is common (Trowbridge and Lentz, 1991), and well characterized by theory (MacCready and Rhines, 1993; Brink and Lentz, 2010a,b). Thus, even though the strength of the main pycnocline is associated with hypoxia, this relationship is not direct, but involves the formation of a secondary thin bottom boundary layer.

Hetland and DiMarco (2008) examined oxygen dynamics on the Louisiana shelf in a three-dimensional hydrodynamic numerical model, attempting to understand the physical processes responsible for the formation of hypoxia. Their study isolated the physical effects that control hypoxic extent by applying simple, idealized models of biological respiration to a relatively complex model of coastal circulation. Hetland and DiMarco (2008) were the first to study oxygen dynamics on the Louisiana shelf in a high-resolution three-dimensional physical model with simple parameterizations of biological processes embedded. They found that by including benthic respiration alone, west of Terrebonne Bay, a hypoxic layer would form in the region where hypoxia is typically observed. The hypoxic layer was associated with a thin bottom boundary layer that would form in this part of the shelf. Fennel et al. (2013) evaluated hypoxia simulations of comprehensive models against monitoring observations, and investigated the sensitivity of hypoxia simulations to factors like model resolution, variations in SOC (Sediment Oxygen Consumption), and choice of physical horizontal boundary treatments. They also showed that hypoxic conditions are restricted to a relatively thin layer above the bottom over most of the shelf and that sediment oxygen consumption is the major oxygen sink leading to hypoxic conditions.

Cross-sections of observed oxygen taken during the LATEX program suggested that hypoxic conditions are found only near the bottom within the bottom boundary layer (Nowlin et al., 1998). Simulated results from Hetland and DiMarco (2008) and Fennel et al. (2013) are in qualitative agreement with these observations.

A primary goal of this section is to examine how stratification, associated with both the main pycnocline and the bottom boundary layer, influences bottom hypoxia. Critical to this goal is the ability to assess whether a hydrodynamic model is able to successfully reproduce observed stratification. Stratification, which may be determined by both temperature and salinity, is harder to simulate compared to temperature and salinity themselves. Any error in simulating temperature or salinity could lead to large errors in stratification, as the gradient operator will tend to increase errors. Previous studies have focused on assessing a model's ability to reproduce tracer and flow fields (e.g., Zhang et al., 2012a; Hetland and DiMarco, 2012), however, the ability of reproducing stratification has not been investigated systematically. Evaluating a model's ability of reproducing stratification is needed and necessary. In this section we present a novel method of comparing different hydrodynamic shelf circulation models to observed stratification.

2.3 Observation

Table 2.1: Research cruises for the Mechanisms Controlling Hypoxia (MCH) project during years 2004-2009

Hypoxia Cruise	Time	Research Vessel	Number of CTD Profiles
2004 MCH01	2-8 April 2004	R/V Gyre	57
2004 MCH02	25 June-1 July 2004	R/V Gyre	60
2004 MCH03	20-27 August 2004	R/V Gyre	63
2005 MCH04	23-29 March 2005	R/V Gyre	104
2005 MCH05	20-26 May 2005	R/V Gyre	102
2005 MCH06	8-14 July 2005	R/V Gyre	142
2005 MCH07	18-24 August 2005	R/V Gyre	231
2007 MCH08	22-29 March 2007	R/V Pelican	225
2007 MCH09	17-20 July 2007	R/V Pelican	110
2007 MCH10	6-9 Sep 2007	R/V Pelican	139
2008 MCH11	16-19 April 2008	R/V Pelican	43
2008 MCH12	17-20 July 2008	R/V Pelican	71
2009 MCH13	7-10 April 2009	R/V Pelican	32
2009 MCH14	28-31 July 2009	R/V Pelican	59

Observational data presented here were obtained aboard the *R/Vs Gyre* and *Pelican* during 14 MCH (Mechanisms Controlling Hypoxia) cruises from 2004 to 2009. Figure 2.2 shows the maps of all the cruises. A summary of the cruises with start and end dates is given in Table 2.1. Vertical profiles of salinity, temperature,

pressure, and DO (Dissolved Oxygen) concentrations were made using a SBE 911 CTD with a SBE43 oxygen sensor. The vertical separation of data of these profiles after processing raw records is 0.5 m. Water samples were taken using Niskin bottles on a 12-bottle rosette. DO concentration of the water samples were analyzed at sea using the Winkler titration method (Carpenter, 1965; Williams and Jenkinson, 1982). All hydrographic sensors were periodically factory calibrated to account for and correct long-term sensor drift. Water samples were analyzed using a Guildline salinometer and compared to the conductivity derived salinity estimates from the CTD. The comparison showed agreement that was within acceptable tolerances for coastal research (i.e., usually within 0.1 psu) (DiMarco, unpublished).

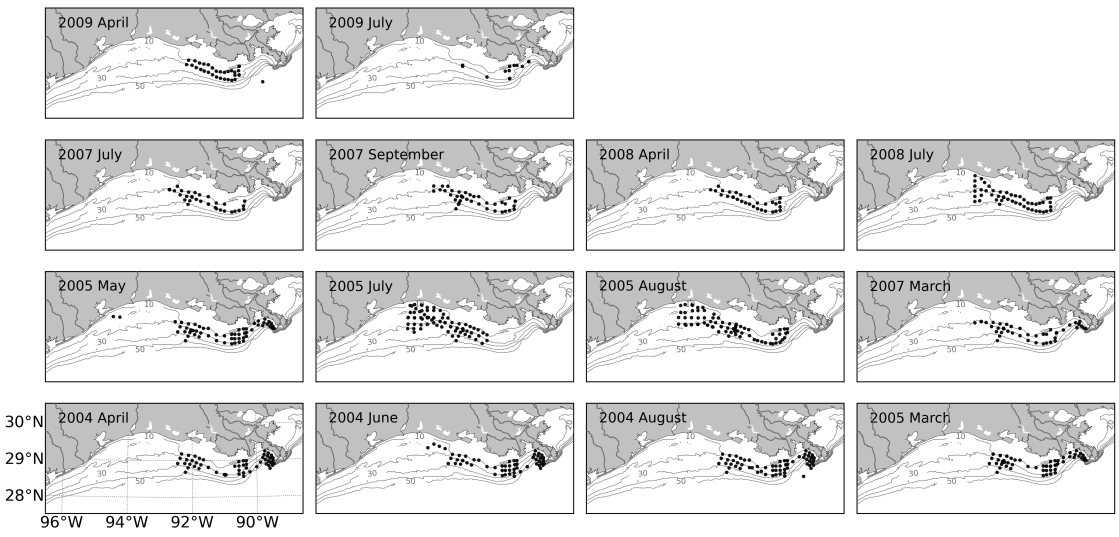

Figure 2.2: The maps for all the cruises. The black points are the locations of observed stations.

2.4 Model description

2.4.1 TXLA hydrodynamic model

Zhang et al. (2012b) describe a high-resolution hydrodynamic model configuration covering the entire Texas-Louisiana shelf and slope, based on the Regional Ocean Modeling System (ROMS), and referred to in this section as TXLA. The model has 30 vertical layers, with a minimum water depth of 3 m, and a maximum water depth greater than 3000 m. The model has a resolution of ∼500 m near the coast, and ∼1-2 km on the outer slope area. At the three open boundaries, a nudging layer of six cells was used to relax the model temperature, salinity and baroclinic velocities toward the Gulf of Mexico Hybrid Coordinate Ocean Model (GOM-HYCOM) (http://www.hycom.org). The nudging time scale used was eight hours at the outermost boundary point, with successively weaker nudging in interior points. Sea surface height and barotropic currents from HYCOM were imposed at the boundaries as Chapman (1985) and Flather (1976) boundary conditions.

The hindcast model is forced with surface momentum, heat and fresh water fluxes from the North American Regional Reanalysis (NARR) data set. Fresh water fluxes from the Mississippi and Atchafalaya Rivers are specified using daily measurements of Mississippi River Transport at Tarbert Landing by the U.S. Army Corps of Engineers. Fresh water fluxes from the other seven rivers (the Nueces, San Antonio, Lavaca, Brazos, Trinity, Sabine, Calcasieu Rivers) were prepared based on the USGS (U.S. Geological Survey) RealTime Water Data for the Nation. For further details on model configuration we refer the reader to Zhang et al. (2012b).

Presently, this model does not have a biogeochemical component due to the large computational expense. However, a simple parameterization of benthic oxygen demand is implemented by introducing a passive tracer representing oxygen in a manner

similar to the benthic respiration case considered by Hetland and DiMarco (2008). Oxygen is initialized at saturated values everywhere based on temperature and salinity (Weiss, 1970). The oxygen at the open boundaries is relaxed to saturation in exactly the same way as the dynamical tracers, and surface values of oxygen are set identically equal to saturated values to represent exchange with the atmosphere. Water from the rivers is saturated with respect to oxygen. The possible effects of photosynthesis increasing water column oxygen above saturated values are not considered. The model specifies benthic respiration based on bottom temperature and oxygen concentrations. The function is

$$\text{Bottom } O_2 \text{ flux} = 6.0 \left[O_2 \text{m}^{-2} \text{days}^{-1}\right] \times 2^{T/10.0^{\circ}\text{C}} \times \left[1 - \exp(\frac{-O_2}{30.0 \mu\text{M } O_2})\right]. \quad (2.1)$$

This is based on data obtained by Rowe et al. (2002). The benthic oxygen flux is applied at the sea floor, as a bottom boundary condition in the model. We refer the reader to Hetland and DiMarco (2008) for further details.

2.4.2 MCH coupled biophysical model

Fennel et al. (2013) used a smaller domain that covers only the Louisiana shelf at a slightly lower resolution, and this model is also analyzed in this study. This model, referred to in this section as MCH, includes both physical and biological components (Fennel et al., 2013). The physical model is based on a hydrodynamic model used by Hetland and DiMarco (2008, 2012); Marta-Almeida et al. (2013). The horizontal resolution is highest near the Mississippi Delta with up to 1 km and telescoped near the open boundaries, such that the lowest in the southwestern corner is about 20 km. The physical model uses several different configurations, all of which use the same horizontal grid but are different in vertical resolution and in the treatment of horizontal boundary conditions (see Table 2.2 for details).

Table 2.2: Overview of model simulations

Run	Vertical Resolution	Horizontal Boundary Treatment
TXLA	30 layers	HYCOM
B20clim	20 layers	climatological
B30HYC	30 layers	HYCOM
B30IAS	30 layers	IASNFS

Temperature and salinity at the boundary are relaxed to a horizontally uniform monthly climatology with a timescale of 1 day for incoming and 10 days for outgoing information. In the configurations, initial and daily boundary conditions were taken from two Gulf of Mexico operational models, which are subsequently referred to as parent models, the Gulf of Mexico operational hybrid coordinate ocean model (HYCOM) (Wallcraft et al., 2009) and the Intra Americas Sea Nowcast Forecast System (IASNFS) (Ko et al., 2008). The models are forced with 3-hourly winds from the NCEP North American Regional Reanalysis (NARR) and climatological surface heat and freshwater fluxes from the study by da Silva et al. (1994a,b). Freshwater inputs from the Mississippi and Atchafalaya Rivers use daily measurements of transport by the U.S. Army Corps of Engineers at Tarbert Landing and Simmesport, respectively. A comprehensive summary of the similarities and differences in the hydrodynamic model results when using different boundary conditions is given by Marta-Almeida et al. (2013).

The biological component of this model uses the nitrogen cycle model described by Fennel et al. (2006). Meanwhile, dissolved oxygen as a state variable and a pa-

rameterization of the air-sea flux of oxygen are included as an extension (Fennel et al., 2013). The nitrogen cycle model is a relatively simple representation that includes two species of dissolved inorganic nitrogen (nitrate, NO_3, and ammonium, NH_4), one functional phytoplankton group, *Phy*, chlorophyll as a separate state variable, *Chl*, to allow for photoacclimation, one functional zooplankton group, Zoo, and two pools of detritus representing large, fast-sinking particles, $LDet$, and suspended, small particles, $SDet$ (Fennel et al., 2006, 2008, 2013).

The equation that describes the biochemical dynamics of oxygen, O_x, is

$$\begin{aligned}\frac{\partial O_x}{\partial t} =& \mu_{max} f(I)(L_{NO_3} R_{O_2:NO_3} \ + \ L_{NH_4} R_{O_2:NH_4}) Phy \\ & - 2\hat{n} NH_4 \\ & - R_{O_2:NH_4}(lZoo + \hat{r}_{SD} SDet + \hat{r}_{LD} LDet),\end{aligned} \tag{2.2}$$

where μ_{max} is the maximum growth rate of phytoplankton, $f(I)$ is a nondimensional light-limitation term, L_{NO_3} and L_{NH_4} correspond to nutrient-limitation due to nitrate and ammonium, respectively, $R_{O_2:NO_3}$ = 138/16 mol O_2/mol NO_3 and $R_{O_2:NH_4}$ = 106/16 mol O_2/mol NH_4 are stoichiometric ratios corresponding to the oxygen produced per mol of nitrate and ammonium assimilated during photosynthetic production of organic matter, $\hat{n}$ is the nitrification flux, l is the zooplankton excretion rate, and $\hat{r}_{SD}$ and $\hat{r}_{LD}$ are the remineralization rates of small and large detritus, respectively (Fennel et al., 2006, 2008, 2013). For the bottom boundary condition on oxygen, the sediment oxygen consumption described by Hetland and DiMarco (2008) is used in all these three configurations. Note that these scenario runs are identical in terms of biology – they only differ in the physics by using different physical horizontal boundary treatments. We refer the reader to Fennel et al. (2006, 2008, 2011, 2013) for further details on model justification, equations, and parameters.

2.5 Method

As an important factor in the formation, maintenance, and destruction of hypoxia, the ability of the model to reproduce observed stratification will be assessed in this study. Stratification refers to the strength of the vertical density gradient; the higher the stratification, the more the water column resists vertical mixing. The stratification frequency, N, is often used to denote the strength of stratification (Brunt, 1927). The stratification frequency, N, is defined as

$$N^2 = -\frac{g}{\rho_0}\frac{\partial \rho}{\partial z}, \tag{2.3}$$

where g=9.8 m s^{-2} is the gravitational acceleration; ρ_0 is the background or reference density value and ρ_0 = 1027 kg m^{-3}; ρ is the density. Bianchi et al. (2010) shows the seasonality of the buoyancy frequency over the Texas-Louisiana shelf. Previous studies (e.g., Hetland and DiMarco, 2008) have demonstrated that the formation of bottom hypoxia is primarily a vertical process – a balance between benthic respiration and vertical mixing. Bottom water is re-oxygenated if ventilation is stronger than oxygen consumption and *vice versa*.

There also are horizontal processes that make a point-by-point comparison difficult. Marta-Almeida et al. (2013); Mattern et al. (2013) argued there is a significant level of unpredictable, nonlinear noise associated with baroclinic instabilities along the Mississippi/Atchafalaya plume front. The noise due to these eddies is seasonal and is greatest during summer upwelling conditions and weaker during nonsummer downwelling; and this noise limits the maximum possible skill for model prediction. Consistent with Marta-Almeida et al. (2013)'s arguments, Mattern et al. (2013) showed that small perturbations in physical forcing lead to large uncertainties in model-simulated hypoxic area estimates. Also, there may be internal waves that

modulate the tracer field on even shorter timescales, without affecting the mean water column properties. Thus, when comparing model results to observations, the peak in stratification may be displaced or the amplitude will be temporarily changed, such that a direct model/data comparison would indicate poor model performance, even in cases where the model correctly predicts stratification in a mean or bulk sense. Thus, bulk metrics that integrate over the entire model state are required to assess the ability of the model to reproduce observed stratification.

Low dissolved oxygen concentrations are often confined to within the bottom boundary layer. The thickness of the bottom boundary layer may be operationally defined as the distance from the bottom to the maximum height at which the vertical density gradient is greater than 0.1 kg/m^4 here. Wiseman et al. (1997) used a different critical value (0.01 kg/m^4) to identify bottom boundary layer. In Fennel et al. (2013), the bottom boundary layer is defined as the layer in which the density change is less than 0.5 kg m^{-3} from the bottom. The choice of the critical value used to define the bottom boundary layer will affect the exact value of the thickness of bottom boundary layer. However, qualitatively different reasonable choices for the critical value will yield the same result, just as Wiseman et al. (1997) states. Sometimes the main pycnocline is close enough to the bottom that the top of the bottom boundary layer and main pycnocline are essentially the same. Operationally, we define the maximum value of vertical stratification to correspond to the main pycnocline, which may or may not be distinct from the bottom boundary layer. Also, this N^2_{max} is used to denote the strength of the total water column stability in a bulk sense.

In order to examine the position of the main pycnocline and bottom boundary layer for the observed profiles in the region of hypoxia, we distinguish three critical layers: the main pycnocline, the top of the bottom boundary layer, and the top of

the hypoxic layer. The top of the hypoxic layer is defined here as the first location above the sea floor where the water ceases being hypoxic. The distance from the free surface to the top of a specific layer is defined as the 'depth' of this layer, while the distance from the sea floor to the top of a layer is defined as the 'thickness' of this layer.

2.6 Results

Among all the observed profiles from the 14 cruises that are examined, bottom dissolved oxygen concentrations range from 0.01 to 5.99 mL L^{-1}, and very different density structures and vertical stratification conditions are encountered from station to station. A collection of different cases from observations is shown in Figure 2.3. The stations in Figure 2.3 a and b correspond to hypoxic conditions and show large to moderate vertical density differences; the stations in Figure 2.3 c and d show large to moderate vertical density differences and are associated with relatively high near-bottom oxygen levels. All the different cases have common characteristic in terms of the vertical structure of properties: the oxygen concentration changes with density gradient and a dramatic drop in oxygen level often occurs below a strong density gradient.

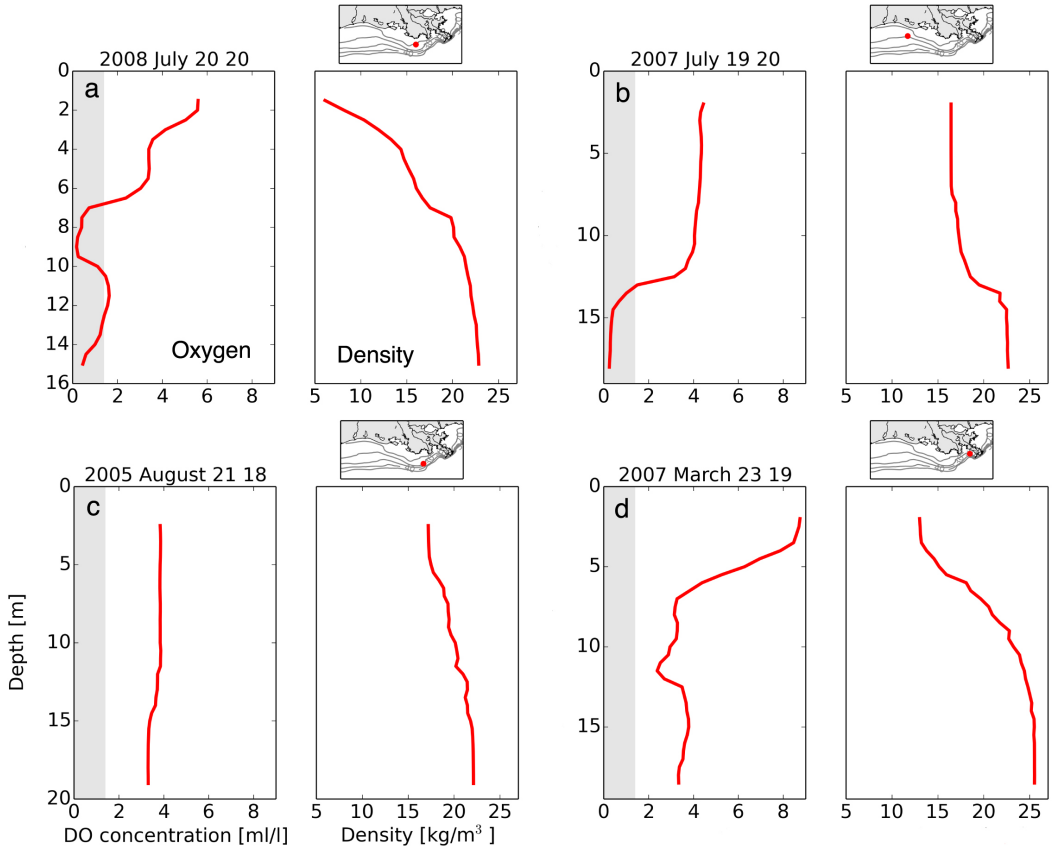

Figure 2.3: A collection of different cases from observations. For each station, the map on top shows the location of the station and the title is the cast time. Both dissolved oxygen concentration and density profiles are shown for each station (red point in the map), the shaded region denotes hypoxic conditions.

However, a strong pycnocline is not always directly associated with hypoxic bottom waters. The critical value of N_{max} for the possible occurrence of low bottom oxygen concentration (<2.4 mL L^{-1}) is 40 cycles/h (0.035 s^{-1}) (Belabbassi, 2006). DiMarco et al. (2010) and Rabalais et al. (1994) suggested that the time scale of the establishment of bottom hypoxia is 1-2 weeks. Stratification must be present long enough for oxygen consumption to occur; only the persistence of a relatively high density gradient that suppresses mixing and ventilation of deeper waters can drive

oxygen to lower levels over time. For example, the station shown in Figure 2.3 d has a dramatic oxygen level drop across the main pycnocline, but the draw down of oxygen in the lower layer is not low enough to be hypoxic.

Examples of observed stratification and dissolved oxygen profiles are compared to simulated values from the MCH model B20clim configuration in Figure 2.4 in order to highlight some of the strengths and weaknesses of the simulations. At the two stations in Figure 2.4 a and b, the model reasonably captures the observed stratification structure as well as oxygen concentration. Note, it is common that dissolved oxygen levels drop below strong vertical stratification. In Figure 2.4 c and d, simulated stratification is weaker than observed, resulting in higher simulated dissolved oxygen levels in the bottom boundary layer as compared to observations. These two profiles illustrate how important it is that models accurately represent stratification. When the region of strong stratification is shifted, so is the oxycline (Figure 2.4 c). When the model under-predicts stratification it over-predicts bottom oxygen levels (Figure 2.4 d), as expected. These examples demonstrate that both the location and magnitude of the strong stratification is important for an accurate reproduction of the oxygen field. An averaged 32% of the observed hypoxic stations are correctly reproduced in the MCH model, see Table 2.3 for details.

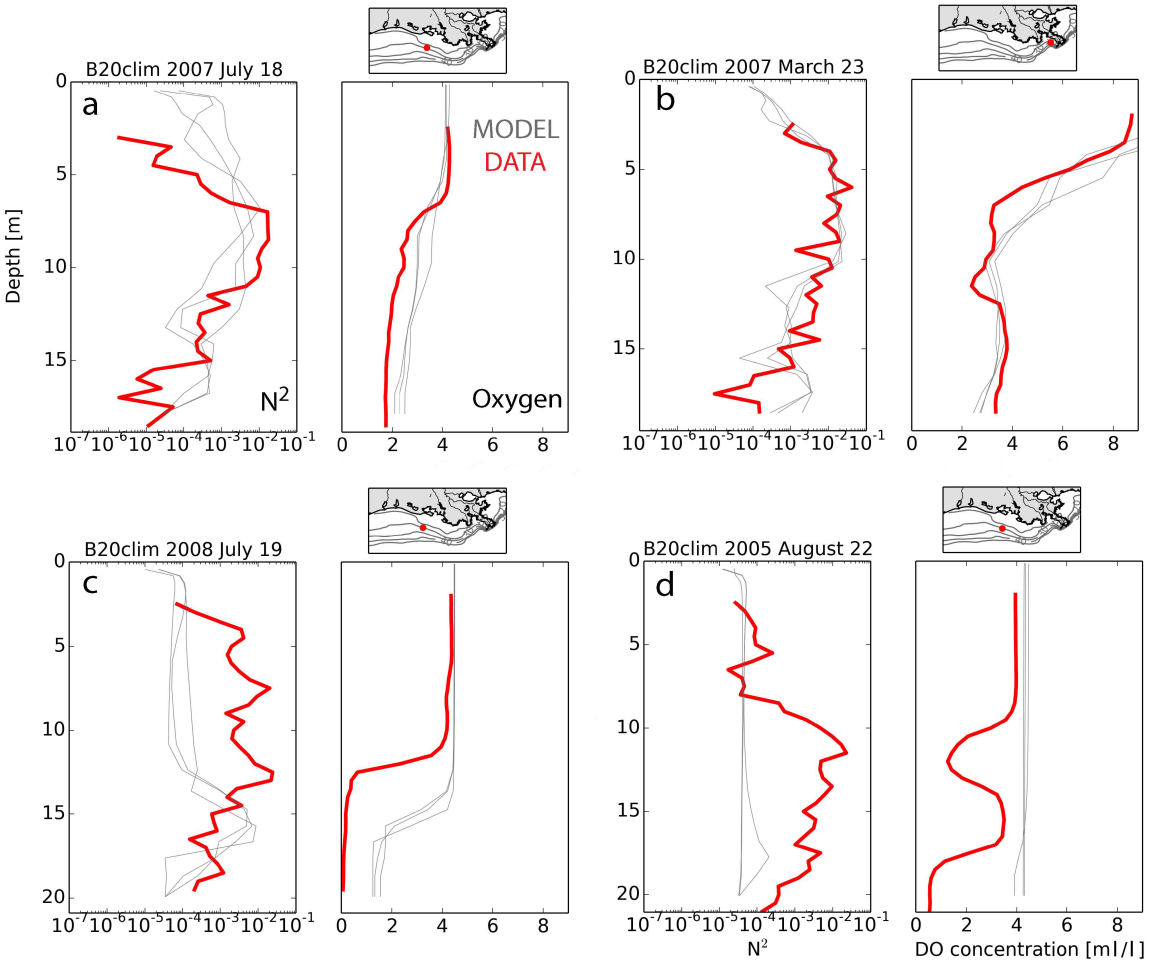

Figure 2.4: Vertical stratification (in logarithmic scale) and dissolved oxygen are shown separately in two panels, red lines are observed profile of properties, while thin gray lines are the simulated properties from the B20clim configuration, three days surrounding the cast time, to show the variability of the profiles.

Table 2.3: Hypoxia prediction during years 2004-2009

	Number of hypoxic stations	Stations predicted correctly as hypoxic (%)
Observation	353	100.00
B20clim	167	47.3
B30HYC	55	15.6
B30IAS	113	32.1

To understand the seasonal variation in the vertical stratification and bottom boundary layer thickness, we selected a location offshore of Atchafalaya Bay (black point in Figure 2.1) within the Atchafalaya River plume, which is strongly influenced by freshwater discharge. The simulated time series of vertical stratification, bottom boundary layer height for TXLA and B30IAS, and bottom dissolved oxygen concentration for B30IAS for the year 2008 (Figure 2.5) are shown. The bottom boundary layer is not defined for September through March when vertical stratification is too weak, the whole water column is almost well mixed and the main pycnocline breaks down ($N^2_{max} < 9.8 \times 10^{-4}$). The bottom boundary layer and the main pycnocline are not distinct from each other for April through May, when a moderately stratified water column establishes and the maximum vertical stratification occurs directly atop the bottom boundary layer. During this time period, the bottom boundary layer is relatively thick.

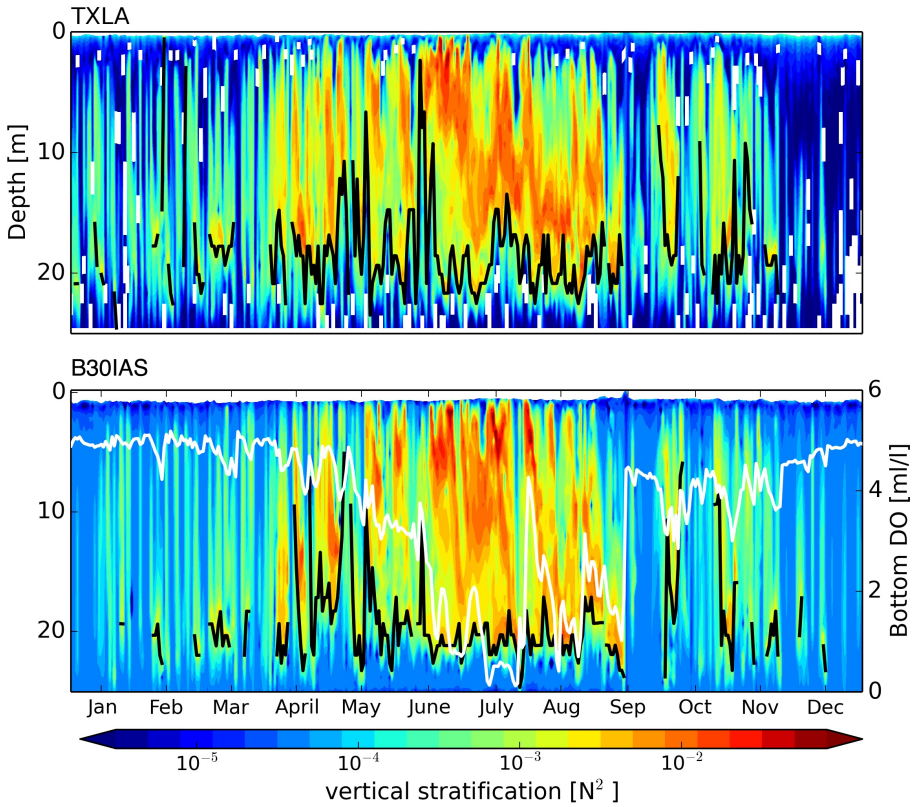

Figure 2.5: The vertical stratification profile time series for the year 2008, for the TXLA model and the MCH B30IAS run; the black line represents the height of the bottom boundary layer and the white line in the B30IAS MCH configuration represents the bottom oxygen concentrations.

A strengthened main pycnocline is distinct from a well-developed thin bottom boundary layer for June through August, when the upper water column is strongly stratified due to the presence of weak, upwelling favorable wind modifying the Mississippi/Atchafalaya River plume; a strong main pycnocline is established in June. The main pycnocline is a prerequisite for the formation of a relatively thin bottom boundary layer, which can accumulate the effect of oxygen consumption (primarily due to sediment oxygen consumption) by inhibiting bottom water ventilation. Bottom dissolved oxygen levels drop dramatically when such a thin bottom boundary

layer forms. The passage of atmospheric fronts in fall leads to enhanced wind mixing and the breakdown of the main pycnocline. At this point, oxygen-rich surface water is mixed downward, exchange with bottom water and the bottom hypoxic water is ventilated. This sequence of events is consistent with the idea that bottom hypoxia formation and destruction are essentially vertical processes, a balance between oxygen ventilation and consumption, in agreement with Hetland and DiMarco (2008). Results shown in Figure 2.5 suggest that a strong main pycnocline provides a necessary pre-conditioning for the existence of a bottom boundary layer to form, and a well-developed thin bottom boundary layer in combination with high rates of sediment oxygen consumption, in turn, is able to maintain low bottom dissolved oxygen.

The observed depth of the main pycnocline vs. the depth of the bottom boundary layer is shown in Figure 2.6; the shading of the points indicates the presence or absence of bottom hypoxia. The points along the diagonal indicate that the main pycnocline and bottom boundary layer are co-located. The points above the diagonal are stations where the main pycnocline is shallower and separated from the bottom boundary layer. The top of the bottom boundary layer is often associated with a small, secondary peak in stratification, below the main pycnocline when the two are distinct. It is this secondary peak in stratification that isolates the bottom boundary layer from the water above, and allows hypoxia to develop within the bottom boundary layer.

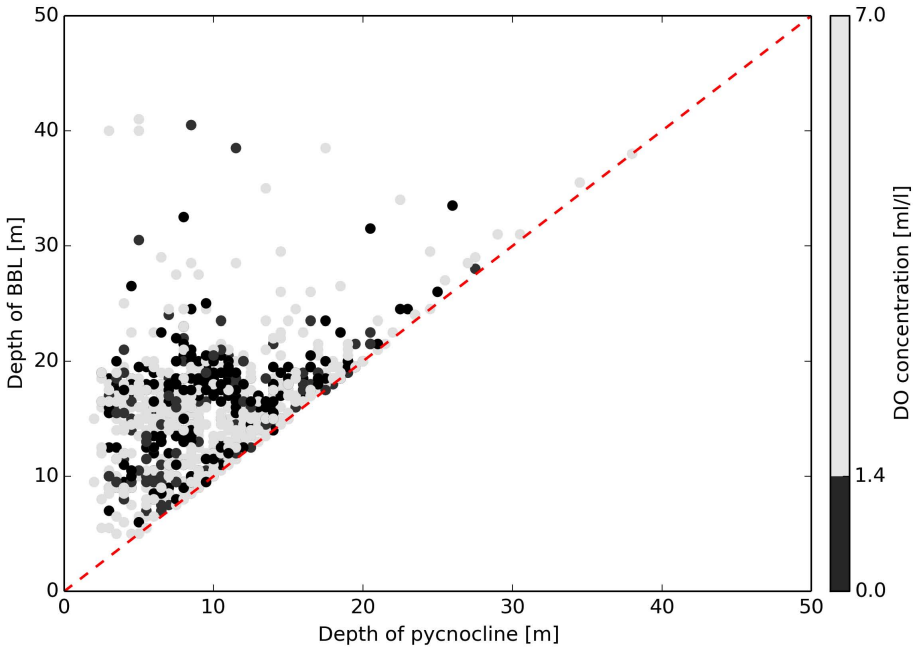

Figure 2.6: Depth of the main pycnocline vs. depth of the bottom boundary layer for all the observed stations, the shading of the points is related to bottom oxygen concentrations, and the dashed line shows the one-to-one line.

The depth differences between the bottom boundary layer and the main pycnocline for all observed hypoxic stations range from 0 to 30 m (Figure 2.6). Operationally, we identify the main pycnocline being distinct from the bottom boundary layer when the depth difference is larger than 15% of the water column depth of the station. In total, a large majority – about 80% – of the observed hypoxic stations (black points in Figure 2.6) have a main pycnocline that is distinct from the top of the bottom boundary layer. Note that no trends in bottom oxygen concentration are present, because this metric does not take into account the strength of stratification, just the relative spatial positions of the top of the bottom boundary layer and main pycnocline.

Additionally, we examine other relationships between hypoxia and the position of

the main pycnocline and bottom boundary layer, similar to the analysis of Wiseman et al. (1997). All the hypoxic stations from 14 cruises are examined to clarify the differences between the main pycnocline and the bottom boundary layer, and their relationships to hypoxia. Figure 2.7 shows the depth and thickness of the main pycnocline and the bottom boundary layer in comparison to the depth and thickness of the hypoxic layer. The depth of the bottom boundary layer and the depth of hypoxic water are almost always co-located while the depth of pycnocline is often shallower than that of the hypoxic water. The rightmost panel shows the bottom boundary layer thickness vs. hypoxic layer thickness, illustrating that the hypoxic layer is typically a bit thicker – about 2 m thicker in the mean – than the bottom boundary layer. Figure 2.8 shows the same analysis for the three MCH configurations. Qualitatively, the models show similar trends, in particular, that the hypoxic layer is most strongly associated with the bottom boundary layer, and is generally thicker by a factor of about 1.5 to 2.

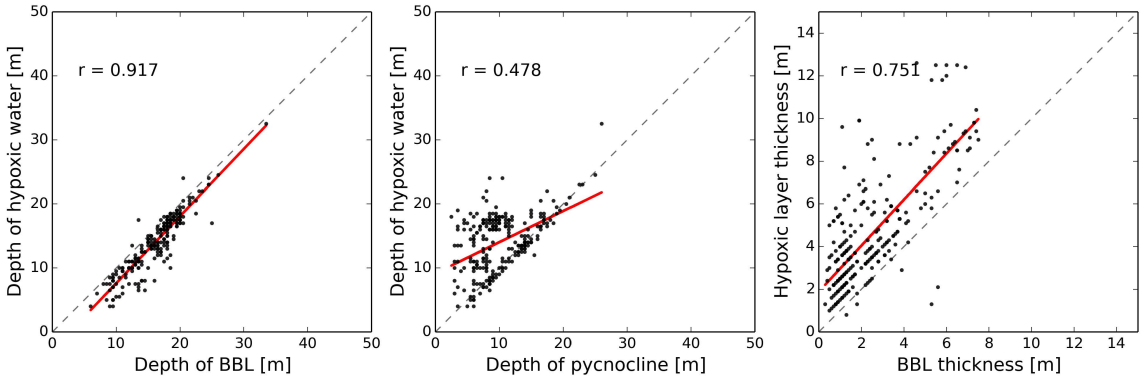

Figure 2.7: The observations used here are shown in table 2.1, only hypoxic stations are selected. Left: depth of the top of the bottom boundary layer vs. the depth of the top of the hypoxic water; middle: depth of the pycnocline vs. the depth of the top of the hypoxic water; right: bottom boundary layer thickness vs. hypoxic layer thickness. The red line represents the slope of the points and the gray dashed line is the one-to-one line.

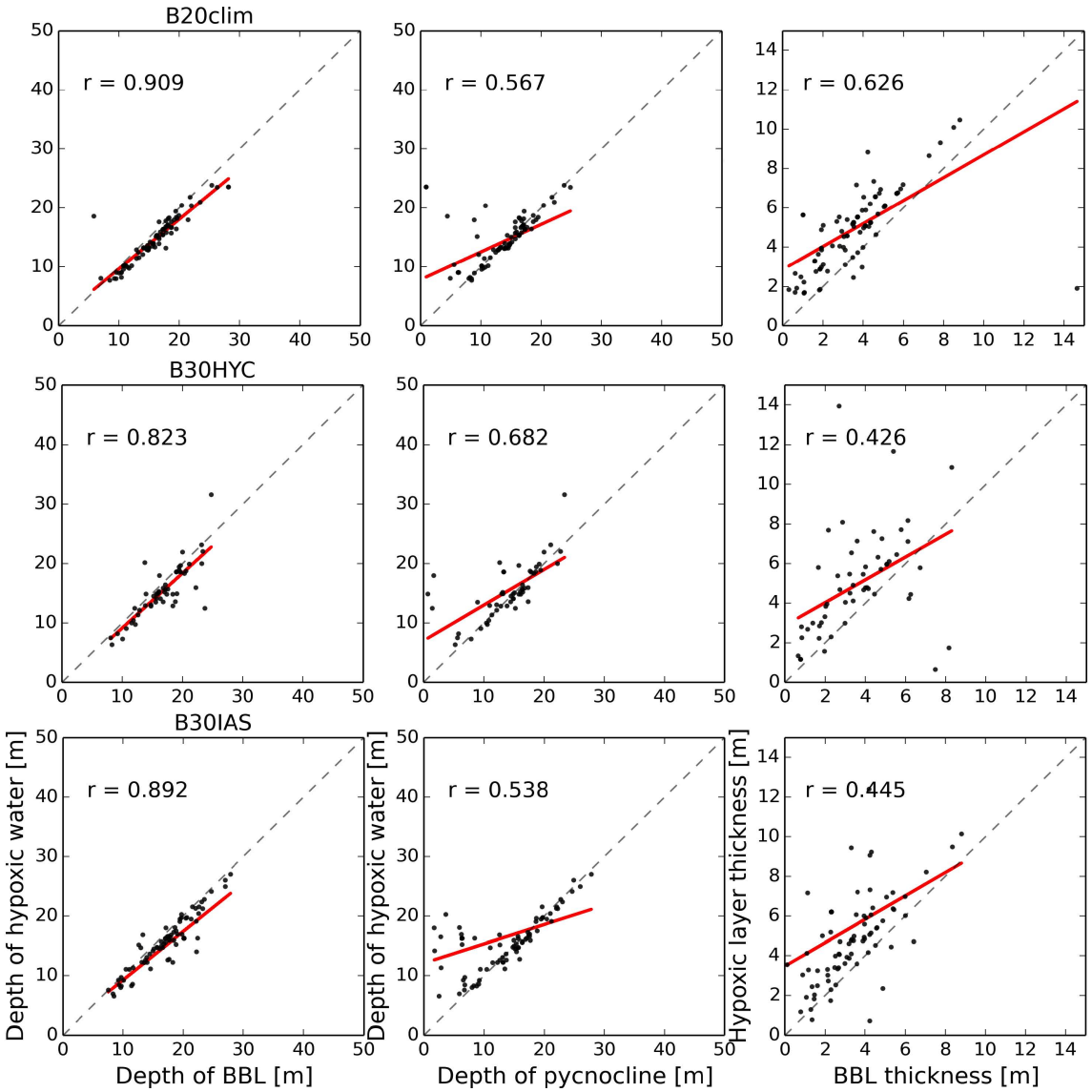

Figure 2.8: The same information as Figure 2.7 for all the MCH models. The model parameters are shown in table 2.2.

Both the observations and simulations indicate that dissolved oxygen concentration changes with vertical stratification (Figure 2.3, Figure 2.4, Figure 2.5). To better assess the ability of the model to reproduce observed stratification, simulated and observed stratification profiles are compared by using a histogram of vertical

stratification weighed by the vertical resolution of the profile at all of the measurement locations. Using histograms of stratification is similar to any bulk water mass analysis – it necessarily integrates over many details. It is the net effect of the various processes occurring at all spatial and temporal scales we are measuring here. Histogram comparisons are shown in Figure 2.9. The gray shaded region denotes the critical vertical stratification range that is necessary but not sufficient for hypoxia to form, as determined by Belabbassi (2006); at higher stratification values, hypoxia is always present in late summer, at lower values, never.

The TXLA model is able to reproduce the observed stratification in a bulk sense, as the simulated and observed stratification histograms overlap, while the MCH model histograms have an offset toward being less stratified than observations suggest. Model error can be further assessed by examining the differences in the histograms of observed and simulated stratification in the range of stratification relevant for the formation of hypoxia in the shaded region. Figure 2.10 shows error histograms, where negative values mean under-prediction of stratification. The TXLA histogram is almost unbiased with the most likely error occurring near zero. However, the error histograms for the MCH configurations are all negatively biased, indicating an underestimation of vertical stratification.

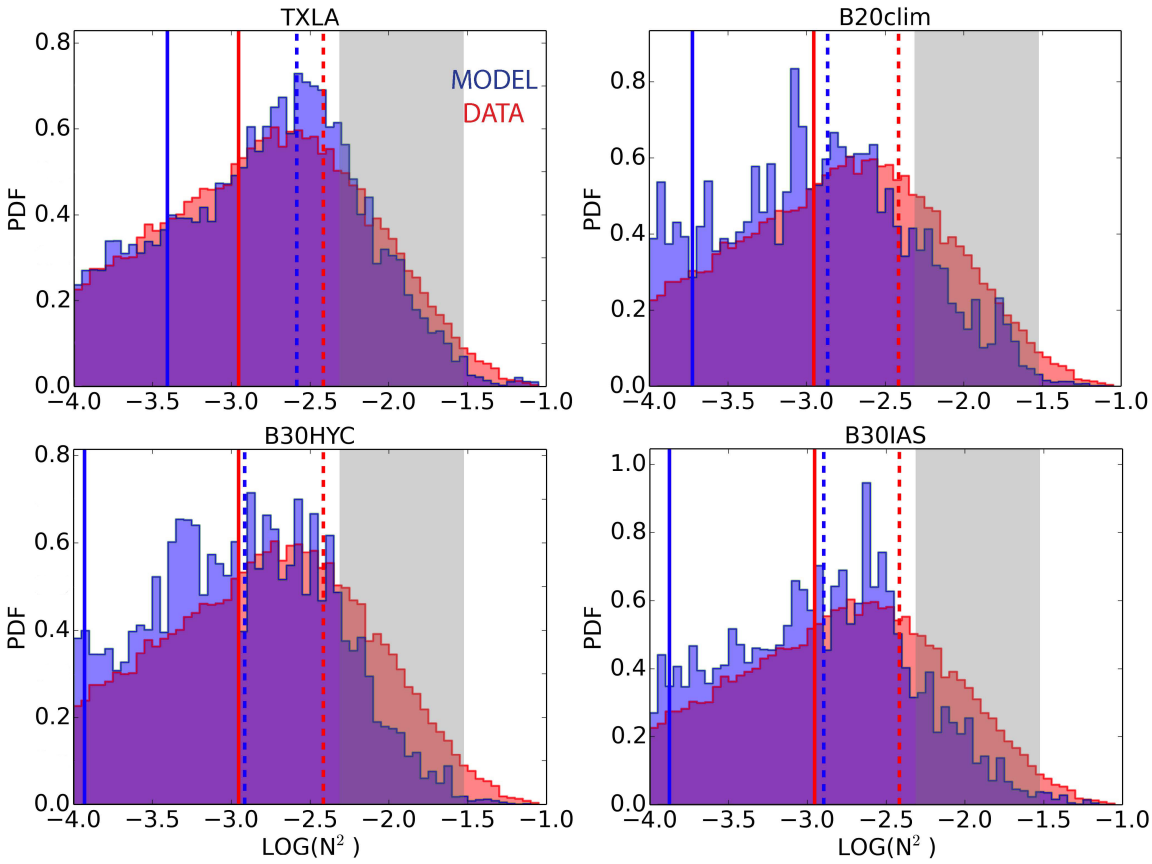

Figure 2.9: Histograms of logarithmic values of vertical stratification for all the measurement stations, red represents observations and blue represents model. The light gray shade denotes the critical vertical stratification range that is necessary but not sufficient for hypoxia formation (40 - 100 cycles/h). Solid and dashed lines are the 50th and 75th percentile, respectively.

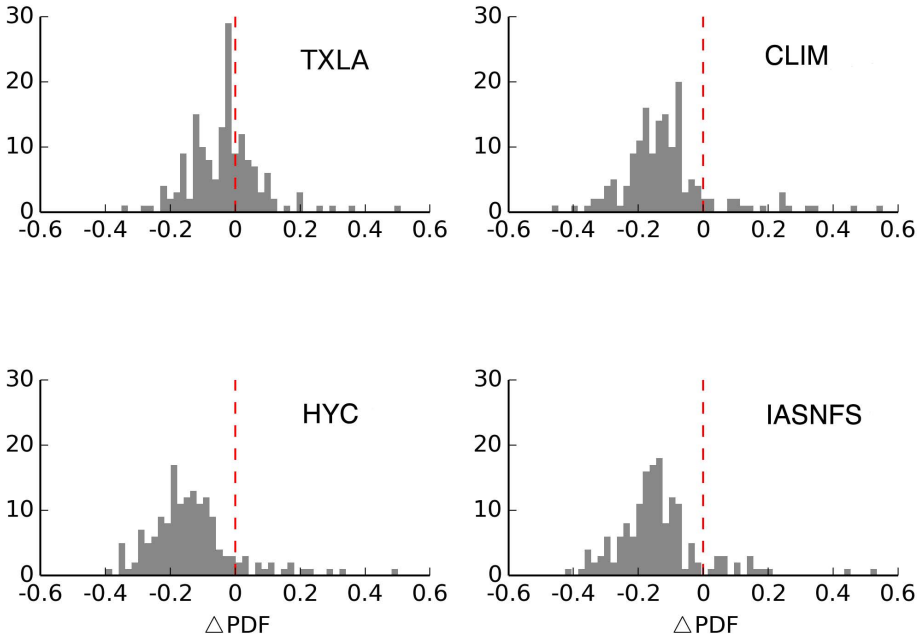

Figure 2.10: The model-data PDF errors of the gray shade region in Figure 2.9.

To understand where the errors are most likely to occur on the shelf, we identified the simulated maximum values for each vertical stratification profile and compare these values to the observed maximum vertical stratification. The left panel of Figure 2.11 shows the observed vs. simulated maximum vertical stratification (on a logarithmic scale) for the TXLA model. Gray points represent stations within 0.5 standard deviations from the diagonal. Colors represent the over- and underestimated stations, and correspond to the colored points on the map in the right panel. The TXLA model captures observed maximum stratification values reasonably well except for a few underestimated stations near the mouth of Atchafalaya Bay. The scatter plots (not shown here) for the MCH models indicate that they are also able to reproduce the observed maximum stratification values, although they have many more underestimated stations, and these locations are usually located in the observed hypoxic domain (Figure 2.12).

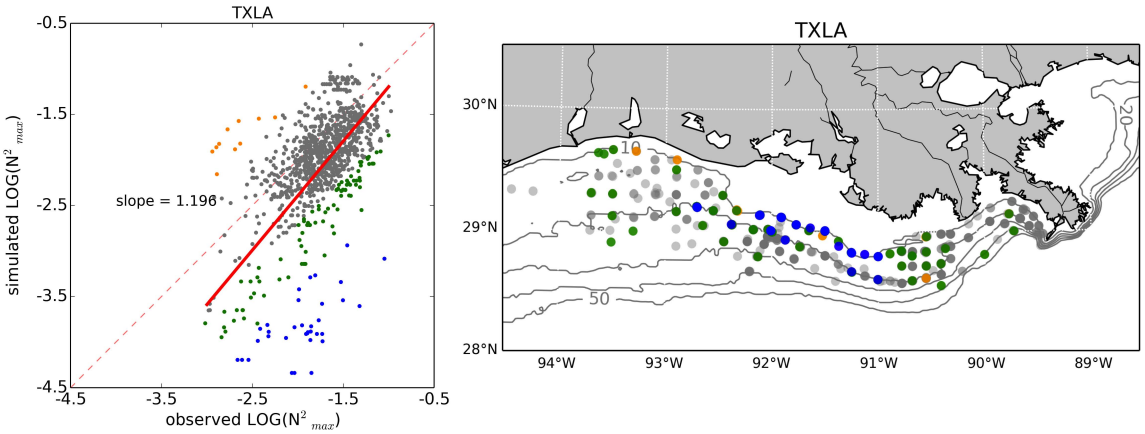

Figure 2.11: Left: the observed vs. TXLA simulated maximum vertical stratification for all measurement stations, the dashed red line represents the one-to-one line and the thick red line represents the slope of all the points. Shading of the points represents the model error, and is relative to the distance of the points to the diagonal. Gray points represent points within 0.5 deviations from the diagonal, colors represent the over- and underestimated stations; and correspond to the colored points on the map in the right panel.

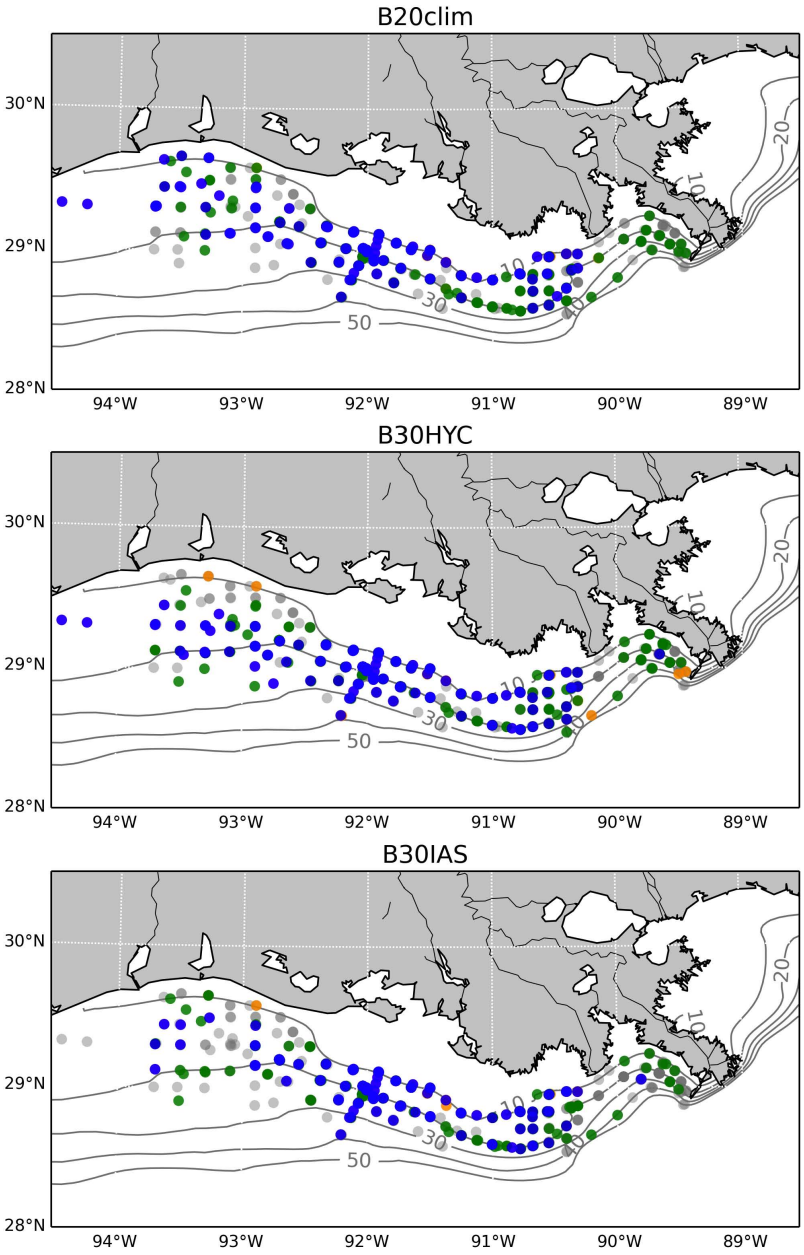

Figure 2.12: This figure shows the same information as the right panel of Figure 2.11 for the MCH models, the scatter plots for observed vs. simulated maximum vertical stratification are not shown here.

2.7 Discussion

Fennel et al. (2013) used different sedimentary oxygen consumption (SOC) treat-

ments, vertical resolutions and horizontal boundary treatments, in order to assess the influence of these factors on hypoxia predictions. In general, both vertical resolution and open boundary conditions had less of an effect than SOC treatment. The different SOC treatments tested included instantaneous remineralization, a parameterization by Hetland and DiMarco (2008) and one by Murrell and Lehrter (2011); the Hetland and DiMarco (2008) parameterization was shown to be the best at simulating hypoxic extent. Fennel et al. (2013) did not investigate the effect of stratification on hypoxia simulations. In this study, three of the MCH configurations (all with the Hetland and DiMarco (2008) SOC treatment) as well as the TXLA model are analyzed, aiming to investigate stratification in the context of hypoxia formation, and what is required to simulate stratification accurately.

The strength of the main pycnocline influences the bottom boundary layer dynamics; the existence of a main pycnocline provides a prerequisite for the formation of a bottom boundary layer(Trowbridge and Lentz, 1991; MacCready and Rhines, 1993; Brink and Lentz, 2010a,b). Thus, a strong frontal pycnocline allows for the formation of a thin bottom boundary layer that persists over parts of the Texas-Louisiana shelf for most of the summer. Bottom boundary layer thickness varies seasonally as does overall stratification primarily due to the combined contribution of seasonal wind patterns and large fresh water discharge. During non-summer (September-May) strong, downwelling-favorable winds force the Mississippi/Atchafalaya plume to the coast, while the vertical stratification over the shelf is reduced by the onshore surface Ekman transport (Cochrane and Kelly, 1986; Nowlin et al., 2005; Zhang and Hetland, 2012). During the summer season, relatively weak, upwelling-favorable wind spreads fresh water seaward at the surface (Cochrane and Kelly, 1986; Nowlin et al., 2005; Zhang and Hetland, 2012), enhancing stratification over the shelf. Thus, during summer, a strong main pycnocline is formed in regions of the shelf where the

Mississippi/Atchafalaya plume is present, and beneath this plume, a thin bottom boundary layer often forms.

The various MCH model configurations all under-predict stratification over the shelf, whereas the TXLA model is able to successfully predict bulk stratification properties over the shelf. Given that the MCH models use a variety of open boundary conditions and vertical resolutions, it appears that the primary factor in successfully simulating stratification is the horizontal resolution of the model. The TXLA model has a horizontal resolution about three times finer than the MCH model. Resolving small-scale circulation features on the shelf, with length scales of $\mathcal{O}(10$ km), is therefore likely critical to the proper simulation of stratification.

Histograms of stratification are determined by the bulk stratification within the water column, i.e. by how much water is present with a particular stratification range, and thus may be considered representative of the model's ability to reproduce the main pycnocline over the entire shelf. However, it is possible that errors in reproducing the weaker stratification associated with the top of the bottom boundary layer may not be as apparent within the histograms of stratification. We assume that proper simulation of the main pycnocline is essential for an accurate simulation of bottom boundary layer processes, but it is not necessarily sufficient. Other processes may act to alter near-bottom conditions. We find that the TXLA model generally seems to over-predict the thickness of the bottom boundary layer, but we leave a detailed comparison of bottom boundary layer dynamics to a future study.

There are known issues with the TXLA model in reproducing stratification. Zhang et al. (2012b) evaluated the TXLA model's ability to reproduce depth-averaged salinity. The calculated model skills indicate that the TXLA model does well in predicting salinity; model skill ranges from 0.28 to 0.78. However, the skill at reproducing temperature, once the seasonal mean has been removed, has an averaged value

smaller than -0.8. The separate effects of salinity and temperature on stratification can be calculated from

$$N_S^2 = -\frac{g\beta}{\rho_0}\frac{\partial S}{\partial z} \tag{2.4}$$

$$N_T^2 = -\frac{g\alpha}{\rho_0}\frac{\partial T}{\partial z} \tag{2.5}$$

where α is the thermal expansion coefficient and β is the saline contraction coefficient. Thus, N_S^2 is the part of the stratification due to salinity stratification alone, and N_T^2 that due to temperature alone. Histograms of N_S^2 (Figure 2.13) indicate that the model's ability to reproduce salinity stratification is reasonable, similar to the ability to reproduce N^2 histograms. However, temperature stratification is underestimated by the model (Figure 2.13). It is not clear what effect this has on the model's ability to reproduce stratification, nor on the model's ability to reproduce sediment respiration, which is thought to be temperature dependent (Hetland and DiMarco, 2008).

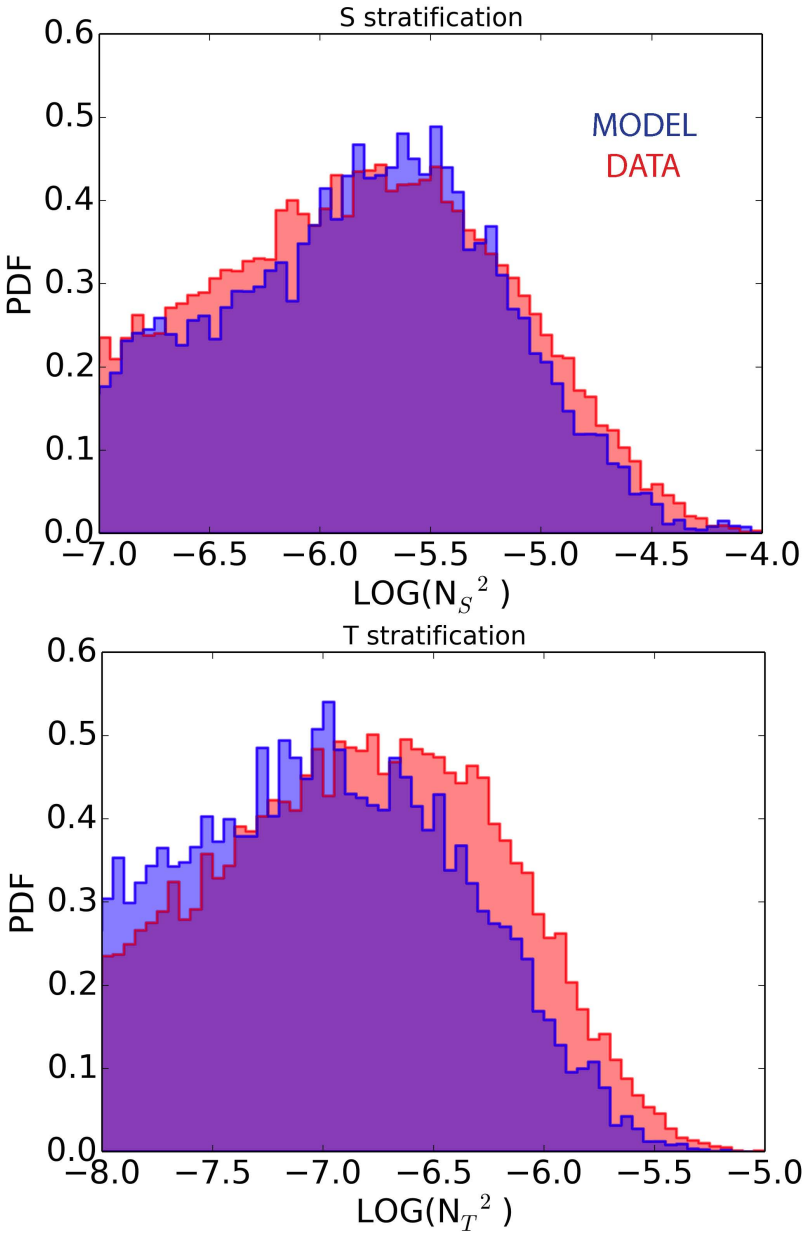

Figure 2.13: Histograms of logarithmic values of salinity stratification (top) and temperature stratification (bottom), respectively, for all the measurement stations. Red represents observations and blue represents the TXLA model.

2.8 Conclusions

Two hydrodynamic model grids are evaluated, the smaller one with various open boundary and vertical grid configurations. Properties of the main pycnocline, bottom boundary layer, and dissolved oxygen concentrations are compared in the context of hydrographic data. The depth of the hypoxic layer is often significantly deeper than that of the main pycnocline, but is almost always associated with the bottom boundary layer; the thickness of the hypoxic layer is about twice the bottom boundary layer thickness. Belabbassi (2006) has related the existence of hypoxia to the maximum water column stratification, following the notion that stratification inhibits mixing and the ventilation of the lower layer. Results presented in this section demonstrate that an intermediate process, the formation of a bottom boundary layer distinct from the main pycnocline, is also important. This is consistent with Hetland and DiMarco (2008) and Fennel et al. (2013).

Hetland and DiMarco (2008) and Fennel et al. (2013) both note the tight relationship between the bottom boundary layer and bottom hypoxia. Around 80% of the observed hypoxic stations in summer have an obviously distinct bottom boundary layer from a main pycnocline. Also, most of these stations are along the 20 m isobath. Previous numerical study indicated that hypoxic conditions are ephemeral near shore, and the most persistent hypoxia centers along the 20 m isobath under benthic respiration demand(Hetland and DiMarco, 2008). Furthermore, DiMarco et al. (2010) observed a meander of the vertical structure of properties, a wave-like structure, in the vertical section taken along 20 m isobath. The near-bottom dissolved oxygen concentrations vary with the crests and troughs of the along shelf density structure (see Fig. 2 of DiMarco et al. (2010)). The active benthic biological processes or the complicated physical dynamics might be the reason for those

observations.

The bottom boundary layer and the main pycnocline play different roles in driving the occurrence of hypoxia. A strong main pycnocline implies a stable water column, which protects and isolates the lower layer from mixing. However, the role that a main pycnocline plays in the formation of bottom hypoxia is not direct. The interaction between a strong main pycnocline and the formation of a thin bottom boundary layer is involved. It provides a prerequisite for bottom boundary layer formation, which in turn inhibits bottom water ventilation and enforces bottom hypoxia. As benthic respiration is often considered the most important sink of oxygen in the western regions affected by seasonal hypoxia, a thinner bottom boundary layer will cause hypoxia to form proportionally faster. The stable main pycnocline may also prime the lower water column for hypoxia, by inhibiting ventilation and lowering oxygen concentrations below the pycnocline through water column respiration.

This study is the first to evaluate the ability of a model at reproducing bulk shelf stratification. The histograms of stratification may be used as a metric to evaluate a hydrodynamic model's ability to reproduce stratification. It was found that the TXLA model is able to reproduce the observed vertical stratification, in a bulk sense, better than any of the MCH model configurations. This improvement in model performance is attributed to the finer horizontal resolution of the TXLA model grid, as other factors are modified in the MCH configurations without any improvement in the ability of the model to simulate observed stratification.

3. PROCESSES CONTROLLING MID-WATER COLUMN OXYGEN MINIMA OVER THE TEXAS-LOUISIANA SHELF

3.1 Overview

We investigate distributions of dissolved oxygen over the Texas-Louisiana shelf using spatially highly resolved observations in combination with a regional circulation model with simple oxygen dynamics. The observations were collected during the MCH program using a towed, undulating CTD profiles collected during the Mechanisms Controlling Hypoxia (MCH) program. Mid-water oxygen minimum layers (dissolved oxygen lower than 3.2 mL L^{-1}) were detected in many transects. These oxygen minimum layers are connected with the bottom boundary layer and follow the pycnocline seaward as a tongue of low oxygen in the mid-water column. T-S diagrams of both observations and simulations imply direct connections between low-oxygen bottom water and the oxygen minimum layer. We examine the dynamics of these oxygen minimum layers in the mid-water column with the help of an existing three-dimensional hydrodynamic model, based on the Regional Ocean Modeling System (ROMS). We calculate convergence within the bottom boundary layer relative to density surfaces and show that there is a convergence in the bottom boundary layer at the location where the pycnocline intersects the bottom. The buoyancy advection forced by bottom Ekman transport creates a convergent flow, and a corresponding intrusion is formed, creating an injection of low-oxygen bottom boundary layer water into the pycnocline. This mechanism explains the observed oxygen minima on the Texas-Louisiana shelf; we consider this as evidence for convergence in the bottom boundary layer and corresponding intrusions of low-oxygen water into the interior of the water column in this region.

3.2 Introduction

The Texas-Louisiana continental shelf is located in the northern Gulf of Mexico, and the Mississippi and Atchafalaya River system is the major source of fresh water, sediment, nutrients and pollutants for this region. Every year the Mississippi and Atchafalaya River system delivers about 5.3×10^2 km^3 of fresh water, 2.1 $\times10^8$ tons of sediment and 0.95 $\times10^6$ tons of nitrogen to this region (Milliman and Meade, 1983; Meade, 1996; Bianchi et al., 2010). The Mississippi and Atchafalaya Rivers drain around 42% of the continental watershed of the United States. The outflow usually peaks in spring and is at a minimum in early fall. The large flux of nutrients leads to eutrophication within the Mississippi/Atchafalaya plume (Lohrenz et al., 1990; Turner and Rabalais, 1994; Fennel et al., 2011), and hypoxic conditions form in the near-bottom waters over the mid-shelf (Rabalais et al., 2002a; Bianchi et al., 2010), at depths ranging from roughly 10 to 50 m.

The wind over the shelf changes seasonally with weak, upwelling-favorable conditions in summer (June-August) and stronger, downwelling-favorable conditions during non-summer (September-May) (Cochrane and Kelly, 1986; Cho et al., 1998; Nowlin et al., 1998, 2005). The seasonal wind patterns, in addition to a strong contribution from buoyancy forcing near the Mississippi and Atchafalaya Rivers, drives the low-frequency circulation on the shelf (Cochrane and Kelly, 1986; Cho et al., 1998; Zhang and Hetland, 2012). A significant portion of the freshwater discharge is trapped on the Louisiana shelf and transported downcoast (westward) by a coastal current (Cochrane and Kelly, 1986; Nowlin et al., 2005; Zhang and Hetland, 2012). During summer, when winds tend to be upweling-favorable, stratification intensifies and inhibits the exchange of oxygen-rich surface water to subpycnocline waters (Wiseman et al., 1997; Hetland and DiMarco, 2008; Bianchi et al., 2010). The strat-

ification due to wind-modified freshwater distribution and the eutrophication due to nutrient loading from the Mississippi River system combine to facilitate bottom hypoxia formation over the shelf (Wiseman et al., 1997; Hetland and DiMarco, 2008; DiMarco et al., 2010; Zhang et al., 2012b; Fennel et al., 2013).

The bottom boundary layer is a thin, near-bottom, well-mixed layer known to exchange water with the interior water column in places where the pycnocline intersects the sea-floor (e.g., Houghton and Visbeck, 1998; Pickart, 2000). The bottom boundary layer responds asymmetrically to the direction of along-shore current over a stratified sloping shelf (e.g., Lentz and Trowbridge, 1991). Ekman transport within the bottom boundary layer is driven by bottom stress associated with along-shore currents, and the direction as well as the magnitude of bottom Ekman transport alters bottom boundary layer thickness. A thicker bottom boundary layer will form under downcoast currents (flow in the sense of Kelvin wave propagation), typically generated by downwelling-favorable winds. The corresponding downslope Ekman transport in the case of downcoast flow will tend to push buoyant water offshore within the bottom boundary layer underneath denser water, destabilizing the water in the bottom boundary layer. The result is mixing and thickening of the bottom boundary layer. However, for upcoast currents driven by upwelling winds, a shoreward Ekman transport will form. The upslope transport will tend to stabilize the bottom boundary layer by advecting heavy water under light and inhibit near bottom mixing, resulting in a thinner bottom boundary layer. These effects are considered to be proportional to the overlying shelf current magnitude (Lentz and Trowbridge, 1991).

Although the bottom boundary layer is typically much thinner than the total water column depth, dynamical processes acting in this layer are essential to many biogeochemical processes, such as hypoxia (Wiseman et al., 1997; Fennel et al., 2013).

Hypoxia is defined as a low dissolved oxygen concentration less than 1.4 mL L^{-1} (equivalent to 63 μM L^{-1} or 2 mg L^{-1}), and it is the threshold at which most oceanic animals evacuate (Rabalais et al., 2002b). Bottom hypoxia is a common seasonal phenomenon over the Texas-Louisiana shelf. The areal extent of bottom hypoxia has been measured annually during the past three decades, with sizes ranging from 7200 to over 20000 km^2 (Rabalais et al., 2007). Notably, low oxygen waters that cause seasonal hypoxia in the northern Gulf of Mexico are typically associated with the bottom boundary layer (e.g., Wiseman et al., 1997; Hetland and DiMarco, 2008; Fennel et al., 2013).

On the continental shelf, dynamical processes within the bottom boundary layer, such as buoyancy advection, can span the entire water column and be essential to momentum balance (e.g., Yankovsky and Chapman, 1997; Trowbridge and Lentz, 1998). Previous studies documented that the vertical shear, generated by buoyancy advection via thermal wind adjustment, reduces the bottom current velocity and thus the bottom stress, changing the Ekman transport within the bottom boundary layer. This, in turn, alters the strength and structure of the interior flow (Trowbridge and Lentz, 1991; MacCready and Rhines, 1993; Garrett et al., 1993; Middleton and Ramsden, 1996). Chapman and Lentz (1997) extended these theories to a three-dimensional circulation; the feedback between the interior flow and the bottom boundary layer plays a crucial role in their model. Time-series measurements collected on the northern California shelf show how the boundary layer flow may have an asymmetric response to the direction of the interior flow, demonstrating that the cross-shore momentum balance includes a dynamically significant buoyancy force resulting from the distortion of isopycnal surfaces within the bottom boundary layer (Trowbridge and Lentz, 1998).

A convergent zone, driven by Ekman transport within the bottom boundary layer,

can be generated at the location where the pycnocline intersects the bottom (e.g., Houghton and Visbeck, 1998). A numerical study by Chapman and Lentz (1994) released buoyant particles into the freshwater inflow, 1.36 m above the bottom at different alongshore locations after the offshore migration of the front was arrested. Some of these remained in the bottom boundary layer until they approached the shoreward edge of the front and were carried vertically upward into the along-shore jet, indicating the location of the convergence. This convergent flow at the foot of the shelfbreak front and the corresponding upwelling circulation within the front in the Middle Atlantic Bight were subsequently studied using a dye tracer injected into the bottom boundary layer (Houghton, 1997; Houghton and Visbeck, 1998). The dye was later found to have been injected up into the water column within the front. Barth et al. (1998) also detected a mid-water region of suspended bottom material emanating from the foot of the front and extending to within 35 m of the surface, 80 m above bottom, providing further evidence of strong convergence within the bottom boundary layer. Pickart (2000) used a synoptic hydrographic section to investigate the characteristic of water injected into the front from the bottom boundary layer, associated with the shelfbreak jet in the Middle Atlantic Bight. Pickart (2000) found the location where the bottom boundary layer detached from the bottom, at the frontal region, and bottom water spread into the interior along an isopycnal layer abutting the front at a pumping speed of 23 m day^{-1}. Also, Pickart (2000) indicates that the detached bottom boundary layer tracks the line of maximum interior convergence, which suggests that intrusions driven by convergence might contribute to the flow along this isopycnal layer.

The primary goal of this section is to identify the dynamical mechanisms that control the mid-water oxygen minima over the Texas-Louisiana shelf. In the model, oxygen is assumed to be saturated at the sea surface and benthic oxygen demand

is the only imposed sink of oxygen. The model reproduces the mid-water oxygen minima qualitatively. Our results demonstrate that the mid-water oxygen minima are actually low-oxygen bottom water intrusions, that the bottom boundary layer dynamics is crucial to the generation of these mid-water oxygen minima, and that the buoyancy advection in the bottom boundary layer is of fundamental importance in injecting low-oxygen bottom water up into the water column along the main pycnocline that intersects the bottom.

3.3 Observations

Eight shelf-wide survey cruises (Table 3.1) over the Texas-Louisiana Shelf were conducted in June and August from 2010 through 2013 to estimate the horizontal areal extent of hypoxia and vertical distribution of DO (Dissolved Oxygen) and other hydrographic properties. Towed, undulating CTD profiles were collected during these cruises (see Table 3.1 for details) to measure water properties along cross-shelf transects. The towed instrument was equipped with a Sea-Bird SBE 43 DO sensor, RINKO DO sensor, Sea-Bird 55 CTD, WET-labs Fluorometer/Turbidity and CDOM (Chromophoric Dissolved Organic Matter) sensors. The system sampled water properties every 0.25 second, and was towed between 2 m above the bottom and 2 m below the surface. During each transect, the ship maintained a constant heading and a tow velocity of 5 knots, along cross-shelf transects designed to be roughly perpendicular to the local bathymetric lines. Each transect took 4-6 hours to complete. CTD casts were made at the inshore and offshore ends of each cross-shelf transect. Water samples from surface, mid-depth, and bottom were collected and analyzed for nutrients, DO concentrations. The Winkler titration method was used to measure DO concentration of the water samples and the results were used to calibrate the SBE 43 electronic sensors. The properties measured through the towed

instrument were compared with the measurement in the lab from discrete water samples to calibrate the electronic probe DO measurements. Cross-shelf transects were not completed in cruises MS1 and MS3 due to equipment failures and weather (DiMarco, unpublished).

Table 3.1: Survey cruise identifiers and their corresponding dates. Total numbers of transects are also included.

Cruise ID	Start date	End date	Transects
MS1	14 Jun 2010	19 Jun 2010	5
MS2	02 Aug 2010	07 Aug 2010	15
MS3	23 Jun 2011	01 Jul 2011	6
MS4	07 Aug 2011	15 Aug 2011	15
MS5	11 Jun 2012	17 Jun 2012	15
MS6	16 Aug 2012	20 Aug 2012	13
MS7	20 Jun 2013	26 Jun 2013	16
MS8	04 Aug 2013	09 Aug 2013	15

3.4 Hydrodynamic model description

The Regional Ocean Modeling System (ROMS) is configured for the Texas-Louisiana shelf, as described by Zhang et al. (2012b). The model has 30 vertical layers, with a minimum mean water depth of 3 m, and a maximum slightly greater than 3000 m. It has a resolution of about ∼500 m in the northern Gulf in the region of the Mississippi and Atchafalaya river sources, and ∼1-2 km further west offshore of the Texas coast. At the three open boundaries, a nudging zone of six cells was used

to relax the model temperature, salinity and baroclinic velocities toward the Gulf of Mexico Hybrid Coordinate Ocean Model (GOM-HYCOM) (http://www.hycom.org). The nudging time scale used was eight hours at the outermost boundary point, with successively weaker nudging in interior points. Sea surface height and barotropic currents from HYCOM were imposed at the boundaries as Chapman (1985) and Flather (1976) boundary conditions.

The hindcast model is forced with surface momentum, heat and fresh water fluxes from the North American Regional Reanalysis (NARR) data set. Fresh water fluxes from the Mississippi and Atchafalaya Rivers are specified using daily measurements of Mississippi River Transport at Tarbert Landing by the U.S. Army Corps of Engineers. Fresh water fluxes from the other seven rivers (the Nueces, San Antonio, Lavaca, Brazos, Trinity, Sabine, Calcasieu Rivers) are specified based on the USGS (U.S. Geological Survey) RealTime Water Data for the Nation. For further details on model configuration we refer reader to Zhang et al. (2012b).

The model has a simple parameterization of benthic oxygen demand and air-sea gas exchange of oxygen in order to describe oxygen dynamics (Hetland and DiMarco, 2008). Oxygen is initialized at saturated values everywhere based on temperature and salinity (Weiss, 1970). Water from the rivers is also saturated with respect to oxygen. Oxygen concentrations at the open boundaries are relaxed to saturation in exactly the same way as the dynamical tracers. The possible effects of photosynthesis increasing water column oxygen above saturated values are not considered (Hetland and DiMarco, 2008).

The model specifies benthic respiration based on bottom temperature and oxygen concentrations. The function is

$$\text{Bottom } O_2 \text{ flux} = 6.0 \left[O_2 \text{m}^{-2} \text{days}^{-1}\right] \times 2^{T/10.0^{\circ}\text{C}} \times \left[1 - \exp(\frac{O_2}{30.0 \mu\text{M } O_2})\right]. \quad (3.1)$$

This formulation was proposed by Hetland and DiMarco (2008) and is based on data obtained by Rowe et al. (2002). The benthic oxygen flux is applied at the sea floor, as a bottom boundary condition in the model. We refer the reader to Hetland and DiMarco (2008) for further details.

3.5 Results

Figure 3.1 shows the study domain with simulated salinity fronts (31 isohaline) for both surface and bottom of June 2011. These thin lines denote the approximate extent of freshwater from river plumes at surface and bottom, respectively. The inshore shelf waters around the Mississippi and Atchafalaya River plumes are markedly fresher due to large freshwater discharge. The shelf is broad and gently sloping to the west of Terrebonne Bay, and the offshore distance of surface and bottom salinity front is close, indicating that the freshwater discharge generates a bottom attached river plume. The shelf is steeper in the eastern part, between the Mississippi River Delta and Terrebonne Bay, and here the surface salinity front is further offshore than that at the bottom, indicating that the river plume is more surface trapped there.

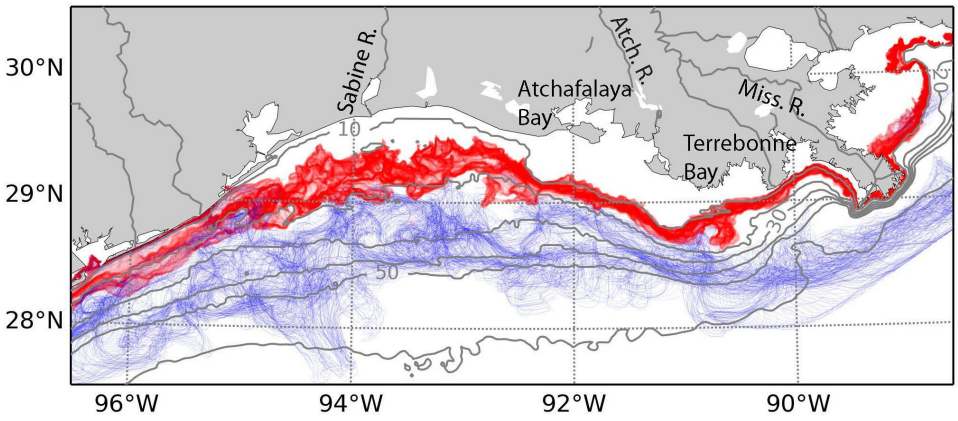

Figure 3.1: The study domain covers much of the Texas-Louisiana continental shelf. Bathymetric contours of 10, 20, 30, 40, 50, 200 m depth are shown on the map. The simulated salinity fronts (31 isohaline) are shown for both surface (blue lines) and bottom (red lines) of June 2011.

Two observed transects of dissolved oxygen concentration are shown in Figure 3.2; transect A is south of Atchafalaya Bay and transect B is west of the Mississippi River Delta. Hypoxic water (orange, DO<1.4 mL L^{-1}) and near-hypoxic, low oxygen water (yellow, 1.4 mL L^{-1}<DO<3.2 mL L^{-1}) are observed near the bottom. Previous studies suggest that this bottom hypoxia formation is a vertical balance between bottom water ventilation and benthic oxygen demand, such that a thin and well-developed bottom boundary layer is essential for hypoxia to form (Wiseman et al., 1997; Hetland and DiMarco, 2008; Fennel et al., 2013). The co-existence of a strong main pycnocline and a persistent thin bottom boundary layer facilitate the formation and persistence of bottom hypoxia. A strong main pycnocline is a pre-requisite for the generation of a bottom boundary layer. The stratification that caps the bottom boundary layer acts as a barrier between low-oxygen near bottom water and well-oxygenated upper layer waters, accumulating the respiratory-oxygen sink while inhibiting oxygen exchange.

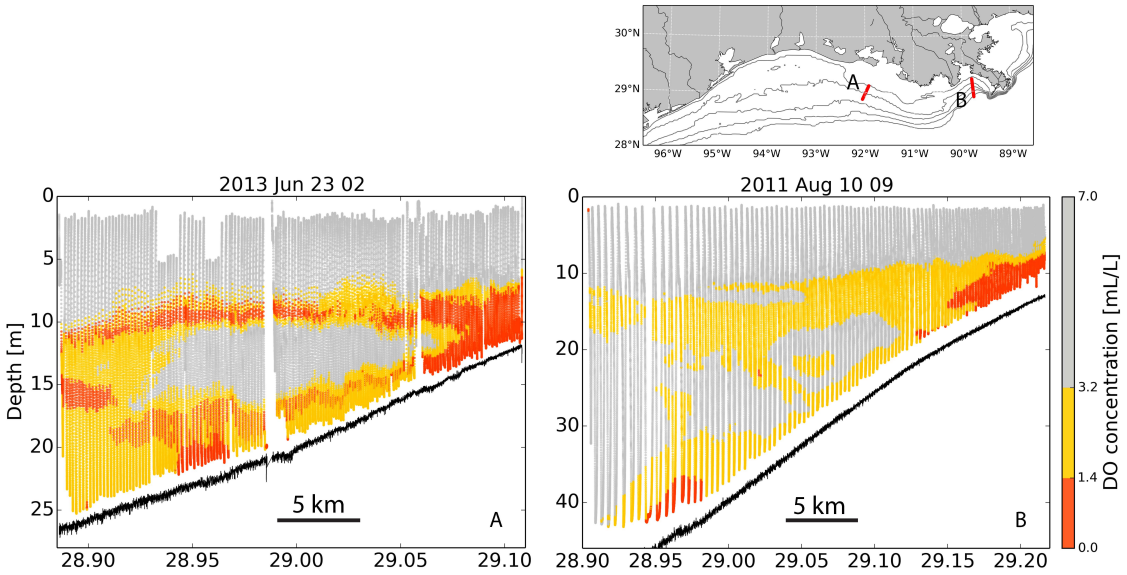

Figure 3.2: Observed dissolved oxygen concentration on two transects. Transect A is south of Atchafalaya Bay and transect B is west of the Mississippi River Delta. Three colors are used to denote different dissolved oxygen conditions. Orange indicates hypoxia (DO<1.4 mL L^{-1}), yellow is defined as near-hypoxic, low-oxygen (1.4 mL L^{-1}<DO<3.2 mL L^{-1}) and gray is any oxygen concentration higher than 3.2 mL L^{-1}.

In addition to the bottom-trapped hypoxia, layers of oxygen minima in the mid-water column are also detected in the transects (see Figure 3.2). Figure 3.3 A1, B1 show the observed dissolved oxygen concentrations for transects A and B, with isopycnals overlayed (thin black lines), and Figure 3.3 A2, B2 show the corresponding T-S diagrams. The low-oxygen layer is co-located with the main pycnocline for both transects. Another noticeable feature of Figure 3.3 A1 is that the near-bottom, low-oxygen water extends up through the water column at 28.97 °N, reaches to within 10 - 12 m of the surface and merges into the main pycnocline low-oxygen layer. The same upward extension of low dissolved oxygen is found in Figure 3.3 B1 at 29.06 °N. Only transect A will be discussed in detail since the two transects have very similar characteristics.

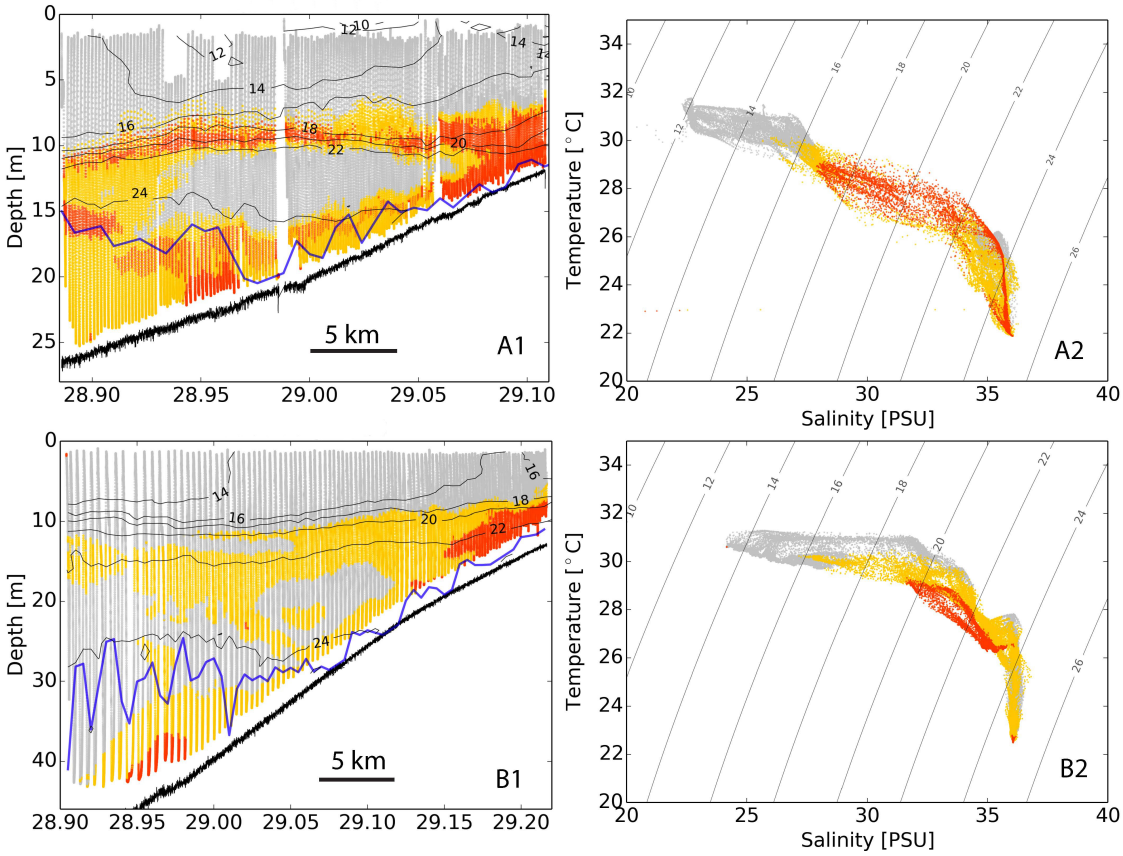

Figure 3.3: A1: the observed dissolved oxygen concentration of transect A from Figure 3.2, black lines overlaid with are the isopycnals and the thick blue line is the top of the bottom boundary layer. A2: the corresponding T-S diagram, and the shading of the points are relative to dissolved oxygen concentration. B1 and B2 are the same informations of transect B from Figure 3.2. The colormap used here is the same as Figure 3.2. The density contours use an interval of 2 kg/m^3 for all panels.

The isopycnals reveal the location of the bottom-attached front; the mid-water oxygen minimum is bounded within the pycnocline and attached to the seafloor at the foot of the front (Figure 3.2). The thickness of the bottom boundary layer here is operationally defined as the distance from the bottom to the maximum height at which the vertical density gradient is greater than 0.1 kg/m^4. This is an operational definition that does not significantly change the results discussed, see Wiseman et al.

(1997).

The bottom boundary layer becomes thinner where the frontal regions intersect the seafloor (the blue lines in Figure 3.3 A1, B1). Also, Figure 3.3 reveals that the bottom near-hypoxic layer becomes thinner shoreward. These are consistent with the conclusion in Section 2, which used survey data to document that the bottom hypoxic layer thickness is highly correlated with the bottom boundary layer thickness, but can be 1.5 or 2 m thicker. Wiseman et al. (1997), Fennel et al. (2013) and Hetland and DiMarco (2008) also demonstrate that the top of the bottom boundary layer is associated with the upper reach of hypoxic bottom water.

We examined transects collected on six cruises, and detected mid-water oxygen minimum layers in many of them. Sometimes the mid-water oxygen minimum layers are similar in extent to those shown Figure 3.2, sometimes they are less pronounced and similar to the ones in Figure 3.4 C. Sometimes, there are more than one mid-water oxygen minimum layer in a single transect (Figure 3.4 D).

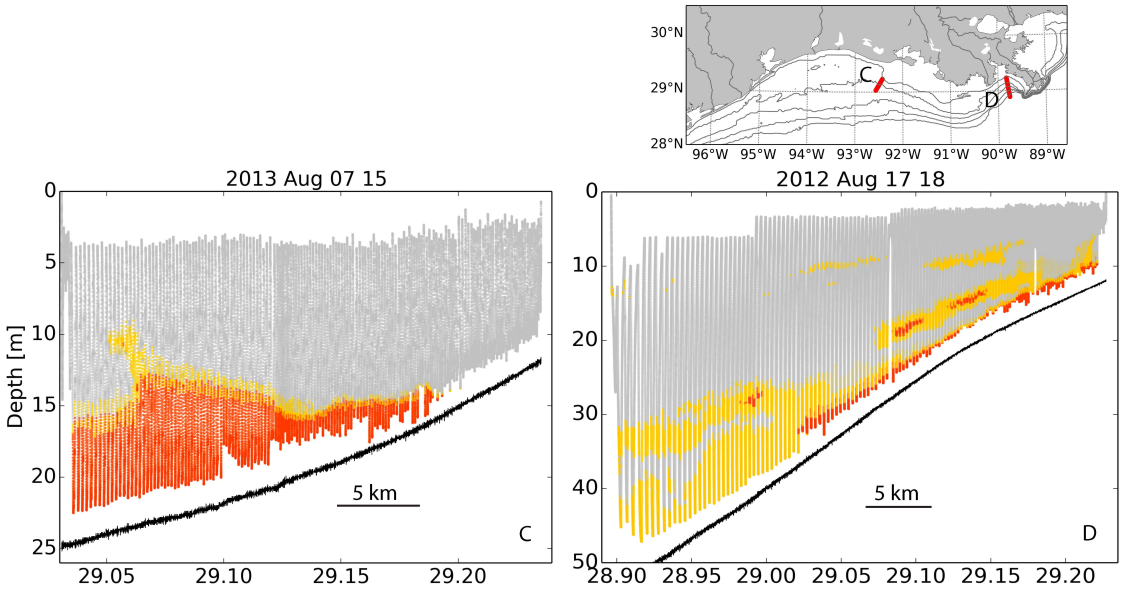

Figure 3.4: Observed dissolved oxygen concentrations of transects C and D, the same colormap from Figure 3.2 is used.

There are two possible reasons that can cause mid-water dissolved oxygen minima. First, dissolved oxygen could be depressed locally by water column respiration, exacerbated by inhibited mixing and reduced ventilation within the pycnocline. Second, the intermediate low oxygen region may be formed by advection from the bottom boundary layer along isopycnals connecting the bottom and the intermediate low oxygen layer, caused by a convergence in the bottom boundary layer. However, it is unlikely that the mid-water dissolved oxygen minima could be generated locally, since there is no reason for the water column respiration to occur at significantly higher rates only in the main pycnocline other than in the water column underneath it as well.

Inspection of the observed T-S diagrams in Figure 3.3 implies a direct connection between low-oxygen water within the bottom boundary layer and that within the mid-water layer. The high density, low dissolved oxygen water masses from the

bottom of Figure 3.3 A2 corresponds to the low-oxygen bottom water underneath the 24 kg m^{-3} isopycnal in A1. Moving to fresher isopycnals along the bottom as well as into the frontal layer (Figure 3.3 A1), the corresponding low oxygen points in the T-S diagram are all connected, without any discernible gap, while crossing multiple isopycnals. This suggests that the mid-water low oxygen layer is directly connected with the low-oxygen bottom water.

We also analyzed the hydrodynamic model results to identify the source of the mid-water column oxygen minima. A transect of simulated oxygen concentration in the vicinity of the observed transect A is shown in Figure 3.5. The simulated dissolved oxygen concentration is generally higher than the actual observed dissolved oxygen concentration, most likely because the model only includes benthic respiration and does not account for water column respiration. The model also shows mid-water oxygen minimum (Figure 3.5) along isopycnals 16 through 18 kg m^{-3} within the stratified front and extending offshore along frontal isopycnals and shoaling toward the surface.

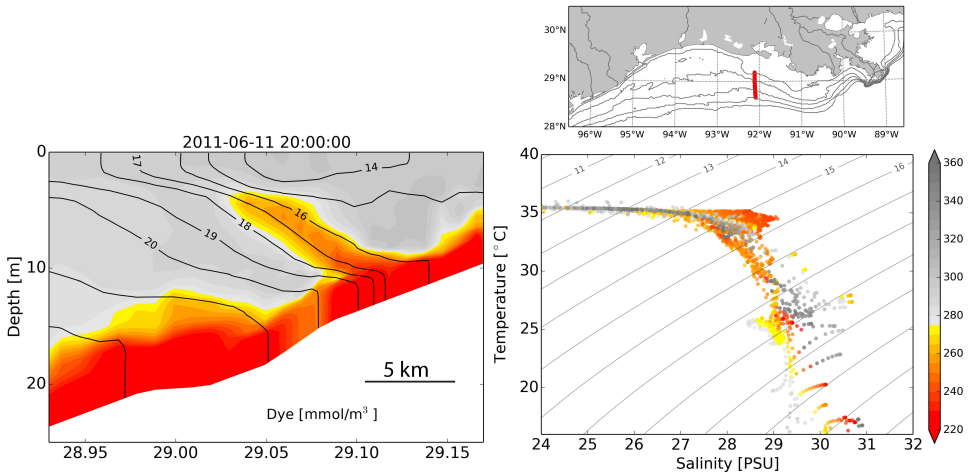

Figure 3.5: Left: the simulated dye tracer concentration of a transect in the vicinity of the observed transect A (around Atchafalaya river plume, see the map on top right). Right: the corresponding T-S diagram, and the shading of the points are relative to dye tracer concentration.

Because the model only uses benthic respiration, the tongue of low dissolved oxygen concentration must ultimately come from the bottom (Figure 3.5). So the model results suggests that the mid-water low-oxygen layer is advected from the low-oxygen bottom water; and the low-oxygen water is associated with a circulation from the bottom boundary layer into the frontal region. The corresponding simulated T-S diagram (right panel of Figure 3.5) also shows that the connection between the low oxygen intrusion and bottom water is continuous. Both the observed mid-water low-oxygen layer structure and the T-S diagram distribution are similar in the simulation. The consistence indicates that the same mechanism is behind observed and simulated mid-water oxygen minima.

Similar to the processes described by Houghton and Visbeck (1998), Barth et al. (1998), and Pickart (2000), the dynamical mechanism of this mid-water dissolved oxygen minimum is that a convergent flow driven by buoyancy advection within

the bottom boundary layer associated with bottom Ekman transport is balanced by an upward flow at the top of the bottom boundary layer, injecting bottom water up along certain isopycnals. The downcoast flow excites offshore bottom Ekman transport within the bottom boundary layer, which can tilt the isopycnals. The tilted isopycnals will be associated with a vertical shear through thermal wind balance; and the near-bottom flow is reduced in regions with strong stratification, reducing the bottom stress and the Ekman transport in these offshore regions in a process similar to that described by MacCready and Rhines (1993). Thus, there will be a convergence in the bottom boundary layer transport, with stronger offshore flow in regions with less stratification seaward of the location where the main pycnocline intersects the bottom. The convergent flow injects bottom water up into the water column and into the interior pycnocline.

To find the convergent zones within the bottom boundary layer over the Texas-Louisiana shelf, first, flow through density surfaces for the bottom layer is calculated using simulated results. In the ocean, the density equation is

$$\frac{\partial \rho}{\partial t} + \vec{u} \cdot \vec{\nabla} \rho = \vec{\nabla} \cdot \vec{f} \tag{3.2}$$

In equation 3.2, ρ is the density field, $\vec{u}$ is the simulated current velocity vector, $\vec{f}$ is the diffusivity term. The total current velocity vector along the bottom, $\vec{u}$, can be divided into three parts, the velocity of the density surface itself $\vec{u_I}$, the flow through the density surface $\vec{u_M}$ and the flow along the density surface $\vec{u_P}$ (Figure 3.6). Since the dot product of $\vec{u_P}$ and density gradient, $\vec{\nabla}\rho$, is zero, $\vec{u_P}$ can be ignored in the equation. In other words, $\vec{u_I} + \vec{u_M}$ is the normal component (in the sense of density

surface) of bottom current velocity. So, equation 3.2 can be rewritten as

$$\frac{\partial \rho}{\partial t} + (\vec{u}_I + \vec{u}_M) \cdot \vec{\nabla} \rho = \vec{\nabla} \cdot \vec{f} \tag{3.3}$$

In equation 3.3, $\vec{u}_I$ is associated with inviscid motions and is reversible, which means the density surface itself can move on- and offshore as well as go back to its original location; $\vec{u}_M$ is associated with mixing and is irreversible. Such that, equation 3.3 can be divided into two components

$$\frac{\partial \rho}{\partial t} + \vec{u}_I \cdot \vec{\nabla} \rho = 0, \tag{3.4}$$

and

$$\vec{u}_M \cdot \vec{\nabla} \rho = \vec{\nabla} \cdot \vec{f} \tag{3.5}$$

Figure 3.6 shows the bottom layer in x-y plane; the gray line represents a density surface along the bottom layer. The isopycnal motions are estimated using equation 3.4 describing the motions of a density surface at the sea floor. Diffusion is ignored, because this equation follows the isopycnal surfaces instead of water parcels. The magnitude of isopycnal motion will be

$$u_I = \frac{|\frac{\partial \rho}{\partial t}|}{|\vec{\nabla} \rho|}. \tag{3.6}$$

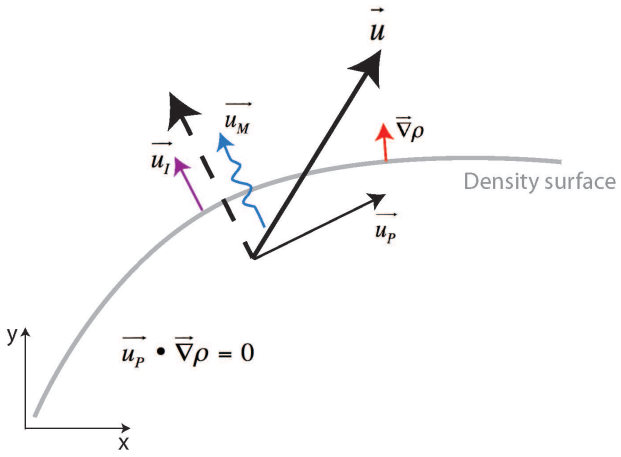

Figure 3.6: Sketch depicting flow along the bottom layer of the model. The gray line is a density surface, the thin black arrow represents current velocity along density surface, the blue arrow represents flow through density surface and the purple arrow represents density surface motion along the bottom.

The motion is perpendicular to the bottom density surface, and the direction of isopycnal motion depends on the sign of the $\frac{\partial \rho}{\partial t}$ term. Water motion along the bottom is calculated directly from the simulated current velocity in the bottom layer. Only the cross-isopycnal flow will advect or flow through the surface isopycnal, and the cross isopycnal component of water motion is obtained using

$$\vec{u}_c = \vec{u} \cdot \frac{\vec{\nabla}\rho}{|\vec{\nabla}\rho|}. \tag{3.7}$$

In this equation $\vec{u}_c$ represents the cross isopycnal component of water motion, and $\frac{\vec{\nabla}\rho}{|\vec{\nabla}\rho|}$ is the unit vector perpendicular to the isopycnal surface. The flow through density surface is obtained by subtracting the isopycnal motion along the bottom from cross isopycnal component of water motion

$$\vec{u}_M = \vec{u} \cdot \frac{\vec{\nabla}\rho}{|\vec{\nabla}\rho|} - \vec{u}_I. \tag{3.8}$$

Instead of the strength of mixing, our interest in this study is the convergence of the flow, relative to the density surfaces, which will then be

$$\xi = \vec{\nabla} \cdot (\vec{u}_c - \vec{u}_I). \tag{3.9}$$

Previous studies used different ways to detect convergent flow and the subsequent intrusion at the foot of the shelfbreak front in the Middle Atlantic Bight (Houghton, 1997; Houghton and Visbeck, 1998; Barth et al., 1998; Pickart, 2000). The measured intrusion into the front had an averaged velocity of 9±2 m day^{-}1 (Barth et al., 1998). However, the Middle Atlantic Bight shelfbreak front is a relatively stationary feature. In the northern Gulf, the temporal change of freshwater discharge alters the stratification structure and the location where the main pycnocline intersects the sea floor; wind forcing can also modify the distribution of buoyancy on the shelf, and shift the pycnocline. Furthermore, in summer, the land-sea breeze excites strong near-inertial flows with 24-h periodicity over the entire Texas-Louisiana shelf (Zhang et al., 2009). Combined, these factors lead to a very transient front over the Texas-Louisiana shelf; isopycnals are pushed on- and offshore, and bottom boundary layer convergence can occur along different isopycnals at various times and locations.

Since the distribution of convergence is patchy as described above, convergence properties in cartesian coordinates may be quite different even for transects in the same vicinity. This will make the interpretation of the convergence and a verification of the consistence of convergence and corresponding intrusion difficult. However, as described above, the intruding of low-oxygen bottom water is along certain isopycnals. A coordinate system that follows density coordinates and is less sensitive to the geographical location of the convergence is necessary and efficient to address these issues. By identifying regions of persistently convergent flow in a particular

range of isopycnals, regions where water is injected into the interior water column can be identified. The way we build a density coordinate is to bin the density field of an analyzed region, and then cast a calculated convergence field into the binned density space, weighted by the volume of each model grid cell. This metric considers the water mass structure of the convergence as a whole and identifies the isopycnals where convergence occurs.

The method described above was employed to estimate the convergence relative to isopycnals over the Texas-Louisiana shelf during June 2011. A region south of Atchafalaya Bay is analyzed (red polygon in the map of Figure 3.7); and then the calculated convergence is cast into a density coordinate. Note that the transect shown in Figure 3.5 is in this red region. Figure 3.7 is a time series of the convergent flow in density space; the time shown in Figure 3.5 is marked with a black arrow. Colors represent convergent or divergent flows; convergent flow implies a net gain of water along a specific isopycnal and divergent flow implies a net loss of water. A divergent flow is generated on June 9th along isopycnal 23 kg m^{-3}, and this divergence lasts for four days while it moves to fresher isopycnals. This divergent flow is bounded by two convergent flows. A time-averaged convergence field in density space clearly shows that the convergent flow is along frontal isopycnals and the divergent flows are along isopycnals underneath the front as well as above the front (Figure 3.8, Figure 3.5). At the time of the transect shown in Figure 3.5, as well as for the time average shown in Figure 3.8, convergence occurs along isopycnals 16.5 through 19 kg m^{-3}. This convergence range is slightly denser than what Figure 3.5 suggests, because of averaging over a large region instead of a single transect.

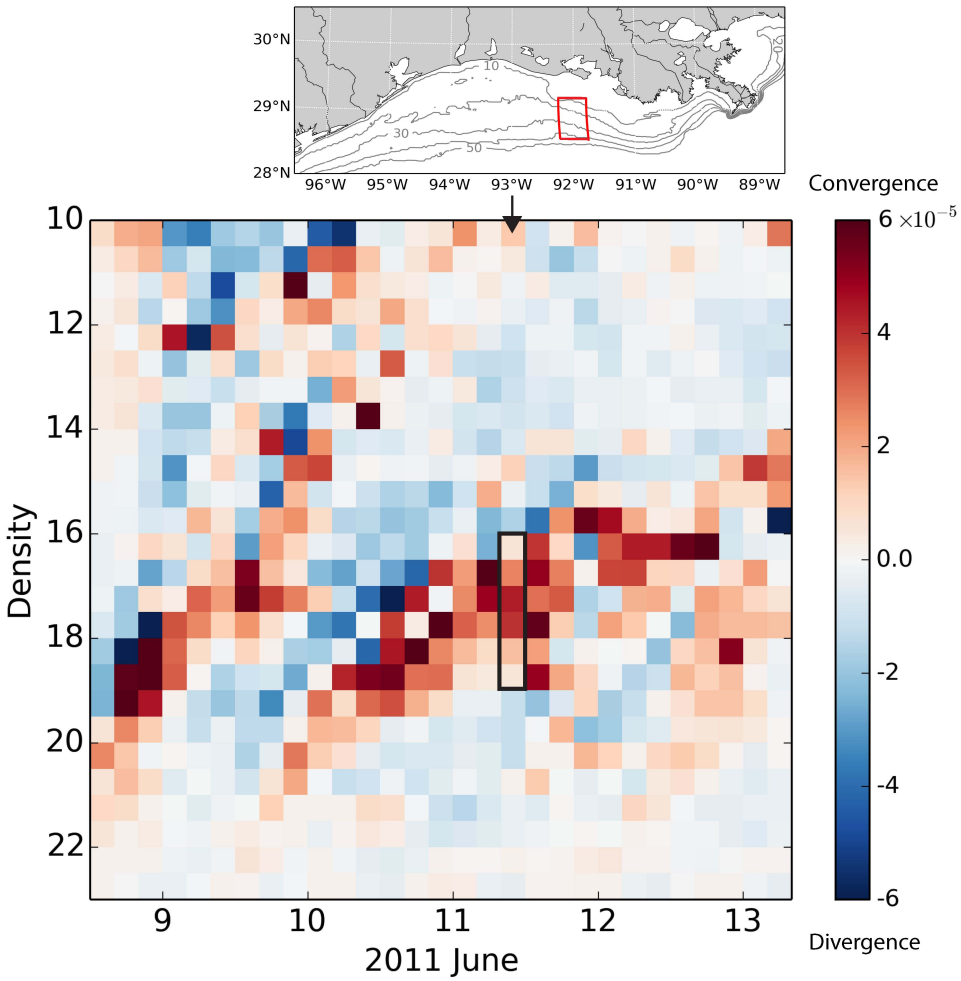

Figure 3.7: Time series of the convergence relative to isopycnals, cast in density space; the red polygon in the map denotes the analyzed region. The black arrow denotes the time step in Figure 3.5, and the black rectangle marks out the convergence range for that time step.

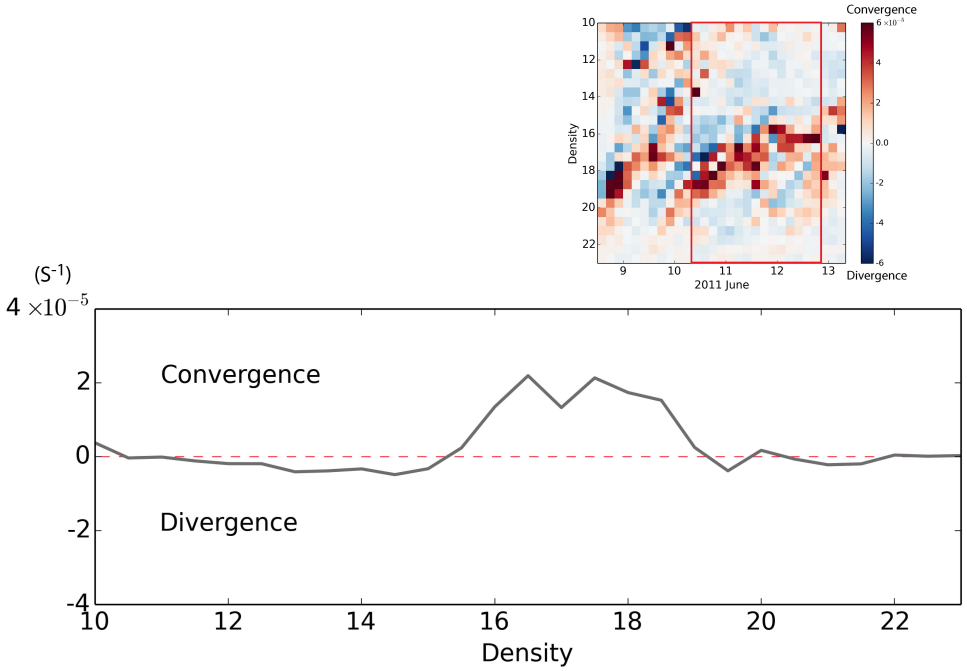

Figure 3.8: A 2.5 days average of the convergence in density coordinate, the averaged time period is denoted by the red rectangle.

3.6 Discussion

Mid-water oxygen minimum layers have often been observed during the eight shelf-wide survey cruises of the MCH program. Analysis of the water properties along these minima indicates that these low-oxygen layers are connected with the low dissolved oxygen bottom water through mixing of water masses. We also examined these mid-water oxygen minima in simulated results from a hydrodynamic model based on ROMS, which uses only benthic oxygen respiration (Zhang et al., 2012b). Similar mid-water oxygen minima are found in the model as in the observations. In the model the low-oxygen layer in the mid-water column must ultimately come from the bottom, as that is its only sink of oxygen. We also used the model to address the dynamical mechanisms of these mid-water low-oxygen layers. Convergent

flow at the bottom, relative to isopycnal surfaces, is strongest in the density classes associated with the oxygen minimum layer. These mid-water oxygen minima are actually intrusions of low oxygen protruding from the bottom boundary layer via buoyancy advection driven convergence, following the main pycnocline.

The temporal evolution of the convergent regions over the Texas-Louisiana shelf indicates that the formation and destruction of convergence is fast, typically lasting only a few days, most likely related to the transient nature of the near-shore frontal region that occurs in water less than 50 m (Hetland and DiMarco, 2008; Bianchi et al., 2010; DiMarco et al., 2010). Further offshore and further from the fresh water sources, convergence becomes weaker or even vanishes, due to the weakening of stratification associated with the Mississippi-Atchafalaya River plume system. The time series of convergence in Figure 3.7 shows two periods of convergence; the first occurs during June 9th-11th (3 days), the other during June 10th-13th (4 days).

The evolution of both convergences shown in Figure 3.7 indicates that the convergent flow first forms along denser isopycnals; the convergent zone moves to fresher isopycnals over time. The mid-water layer structure of properties is also described and supported by Houghton (1997), Houghton and Visbeck (1998), Barth et al. (1998), and Pickart (2000). Different from the convergent flow at the foot of the stationary front in the Middle Atlantic Bight (Houghton, 1997; Houghton and Visbeck, 1998; Barth et al., 1998; Pickart, 2000), this transient feature is unique for a river plume shelf. A convergence in the bottom boundary layer transport can form at the location where the arrest or reversal in the Ekman transport occurs, which is most likely the location where the front intersects the seafloor. The migrating convergent zone corresponds to the transient front over the Texas-Louisiana shelf. And the convergent zone stops moving to fresher isopycnals when the front is well developed and totally arrested. A one-day long stable convergence occurs along isopycnals 16.5

through 19 kg m^{-3}, facilitating the large low oxygen intrusion (Figure 3.5). After that the convergence becomes weaker and the intruding is halted.

The buoyancy-driven convergence in the bottom boundary layer and the corresponding intrusion are essential in forming the mid-water column low-oxygen layer. Hetland and DiMarco (2008) indicate that water column respiration could be important for the formation of hypoxia over the Texas-Louisiana shelf, especially for the region between the Mississippi River Delta and Terrebonne Bay. It is possible that this type of respiration could also contribute to the formation of the detected mid-water low oxygen layer, especially for the large main pycnocline bounded low oxygen layers. However, it seems unlikely that water column respiration would occur at significantly higher rates only in the main pycnocline. Also, low oxygen intrusions were observed in the hydrodynamic model, which ignores water column respiration.

3.7 Conclusions

We have investigated the dynamical mechanisms of the mid-water column dissolved oxygen minima that have been observed using high-resolution towed, undulating CTD profiles. The convergence relative to density surfaces calculated based on a hydrodynamic model results reveals that the mid-water low-oxygen layer is consistent with the bottom convergent flow and the corresponding intrusion of bottom water (Figure 3.5, Figure 3.7), demonstrating the existence of coastal intrusions driven by the near bottom convergence generated by the buoyancy flux within the bottom boundary layer over the Texas-Louisiana shelf.

The dynamical mechanism of the mid-layer, low-oxygen tongue is a convergent flow and the corresponding intrusion of bottom water produced by buoyancy flux via bottom Ekman transport. Downslope Ekman transport advects buoyant water offshore, and meanwhile concentrates near-bottom isopycnals and enhances lateral

density gradients, driving frontogenesis. The thermal wind adjustment within the bottom boundary layer, associated with an enhanced lateral density gradient at the foot of the front, leads to a reduction of along-shore flow near bottom, which can shut down the offshore Ekman transport at the foot of the front (Trowbridge and Lentz, 1991; MacCready and Rhines, 1993; Chapman and Lentz, 1997). The bottom boundary layer continues to transport buoyant water offshore, hence moves the entire front offshore, until eventually the vertical shear causes an arrest or reversal in the bottom Ekman transport across the entire base of the front, thus eliminating the offshore buoyancy advection in the bottom boundary layer. At this point, the density front is well developed and stops migrating offshore, and buoyancy advection is arrested. Thus, there will be a convergence formed at the location where the well-developed main pycnocline intersects the bottom.

The temporal evolution of the simulated low oxygen intrusion in Figure 3.5 reveals that the low oxygen shoals 8 m along the frontal isopycnals from the bottom in 20 hours, equivalent to an intrusion velocity of about 10 m day^{-1}, which is similar to what Houghton and Visbeck (1998) and Barth et al. (1998) suggested. The buoyancy advection in the bottom boundary layer is essential to the bottom boundary layer structure itself; meanwhile, the frontogenesis driven by this can alter the overlying flow field. Furthermore, the buoyancy advection in the bottom boundary layer has important implications for the concentration of material on the offshore side of the front and the biogeochemistry of the shelf; convergence generates intrusions of nutrients or other materials from the bottom.

4. CONVERGENT FLOW WITHIN THE BOTTOM LAYER AND A CORRESPONDING UPWARD BOTTOM MATERIAL FLUX: AN IDEALIZED STUDY

4.1 Overview

Buoyancy advection along a sloping, stratified bottom forces isopycnal distortions and sets up horizontal density gradient, thus frontogenesis. The near-bottom alongshore velocity, hence the bottom stress, within the front will eventually be brought to rest or reverse by means of the thermal wind shear resulting from the horizontal density gradient. A convergent flow can be generated at the location where the buoyancy transport vanishes or reverses, which is most likely the location where the front intersects the seafloor. This theory is revisited in this section, and a simple two-dimensional model is used to quantify the relationship between the convergent flow and a corresponding upward flux of bottom materials, water age is also introduced via activating two passive tracers to orientate the source of water masses. Cross-shore section of water age distributions indicate that the model reproduced the similar bottom water intrusions, and the size of intrusions are directly controlled by the strength of the convergent flow. A variety of initial stratification structures and Coriolis parameters are configured; the convergent flow along the bottom layer as well as the upward tracer flux through a reference plane above the bottom are computed using the model results. Slope parameter, $\delta = \alpha / \frac{M^2}{N^2}$, represents the slope of bathymetry compared to the slope of isopycnals with the bottom slope α, the horizontal stratification M^2 and the vertical stratification N^2. The upward flux of bottom material is found to change logarithmically with the convergent flow, and the upward tracer flux and the net tracer flux through the reference plane decrease

with increasing slope parameters logarithmically.

4.2 Introduction

An upward intrusion of bottom water properties along frontal isopycnals has been investigated previously in different regions (e.g., Houghton and Visbeck, 1998; Pickart, 2000). Houghton (1997), Houghton and Visbeck (1998), Barth et al. (1998) and Pickart (2000) used different methods to study the upwelling circulation at the foot of the shelfbreak front in the Middle Atlantic Bight, which is a stationary isopycnal front. Houghton (1997) and Houghton and Visbeck (1998) used a dye tracer injected into the bottom boundary layer, which was later found to have been injected up into the water column within the front. Barth et al. (1998) detected a mid-water region of suspended bottom material emanating from the foot of the front and extending upward to near-surface along frontal isopycnals. Subsequently, Pickart (2000) used a synoptic hydrographic section to find that the bottom water spread into the interior along an isopycnal layer abutting the front. In Section 3, we used towed, undulating CTD profiles and a three-dimensional hydrodynamic model to identify a mid-water column oxygen minima over the Texas-Louisiana shelf (Figure 4.1). The direct connection between low-oxygen water within the bottom boundary layer and that within the middle water layer shown in the T-S diagrams implies an intrusion of bottom low-oxygen water into the middle water column. Different from the shelfbreak front in the Middle Atlantic Bight, the buoyancy transport within the bottom boundary layer changes directions as well as magnitudes fast over the Texas-Louisiana shelf, resulting in transient fronts thus the intrusions of bottom water.

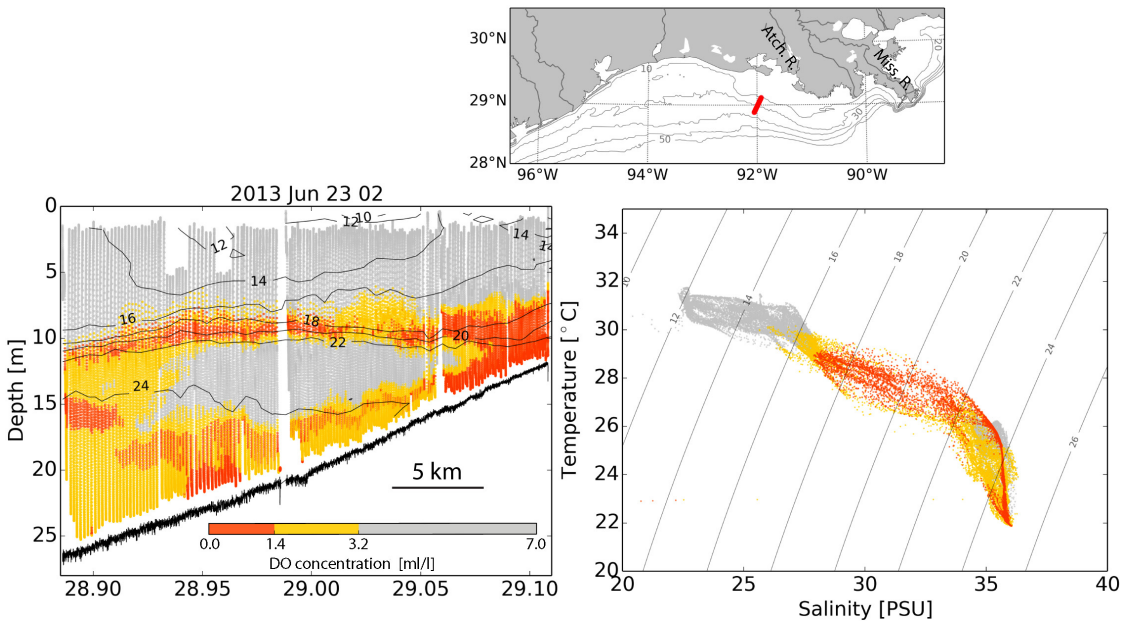

Figure 4.1: Left: cross-shore observed dissolved oxygen concentration, south of Atchafalaya Bay over the Texas-Louisiana shelf (red line in the map). Three colors are used to denote different dissolved oxygen conditions. Orange indicates hypoxia (DO<1.4 mL L^{-1}), yellow is defined as near-hypoxic, low-oxygen (1.4 mL L^{-1}<DO<3.2 mL L^{-1}) and gray is any oxygen concentration higher than 3.2 mL L^{-1}. Right: T-S diagram for the transect, the shading of the points is relative to oxygen concentration.

The dynamical mechanisms behind this bottom water intrusion are buoyancy advection within the bottom boundary layer and subsequent convergent flow generated at the location where the frontal isopycnals intersect the bottom. The cross-shore bottom Ekman transport and buoyancy arrest theory above a slopping, stratified bottom is well known (e.g., Lentz and Trowbridge, 1991; Chapman and Lentz, 1994; Yankovsky and Chapman, 1997; Brink and Lentz, 2010a). The bottom boundary layer is a near-bottom, thin, well-mixed layer known to exchange water with the interior water column in places where the pycnocline intersects the sea-floor (e.g., Houghton and Visbeck, 1998; Pickart, 2000). Along-shore flow gives rise to cross-

shore bottom Ekman transport, and therefore sets up lateral density gradient and forces frontogenesis over a sloping, stratified bottom. The lateral density gradient within the front acts, through thermal wind balance, to bring the along-shore velocity near the bottom toward rest or a reversal. Thus Ekman transport within the bottom boundary layer across the base of the front, which is driven by bottom stress associated with along-shore flow, will vanish or reverse. A convergence in the bottom boundary layer transport can form at the location where the arrest or reversal in the Ekman transport occurs, which is most likely the location where the front intersects the sea-floor (Chapman and Lentz, 1994; Houghton, 1997; Houghton and Visbeck, 1998).

This bottom water intrusion topic is revisited here using a simple two-dimensional model. In the model, water age is introduced by activating two passive tracers for near-bottom layer to track the paths of water masses. Configurations with different initial stratification conditions are executed (Table 4.1) and the primary goal of this section is to quantify the relationship between the convergent flow and bottom water intrusion and investigate how slope parameter influences bottom material fluxes.

Table 4.1: List of model runs with parameters. Bottom slope $\alpha = 0.001$, and Richardson number $Ri = 1.0$ for all the configurations.

Run No.	$N^2 \times 10^4$	$M^2 \times 10^6$	f $\times 10^4$	δ
1	1.80	0.9000	0.671	0.200
2	2.40	0.8000	0.516	0.300
3	3.09	0.6190	0.352	0.500
4	4.17	0.5000	0.245	0.830
5	4.00	0.4000	0.200	1.000
6	5.46	0.3500	0.150	1.532
7	4.60	0.2140	0.100	2.156
8	4.00	0.1000	0.050	4.000
9	6.45	0.0838	0.033	7.695

4.3 Methods

4.3.1 Water age

Water age can not be observed directly, and usually transient tracers are used in numerical models to infer water age, which generally suggests the elapsed time since the water was last in contact with the tracer source.

Water age is computed following Delhez et al. (1999), Deleersnijder et al. (2001), Delhez and Deleersnijder (2006) and Zhang et al. (2010). Assuming that the position vector of any point in the domain of interest reads $\mathbf{x} = (x, y, z)$. The equation governing the evolution of the age distribution function, $c(t, \mathbf{x}, \tau)$, of a water parcel

located at $\mathbf{x}$ at time t containing dissolved tracer is

$$\frac{\partial c}{\partial t} = p - d - \boldsymbol{\nabla} \cdot (\mathbf{u}c - \mathbf{K} \cdot \boldsymbol{\nabla} c) - \frac{\partial c}{\partial \tau} \tag{4.1}$$

where τ is the age (i.e., the time since the tracer was released into the water); p and d are the rates of production and destruction, respectively (i.e., the source and sink terms; in this section, these terms are zeros, with production effectively entering only at the bottom); $\mathbf{u}$ is the current velocity; and $\mathbf{K}$ is the eddy diffusivity tensor. The last term on the right-hand side is related to the aging of the tracer, i.e. the process by which the age of every water parcel tends to increase by a certain amount of time as time progresses by the same amount of time.

Assuming that the age is positive definite, the concentration of tracer in the fluid is

$$C(t, \mathbf{x}) = \int_0^\infty c(t, \mathbf{x}, \tau) d\tau \tag{4.2}$$

Then integrate Eq. 4.1 over τ, taking into account Eq. 4.2 and the common-sense boundary conditions, $\lim_{x \to \infty} c(t, \mathbf{x}, \tau) = 0$, to get the equation of the time rate of change of the total concentration of the tracer

$$\frac{\partial C}{\partial t} = P - D - \boldsymbol{\nabla} \cdot (\mathbf{u}C - \mathbf{K} \cdot \boldsymbol{\nabla} C), \tag{4.3}$$

with the source of tracer $P(t, \mathbf{x}) = c(t, \mathbf{x}, \tau = 0) + \int_0^\infty p(t, \mathbf{x}, \tau) d\tau$ and the sink $D(t, \mathbf{x}) = \int_0^\infty d(t, \mathbf{x}, \tau) d\tau$. Eq. 4.3 is the conservation equation solved in numerical circulation models.

The mean age $a(t, \mathbf{x})$ is given based on the definition of the age distribution function, $a(t, \mathbf{x}) = \frac{1}{C(t, \mathbf{x})} \int_0^\infty \tau c(t, \mathbf{x}, \tau) d\tau$. An age concentration tracer, $\alpha(t, \mathbf{x})$, is

defined as

$$\alpha(t, \mathbf{x}) = C(t, \mathbf{x})a(t, \mathbf{x}), \tag{4.4}$$

and we reasonably assume that the age distribution function verifies $\lim_{x\to 0} \tau c(t, \mathbf{x}, \tau) = 0 = \lim_{x\to\infty} \tau c(t, \mathbf{x}, \tau)$. Then, multiplying Eq. 4.1 by τ, integrating over τ, we obtain the age concentration equation

$$\frac{\partial \alpha}{\partial t} = C + \pi - \delta - \boldsymbol{\nabla} \cdot (\mathbf{u}\alpha - \mathbf{K} \cdot \boldsymbol{\nabla}\alpha), \tag{4.5}$$

with $\pi(t, \mathbf{x}) = \int_0^\infty \tau p(t, \mathbf{x}, \tau) d\tau$ and $\delta(t, \mathbf{x}) = \int_0^\infty \tau d(t, \mathbf{x}, \tau) d\tau$. So the age concentration α satisfies an equation similar to that governing the evolution of the concentration of tracer. As the independent variable τ will rarely be used, for simplicity, to call the variable a the 'age' rather than the 'mean age', which will be the 'water age' in this section.

4.3.2 Nondimensional parameters

Stratification refers to the strength of the density gradient, and buoyancy is directly related to water stratification. Start with the inviscid, Boussinesq equation of vertical-momentum $B = -\frac{p_z}{\rho_0}$, where $B = g(\rho_0 - \rho)/\rho_0$ is the buoyancy. So that, vertical stratification is defined as $N^2 = B_z$; and horizontal stratification is defined as $M^2 = B_y$ if assuming no along-shore (x direction) density gradient.

Two important nondimensional parameters based on vertical and horizontal stratification are used in this section. First will be the Richardson number

$$Ri = \frac{N^2}{(u_z)^2} = \frac{N^2 f^2}{M^4}, \tag{4.6}$$

where u_z is the vertical gradient of along-shore flow and f is the Coriolis parameter.

And the second one is the slope parameter (Blumsack and Gierasch, 1972)

$$\delta = s\sqrt{Ri} = \frac{\alpha N}{f}\frac{Nf}{M^2} = \frac{\alpha}{\frac{M^2}{N^2}} = \frac{\text{Bottom slope}}{\text{Isopycnal slope}}, \tag{4.7}$$

where $s = \frac{\alpha N}{f}$ is the slope Burger number, measuring the important of bottom slope α.

4.4 Model description

We set up a simple two-dimensional model using the Regional Ocean Modeling System (ROMS; available online at http://www.myroms.org) here. The ocean (Figure 4.2) has 30 vertical layers, with a minimum water depth of 5 m (h_0) at the coast and lying above a sloping bottom at $H = h_0 + \alpha y$. The bottom slope, $\alpha = 0.001$, is uniform everywhere in the model domain. The horizontal resolution is 1 km, and the domain size is 130 km in the along-shore direction and 130 km in the cross-shore direction. The model is an reentrant domain with periodic along-shore boundaries, closed coastal and open offshore boundaries. The three-dimensional variables for the offshore open boundary condition use a simple no-gradient condition. Sea surface height and barotropic currents use a Chapman/Flather combination (Chapman, 1985; Flather, 1976).

The initial configuration of the tracer fields for a standard case are shown in Figure 4.2. The ocean has a constant, horizontally uniform initial vertical stratification which is controlled only by temperature throughout the domain. Inshore of 50 km, the ocean has a constant initial horizontal stratification controlled only by salinity. Horizontal and vertical stratification are conservative through a linear equation of state

$$\rho = 1027.0 \times (1.0 + 7.6 \times 10^{-4}(S - 35.0) - 1.7 \times 10^{-4}(T - 25.0)) \tag{4.8}$$

so that the horizontal and vertical density gradient can be explicitly formed through the combination of horizontal (salinity) and vertical stratification (temperature) (see Figure 4.2). The ocean is initially at rest and has no other forcing with potential energy anomaly the only forcing in the system. As a convenient measure, the potential energy anomaly is the amount of mechanical energy required to instantaneously homogenize the water column with a given density stratification (Simpson, 1981; Burchard and Hofmeister, 2008; De Boer et al., 2008). Table 4.1 lists the configurations with necessary parameters arise from this section.

To simulate the age of water in the model domain, two tracers are activated in the ROMS model with zero initial concentrations. The first is conservative and satisfies Eq. 4.3 with unit concentration (per m^3) at the bottom layer, whereas the second represents the water age concentration and satisfies Eq. 4.5. The water age concentration is zero at the bottom, and the water age is computed with Eq. 4.4. Regions where the first tracer concentration is lower than 10^{-4} are assumed to be free of bottom water, and the age there is undefined.

4.5 Standard case

Table 4.1 lists 9 model runs, the Richardson numbers of which are the same, and run 5 is the standard case. Figure 4.2 shows the model domain as well as the initial condition of the standard case. Potential energy will be released and isopycnals will start to distort and force buoyancy advection along the bottom once the model starts.

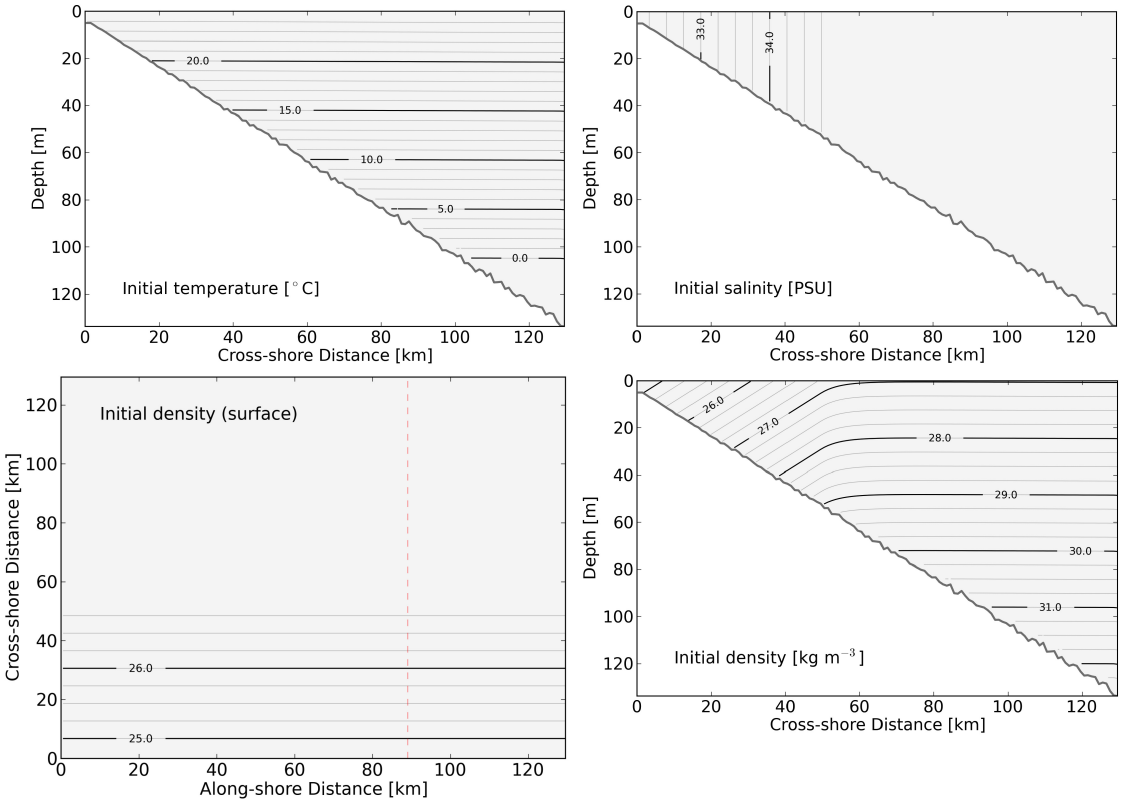

Figure 4.2: The model domain and initial conditions for the standard case.

A vertical cross section (the red dashed line in the plan view of initial density in Figure 4.2) of simulated water age at day 8 is shown in Figure 4.3. The age at the blank regions are undefined since the tracer concentration is lower than 10^{-4} there. The water age at the bottom is zero as the model designed. The same features of properties of water in the middle water column as previous studies (Houghton and Visbeck, 1998; Barth et al., 1998; Pickart, 2000) detected are reproduced. The bottom water is injected upward along frontal isopycnals, and two low-age (lower than three days) bottom water intrusions penetrate the bottom boundary layer and are formed. The bottom boundary layer here is defined as the layer in which the density change is less than 0.5 kg m^{-3} from the bottom.

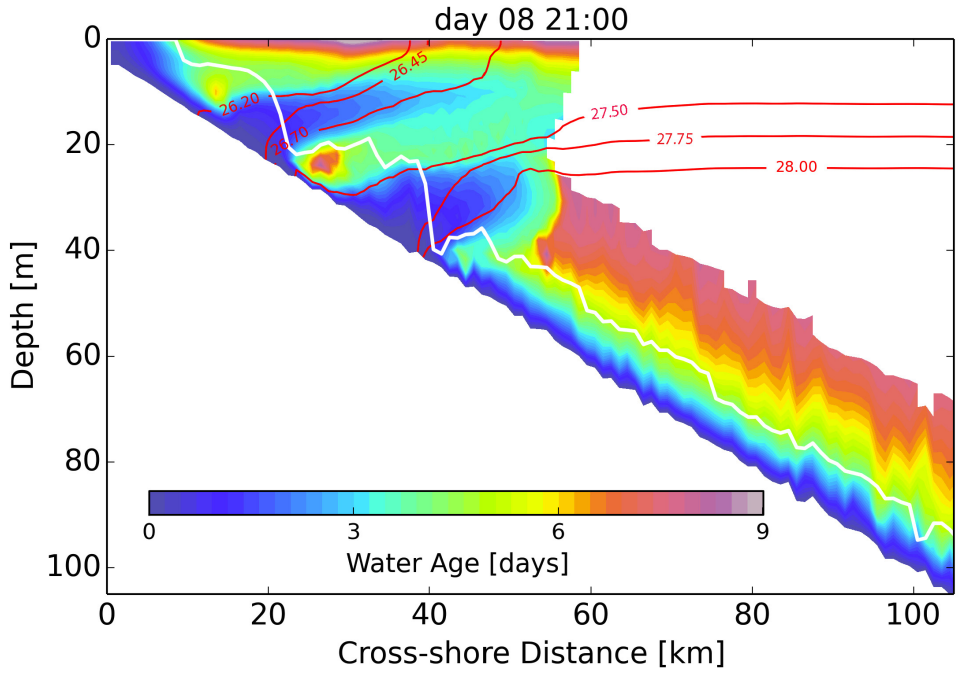

Figure 4.3: Cross-shore section of simulated water age at day 8 from standard case, the transect is denoted by the red dashed line as shown in Figure 4.2. The white line represents the top of the bottom boundary layer, and the red lines are isopycnal contours.

To examine these low-age water intrusions within the whole model domain, a histogram of water age weighted by the volume of each model grid cell in density space is introduced in Figure 4.4. All the low-age waters underneath the bottom boundary layer (see Figure 4.3) are excluded in the histogram to ensure that all the low-age waters shown are from the intrusions in the interior. There are three main patches of large-volume water mass. The first is the high-age, high-density water mass occupying isocpycnals 28 through 31.5 kg m^{-3} and age of 5 through 8 days. This indicates high-age waters underneath isopycnal 28 kg m^{-3} like Figure 4.3 shows. The other two are low-age waters along ispycnals 26.2 through 27 kg m^{-3} and 27.5 through 28 kg m^{-3}, respectively. These waters imply the existence of bottom low-age

water extensions in the interior, demonstrating the intrusions of low-age water. The consistence between Figure 4.3 and Figure 4.4 indicates that the two bottom low-age water intrusions along frontal isopycnals are common features in the whole model domain.

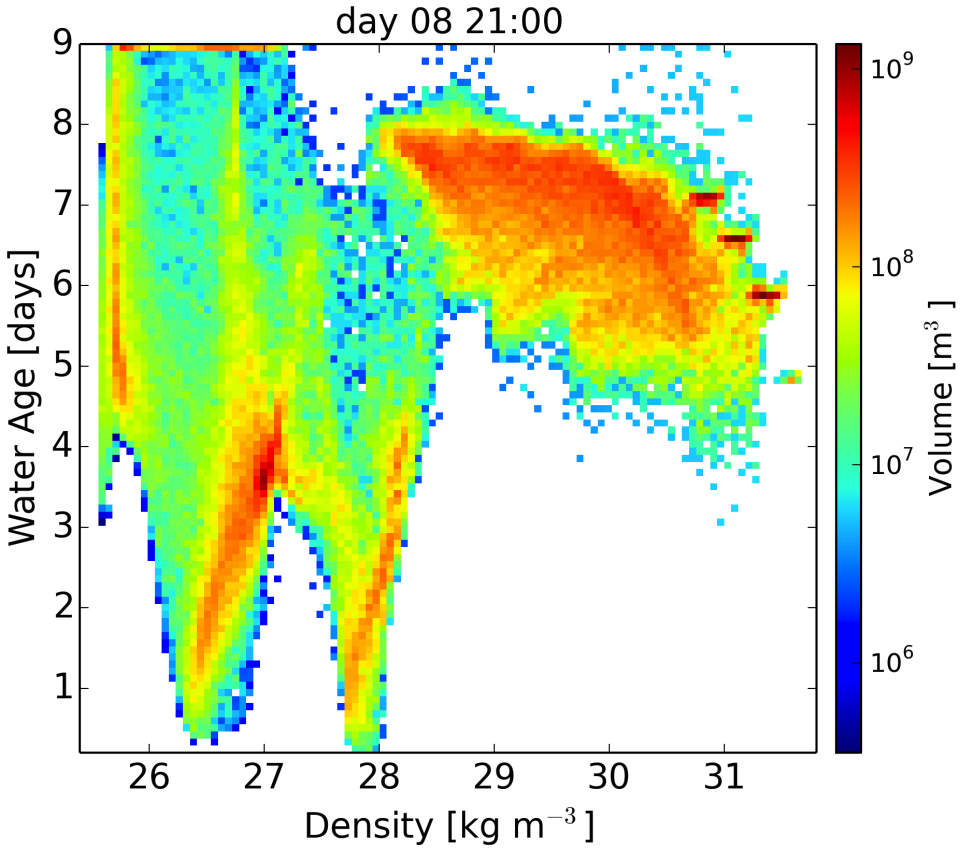

Figure 4.4: The histogram of water age in density space for the whole model domain, weighted by the volume of each grid cell (standard case). This is the same time as shown in Figure 4.3. All the waters underneath the bottom boundary layer are excluded with all the low-age water only come from the intrusions of bottom water penetrating the bottom boundary layer.

Following Section 3, the convergence along the bottom layer is computed for the whole model domain and then cast into a density coordinate (Figure 4.5). The way

we build a density coordinate is to bin the density field of an analyzed region, and then cast a computed convergence into the binned density space, weighted by the area of each model grid point. This metric considers the water mass structure of the convergence as a whole and identifies the isopycnals where convergence occurs. Red represents convergence, indicating a net gain of water along the isopycnal; while blue represents divergence, indicating a net loss of water. There are two main convergence formed, separated by a narrow divergence. The first convergence starts to form and strengthens at day 2, and the temporal evolution of water age indicates that an intrusion driven by the convergent flow starts to extend upward along frontal isopycnals two days later. The second convergence starts to form at day 4, and a corresponding intrusion also starts around two days later. Figure 4.5 suggests that these two convergence both migrate to fresher isopycnals slightly over time.

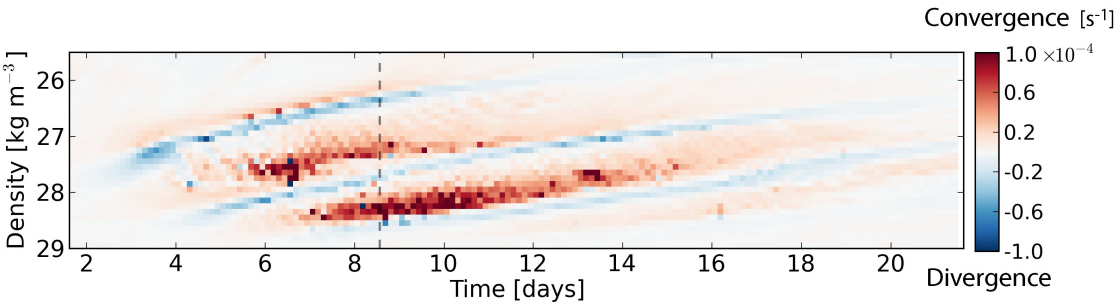

Figure 4.5: The time series of convergent flow in density coordinates for standard case. Red represents convergence, indicating a net gain of water; blue represents divergence, indicating a net loss of water.

Upward tracer flux through a reference plane is computed to quantify the strength of the intrusions within the model domain. Figure 4.3 indicates that the intrusion injects the tracer along frontal isopycnals into the interior otherwise the tracer is confined underneath the bottom boundary layer within an average of 5 m above the bottom. So it is reasonable to assume that all the tracer fluxes above the bottom boundary layer are caused by the intrusions. Net flux, net flux of the upward flux due to convergence and downward flux due to divergence, through the reference plane is also computed. Figure 4.6 (a) shows a cross section of the simulated density field with cross-shore vs. scaled vertical current velocity ($\times 10^3$) quivers (the same time as Figure 4.3), and the velocity field suggests convergent flows at the foot of the frontal isopycnals. The distance between the bottom and the reference plane A is δh, and the upward tracer flux through plane A is computed from $F = \int_A \mathbf{w}C \cdot d\mathbf{A}$. Figure 4.6 (b) shows the upward tracer flux and net flux with different values of δh, which both peak at around 4 m above the bottom.

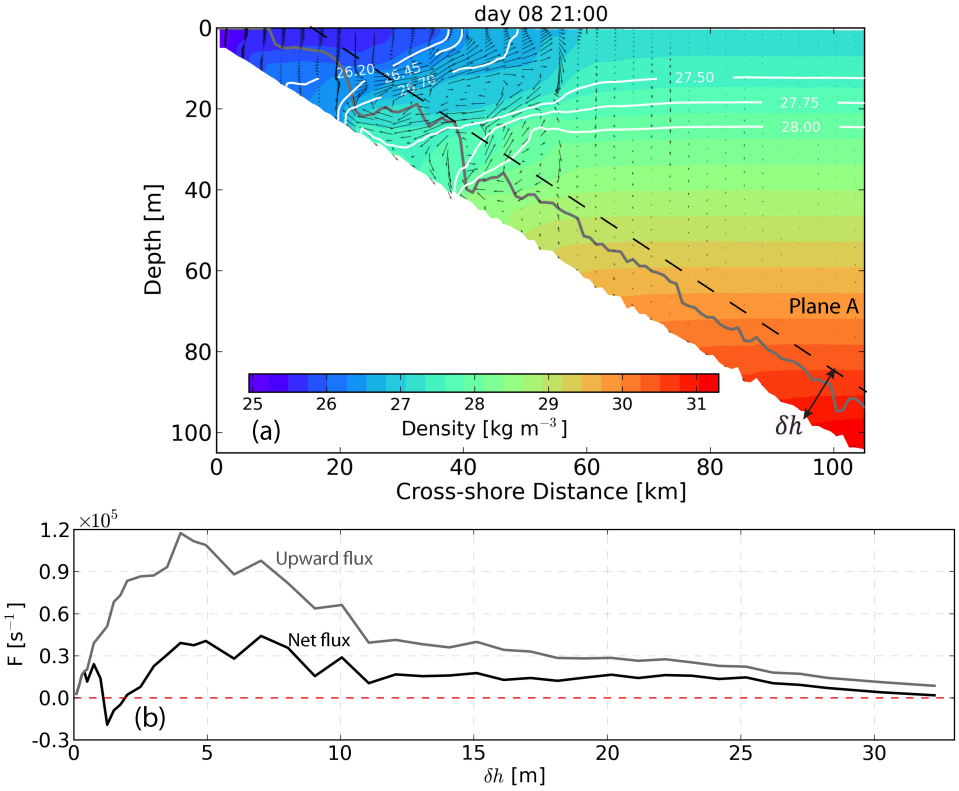

Figure 4.6: (a). cross-shore section of simulated density distribution with velocity field overlaid for standard case, the same transect and the same time as shown in Figure 4.3. The gray line represent the top of the bottom boundary layer and the white lines are the same isopycnal contours as shown in Figure 4.3. The black dashed line is a reference plane and δh is the distance between the bottom and the plane A; (b). the upward flux (gray line) and the net flux (black line) through plane A in relation to δh.

4.6 Case comparisons and discussions

A list of model runs with different initial stratification conditions are configured (Table 4.1) to examine how slope parameter influences the convergent flow and a corresponding intrusions and quantify the relationship between convergent flow and upward flux of bottom water. Slope parameter represents the slope of the bathymetry compared to the slope of the isopycnals. The slope of bathymetry is

constant throughout the configurations, thus the bigger the slope parameter, the smaller the slope of isopycnals and the closer the total stratification structure to a horizontally homogenous stratification. Buoyancy advection along the bottom can be excited via distorting isopycnals along the bottom through releasing the tilted isopycnals from the initial conditions, resulting in convergence/divergence.

Convergent flows are computed and cast into density coordinates following the same method. The convergence/divergence ξ scales substantially as $\frac{U}{L}$, where U is the horizontal velocity scale and L is the horizontal length scale; and $U \sim \frac{M^2 H}{f}$ according to thermal wind balance, where H is the vertical length scale. Thus $\xi \sim \frac{M^2 H}{fL} = A\frac{M^2}{f}$ with a constant $A = \frac{H}{L}$, indicating that the convergence/divergence is proportional to the ratio of initial horizontal stratification and Coriolis parameter. The initial horizontal stratification and Coriolis parameter take a variety of values among different cases, to compare different cases, the convergent/divergent flows are normalized by initial M^2/f. Figure 4.7 shows the time series of normalized convergent/divergent flow (ξ^*) in density space for all the model runs. For small slope parameter cases, such as model runs 1 and 2, the convergence is chaotic and relatively strong during most of the time. The convergence becomes more organized with increasing slope parameters, however, the convergence becomes extremely weak while the slope parameter is large, such as model runs 7 through 9.

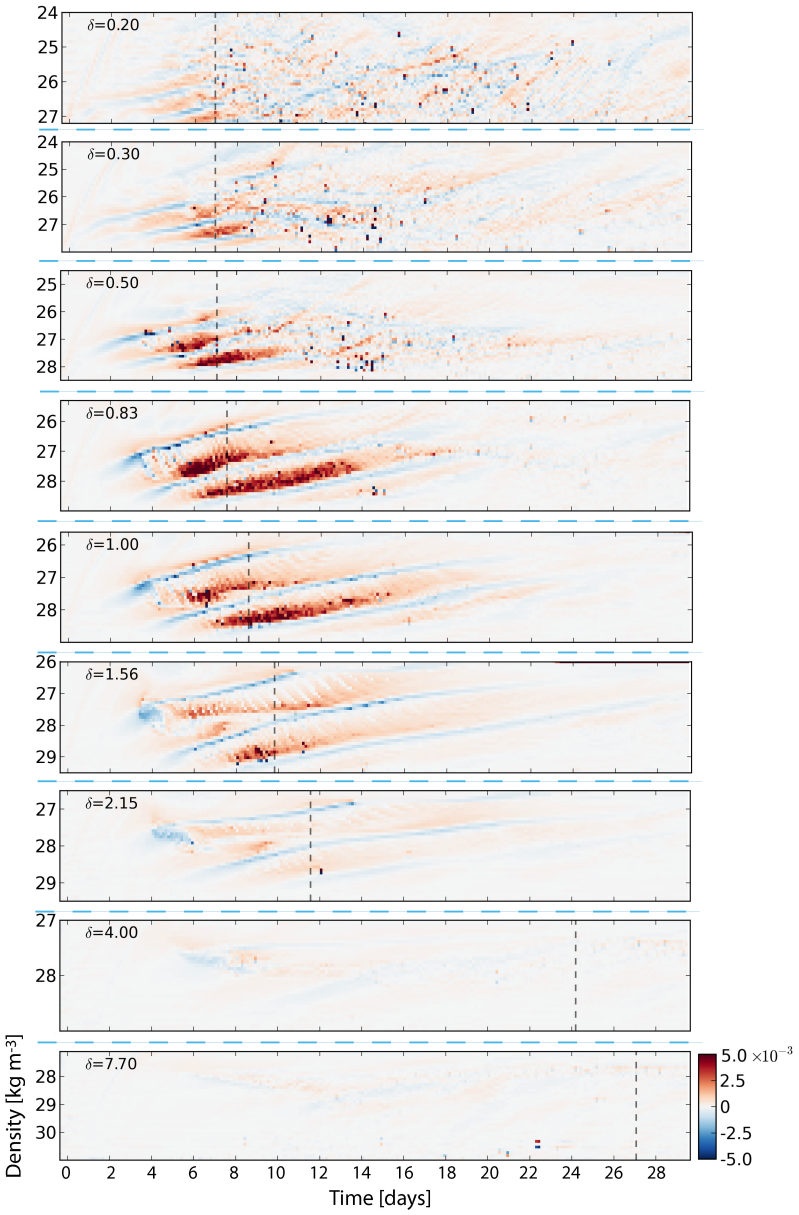

Figure 4.7: The same information as presented in Figure 4.5 for all the model runs. To compare different cases, the convergent flows are normalized by initial M^2/f. The black dashed lines denote the maximum intrusions for different cases.

Figure 4.7 implies that the strength of convergent flow decreases with increasing slope parameter significantly. Under small slope parameters, strong distortions of

isopycnals and buoyancy transport along the bottom are excited, resulting in motions of isopycnals themselves and frontogenesis near the bottom. Intense mixing occurs along frontal isopycnals, and previous studies define this mixing as the buoyancy and momentum transport across isopycnal surfaces (i.e., convergence here) in estuarine and coastal regions (Sherman et al., 1978; Ivey et al., 2008; Stacey et al., 2011; Horner-Devine et al., 2015). Thus, cross-isopycnal motions will also be resulted from the distortion of isopycnals, especially for strong buoyancy advection cases. Under large slope parameters, relatively flat slope of isopycnals gives rise to weak distortions of isopycnals, suggesting that mixing, thus cross-isopycnal motion, at the bottom layer is inhibited.

The temporal evolutions of water age indicate that the temporal and spacial features of bottom water intrusions among model runs are different. Runs 1 through 3 are energetic, and intrusions of bottom water are generated only within 2 days after the model runs start. Multiple large intrusions can be generated under such conditions and they are all extremely transient (along variable isopycnals), which is consistent with the chaotic convergent flow (Figure 4.7). These intrusions are transitory (several hours usually); old intrusions are halted and new ones are generated randomly within 50 km inshore. Intrusions of bottom water under runs 4 and 5 are also formed fast, at day 4, however, those intrusions are relatively stationary. Once an intrusion is generated and reaches its maxima, it can last for around 10 days till the convergent flow that is supporting this intrusion is too weak. It takes longer for large slope parameter cases to generate an intrusion and reach its maxima; the black dashed lines in Figure 4.7 denote the occurrence of the maximum intrusions. Figure 4.8 shows the maximum intrusions for different cases; the white lines are the contour lines of water age equals 3 days. Large convergent flows result in large bottom water intrusions and *vise versa*.

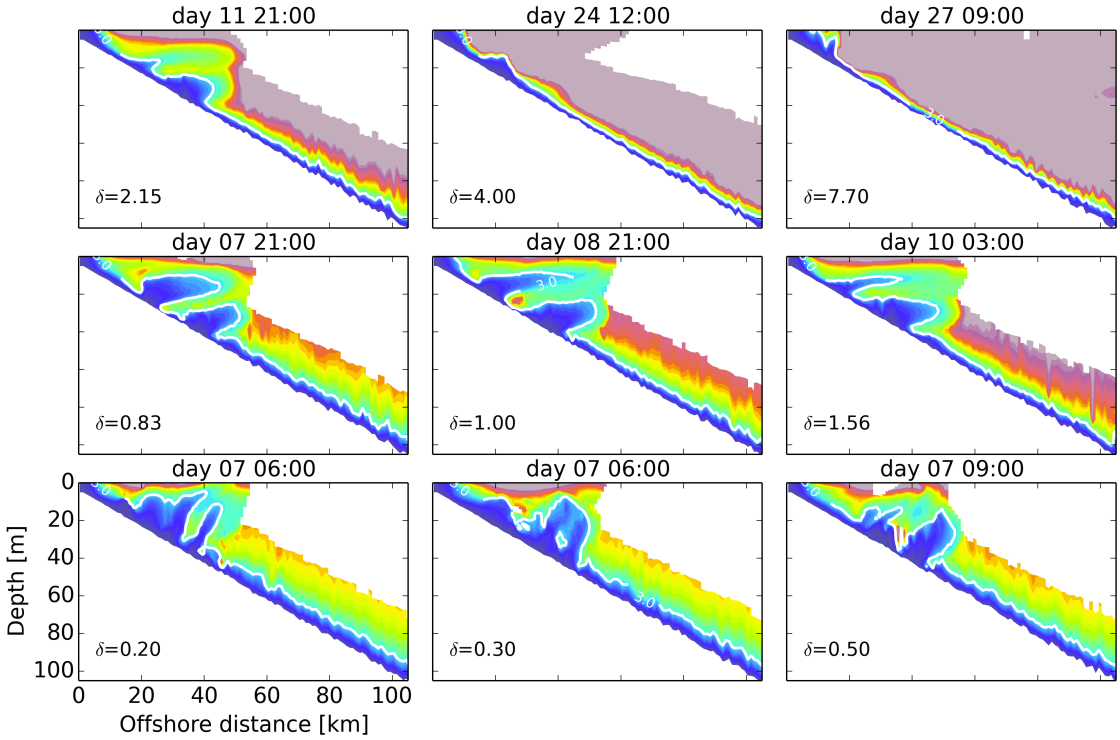

Figure 4.8: Cross-shore sections of simulated water age at the maximum intrusion time steps (see the black dashed lines in Figure 4.7). The white lines are the water age contours of three days.

The consistence between convergent flow and water age suggests a direct connection between the convergent flow and upward flux of bottom tracer (bottom materials). Other than casting the computed convergent flow into density space, the convergent flow in Cartesian coordinates is used to investigate the relationship between the convergent flow and the upward tracer flux. Integrating the convergent flow (positive values in convergence/divergence) within the domain to get the total convergence ξ_{sum}, which causes the integrated upward tracer flux F through a reference plane. According to scales analysis, the upward flux is also proportional to the ratio of initial horizontal stratification and Coriolis parameter. To compare different cases, both the upward tracer flux and total convergent flow are normalized

by the initial M^2/f, and the flux is averaged in relation to δh for each time step. Figure 4.9 shows normalized total convergent flow (ξ^*_{sum}) vs. averaged upward tracer flux (F^*_{ave}) on logarithmic scales for all the cases; each point represents one time step and the shadings of the points are relative to slope parameters. The black line is the regression curve, which indicates that upward tracer flux (F^*_{ave}) is proportional to $(\xi^*_{sum})^{1.29}$.

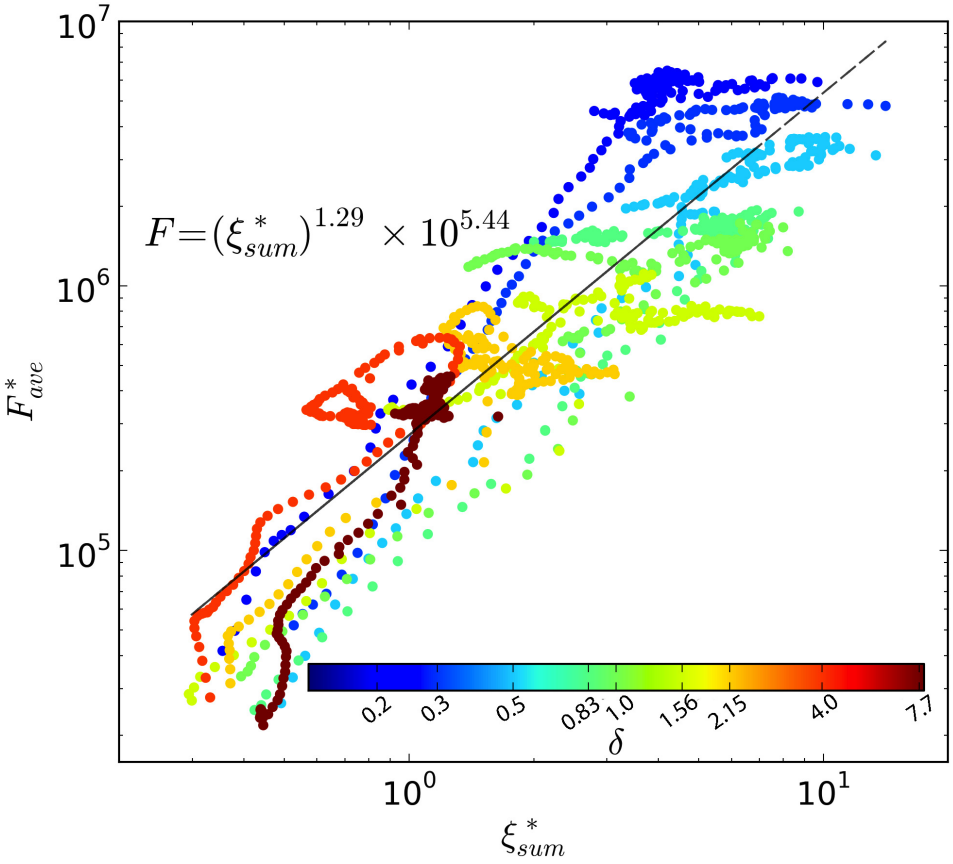

Figure 4.9: Normalized total convergent flow vs. normalized upward trace flux on logarithmic scales, the shading of the points are relative to slope parameter values. The black line is the linear regression line for $log(\xi^*_{sum})$ and $log(F^*_{ave})$.

The simulated results imply that upward tracer flux increases linearly with total

convergent flow on logarithmic scales (Figure 4.9). Chapman and Lentz (1994) released buoyant particles into the freshwater inflow at different alongshore locations and 1.36 m above the bottom after the isopycnal front was well developed in a numerical study. Some of these remained in the bottom boundary layer until they approached the shoreward edge of the front and were carried vertically upward along frontal isopycnals into the along-shore jet. Subsequently, a convergent flow at the foot of the shelfbreak front and the corresponding upwelling circulation within the front in the Middle Atlantic Bight were detected using a dye tracer injected into the bottom boundary layer (Houghton, 1997; Houghton and Visbeck, 1998). The dye was later found to have been injected into the water column within the front. A mid-water region of suspended bottom material emanating from the foot of the front and extending to within 35 m of the surface, 80 m above bottom was also observed within the front in the Middle Atlantic Bight (Barth et al., 1998). Mid-water column oxygen minima was identified to be related to the convergent flow near Mississippi and Atchafalaya River plumes over the Texas-Louisiana shelf region (Section 3). Previous studies all suggested a direct connection between the existence of a convergent flow at the foot of the front region and a corresponding upwelling of bottom materials. Figure 4.9 is in agreement with previous studies, furthermore it quantifies the convergent flow and bottom tracer flux mathematically based on results of the simple two-dimensional model.

Upward tracer fluxes and net fluxes are compared in relation to slope parameters to examine the influence of slope parameter on upward bottom material flux. The normalized flux (i.e., upward flux or net flux) is averaged in relation to δ for each time step, and the maximum flux is selected via selecting the maximum value of the averaged flux. Figure 4.10 (a) shows slope parameter vs. the normalized maximum flux on logarithmic scales while Figure 4.10 b shows slope parameter vs.

the normalized maximum net flux on logarithmic scale; both decrease with increasing slope parameter linearly. Smaller slope parameters give rise to larger maximum fluxes and *vise versa* (Figure 4.10). Smaller parameters result in intense mixing along frontal isopycnals at the foot of the front, leading to strong flows through isopycnal surfaces, thus convergent flows. The convergent flow has a direct connection with bottom water intrusion and will be balanced via upward fluxes.

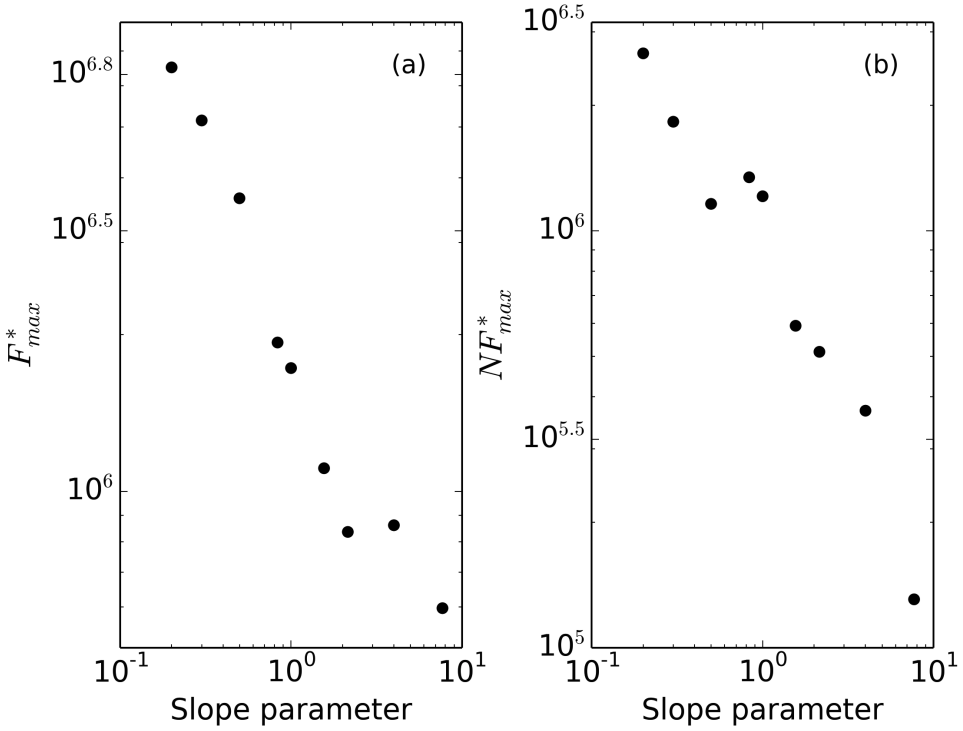

Figure 4.10: (a). slope parameter vs. the maximum upward tracer flux; (b). slope parameter vs. the maximum net tracer flux. These are all on logarithmic scales.

4.7 Summary

A convergent flow and the corresponding intrusions are investigated using a simple two-dimensional model, and the similar intrusions as previous studies (e.g., Houghton

and Visbeck, 1998; Barth et al., 1998) detected are reproduced. Water age is introduced to represent the elapsed time since the water was last in contact with the tracer source, thus the bottom water. The location of convergence and upward extensions of bottom waters are denoted by low-age waters. Mixing represents the buoyancy transport through isopycnals in coastal and estuarine regions (Sherman et al., 1978; Ivey et al., 2008; Stacey et al., 2011; Horner-Devine et al., 2015), instead of quantifying mixing, the convergence of velocity field along the bottom layer is computed following the method described in Section 3.

A variety of initial stratification and Coriolis parameter are used in the model to examine the influence of slope parameter on the convergent flow and corresponding flux of bottom tracer through a reference plane above the bottom. In agreement with the previous studies (Houghton, 1997; Houghton and Visbeck, 1998; Barth et al., 1998; Pickart, 2000), this section proved mathematically that the upward bottom material flux is directly connected with the convergent flow, which is driven by buoyancy advection along the bottom. Small slope parameter cases are extremely energetic and give rise to large, transient intrusions; intrusions become more stationary while slope parameter increases, and convergent flow becomes extremely weak and intrusions are rarely generated under large slope parameters (larger than 2), see Figure 4.8 for details. The simulated results indicate that the bottom material flux decreases linearly with increasing slope parameter on logarithmic scales (Figure 4.10).

The buoyancy advection driven convergence in the bottom boundary layer generates intrusions of nutrients or other materials from the bottom, it has important implications for the concentration of material on the offshore side of the front and the biogeochemistry of the shelf. Over a sloping, stratified shelf, buoyancy advection along the bottom layer is significant, such as the Texas-Louisiana shelf, especially the Mississippi and Atchafalaya River plumes regions. Thus, those buoyancy advection

related processes is essential for the shelf biogeophysical dynamics. According the Figure 4.9, the upward flux of bottom material can be estimated via computing the convergence/divergence of the interested regions. The combination of bathymetry and the stratification structure controls the amount of bottom material fluxes. Applying these methods to realistic shelves can provide important informations for other biogeochemical studies.

5. CONCLUSIONS

The Texas-Louisiana shelf has unique coastal dynamics because of the combination of seasonal wind signal, freshwater discharge from the Mississippi and Atchafalaya Rivers and strong inertial oscillation during summer. Strong stratification established during summer and subsequently well-developed thin bottom boundary layer inhibit oxygen exchange between bottom water and water atop the bottom boundary layer, facilitating bottom hypoxia formation and maintenance. In addition to this bottom hypoxia, strong signals of inertial oscillation combine with wind modified freshwater distribution result in transient freshwater front, leading to significant bottom boundary layer dynamics. The bottom boundary layer dynamics is essential for other physical and biochemical processes. Both observations and numerical modeling are used to study the dynamics over the Texas-Louisiana shelf in this dissertation.

The models' skill of reproducing the observed stratification were evaluated using six-years' CTD profiles collected during MCH program. Over a sloping, stratified shelf, stratification structures are of importance for shelf dynamics; stratification controls bottom hypoxia formation and destruction, and it forces buoyancy distribution over the shelf. It is necessary and important to evaluate a hydrodynamic model's ability to reproduce observed stratification. Previous study (Belabbassi, 2006) used the maximum value of observed vertical stratification to investigate bottom hypoxia, and direct connections between the maximum vertical stratification and low dissolved oxygen concentration were found. However, the significantly unpredictable, nonlinear noise associated with baroclinic instabilities along the river plume fronts can alter the location of the front or the magnitude of the shear. Those processes limit the

maximum possible skill for model predictions. According to point-by-point comparisons of maximum vertical stratification, even the models which already proved to be able to predict observed hypoxic area reasonably give a poor result. Histograms of vertical stratification, a bulk metric that integrate over the entire model state, is more robust to assess the ability of the model to reproduce observed stratification. Using this method, both the TXLA model and the MCH model reproduced the observed stratification successfully. The TXLA model is the best among all the models with unbiased stratification difference, which three MCH configurations biased to underestimated side slightly. Histogram of vertical stratification is an efficient metric to evaluate hydrodynamic model's ability of reproducing observed stratification, and can be applied to any shelf easily.

Beside the vertical stratification itself, bottom boundary layer is also of importance for the formation and maintenance of bottom hypoxia over the Texas-Louisiana shelf. Strong vertical stratification provides a necessary pre-conditioning for a well-developed, thin bottom boundary layer to form. The top of the bottom boundary layer can be considered as a secondary pycnocline of the water column and acts as a barrier to inhibit exchange of oxygen between bottom boundary layer and the water above, maintaining bottom low dissolved oxygen.

In additional to the bottom hypoxia, transects of high-resolution towed, undulating CTD profiles collected during MCH program also detected mid-water column low dissolved oxygen layer bounded by the frontal isopycnals. The TXLA model is used to investigate the dynamical mechanisms behind those mid-water oxygen minima. With bottom sediment demand the only oxygen sink of the system, the low-oxygen water layer in the middle water column much be advected from the bottom. Buoyancy advection driven by bottom Ekman transport causes the distortion of isopycnals, resulting in frontogenesis. Intense mixing can occur along frontal isopycnals

and lead to flows through density surfaces. Rather than quantifying the complicated turbulent mixing, convergent flow along the bottom layer is computed and cast into a density coordinates, proving the mid-water oxygen minima an intrusion of bottom low-oxygen water. Strong horizontal density gradient within the front acts to bring the near-bottom along-shore velocity, hence the bottom stress, to rest. A convergence will be generated at the location where the frontal isopycnals intersects the seafloor. Different from the stationary upwelling circulation at the foot of the front in the Middle Atlantic Bight, the direction as well as the magnitude of the buoyancy advection along the bottom changes frequently because of the unique dynamics over the Texas-Louisiana shelf, resulting in transient intrusions of bottom waters.

To better understand the convergent flow along the bottom and those corresponding intrusions of bottom water, a simple two-dimensional model is set up in chapter four. Two passive tracers were activated at the bottom layer of the model to calculate water age, which represents the elapsed time since the water was last in contact with the bottom. The intrusions of bottom water are reproduced in the configurations, and the same method as chapter three was used to calculate the convergent flow of the bottom layer. The cross-shore water age distribution implied that the bottom tracer is injected along the frontal isopycnals into the middle water column otherwise it will be confined within the bottom boundary layer. Thus the upward tracer flux through a reference plane was calculated to represent the strength of the intrusion. The upward flux of bottom tracer was found to change logarithmically with the convergent flow, and the flux increases linearly with increasing convergent flow on logarithmic scales. Applying the convergent flow to realistic shelves, the upward flux of bottom materials can be easily estimated. Slope parameter, the slope of bathymetry compared to the slope of isopycnals, also has influence on upward bottom material fluxes. The smaller the slope parameter the larger the maximum

upward and net flux of bottom material will be and *vise versa*.

All of above, it is essential for a hydrodynamic model to reasonably reproduce the shelf stratification for other physical and biogeochemical processes over the Texas-Louisiana shelf; and the bottom boundary layer dynamics over the shelf is of importance for near-bottom density structure, buoyancy transport and bottom material transport and so on; the histogram of the vertical stratification and the convergent flow along the bottom layer are efficient methods for coastal dynamics and can be applied to other shelf studies.

REFERENCES

Barth, . A., Bogucki, D., Pierce, S. D., and Kosro, P. M. (1998). Secondary circulation associated with a shelfbreak front. *Geophys. Res. Lett.*, 25(15):2761–2764.

Belabbassi, L. (2006). *Examination of the relationship of river water to occurrences of bot- tom water with reduced oxygen concentrations in the northern Gulf of Mexico.* PhD thesis, Texas A&M University.

Bianchi, T. S., DiMarco, S. F., Jr., J. H. C., Hetland, R. D., Chapman, P., Day, J. W., and Allison, M. A. (2010). The science of hypoxia in the Northern Gulf of Mexico: A review. *Sci. Total Environ.*, 408(7):1471–1484, doi:10.1016/j.scitotenv.2009.11.047.

Blumsack, S. L. and Gierasch, P. (1972). Mars: The effects of topography on baroclinic instability. *J. Atmos. Sci.*, 29(6):1081–1089.

Brink, K. H. and Lentz, S. J. (2010a). Buoyancy arrest and bottom Ekman transport, Part I, Steady flow. *J. Phys. Oceanogr.*, 40:621–635.

Brink, K. H. and Lentz, S. J. (2010b). Buoyancy arrest and bottom Ekman transport: Part II, Oscillating flow. *J. Phys. Oceanogr.*, 40:636–655.

Brunt, D. (1927). The period of simple vertical oscillations in the atmosphere. *Q. J. R. Meteorol. Soc.*, 53(221):30–32.

Burchard, H. and Hofmeister, R. (2008). A dynamic equation for the potential energy anomaly for analysing mixing and stratification in estuaries and coastal seas. *Estuarine, Coastal and Shelf Science*, 77:679–687.

Carpenter, J. H. (1965). The Chesapeake Bay Institute technique for the Winkler dissolved oxygen method. *Limnol. Oceanogr.*, 10(1):141–143.

Chapman, D. C. (1985). Numerical treatment of cross-shelf open boundaries in a

barotropic coastal ocean model. *J. Phys. Oceanogr.*, 15(8):1060–1075.

Chapman, D. C. and Lentz, S. J. (1994). Trapping of a coastal density front by the bottom boundary layer. *J. Phys. Oceanogr.*, 24:1464–1479.

Chapman, D. C. and Lentz, S. J. (1997). Adjustment of stratified flow over a sloping bottom. *J. Phys. Oceanogr.*, 27(2):340–356.

Cho, K., Reid, R. O., and Nowlin, W. D. (1998). Objectively mapped stream function fields on the Texas-Louisiana shelf based on 32 months of moored current meter data. *J. Geophys. Res.*, 103(C5):10,377–10,390.

Cochrane, J. D. and Kelly, F. J. (1986). Low-frequency circulation on the Texas-Louisiana continental shelf. *J. Geophys. Res.*, 91(C9):10,645–10,659.

da Silva, A. M., Young-Molling, C. C., and Levitus, S. (1994a). Vol. 1: Algorithms and Procedures. NOAA Atlas NESDIS 6. Technical report, U.S. Gov. Printing Office, Washington D.C.

da Silva, A. M., Young-Molling, C. C., and Levitus, S. (1994b). Vol. 2: Anomalies of Directly Observed Quantities. NOAA Atlas NESDIS 7. Technical report, U.S. Gov. Printing Office, Washington D.C.

De Boer, G. J., Pietrzak, J. D., and Winterwerp, J. C. (2008). Using the potential energy anomaly equation to investigate tidal straining and advection of stratification in a region of freshwater influence. *Ocean Modelling*, 22:1–11.

Deleersnijder, E., Campin, J. M., and Delhez, E. J. M. (2001). The concept of age in marine modelling: I. Theory and preliminary model results. *J. Mar. Sys.*, 28:229–267.

Delhez, E. J. M., Campin, J. M., and Deleersnijder, E. (1999). Toward a general theory of the age in ocean modelling. *Ocean Modelling*, 1:17–27.

Delhez, E. J. M. and Deleersnijder, E. (2006). The boundary layer of the residence time field. *Ocean Dynamics*, 56:139–150.

DiMarco, S. F., Chapman, P., Walker, N., and Hetland, R. D. (2010). Does local topography control hypoxia on the eastern Texas–Louisiana shelf? *J. Mar. Sys.*, 80:25–35.

Fennel, K., Hetland, R., Feng, Y., and DiMarco, S. (2011). A coupled physical-biological model of the Northern Gulf of Mexico shelf: model description, validation and analysis of phytoplankton variability. *Biogeosciences*, 8:1881–1899.

Fennel, K., Hu, J., Laurent, A., Marta-Almeida, M., and Hetland, R. (2013). Sensitivity of hypoxia predictions for the Northern Gulf of Mexico to sediment oxygen consumption and model nesting. *J. Geophys. Res.*, 118:990–1002.

Fennel, K., Wilkin, J., Levin, J., Moisan, J., O'Reilly, J., and Haidvogel, D. (2006). Nitrogen cycling in the Mid Atlantic Bight and implications for the North Atlantic nitrogen budget: Results from a three-dimensional model. *Global Biogeochemical Cycles*, 20:GB3007, doi: 10.1029/2005GB002456.

Fennel, K., Wilkin, J., Previd, M., , and Najjar, R. (2008). Denitrification effects on air-sea CO2 flux in the coastal ocean: Simulations for the Northwest North Atlantic. *Geophys. Res. Lett.*, 35:L24608, doi:10.1029/2008GL036147.

Flather, R. A. (1976). A tidal model of the northwest Euopean continental shelf. *Memoires de la Societe Royale des Sciences de Liege*, 10(6):141–164.

Garrett, C., MacCready, P., and Rhines, P. B. (1993). Boundary mixing and arrested Ekman layers: Rotating stratified flow near a sloping boundary. *Annu. Rev. Fluid Mech.*, 25:291–323.

Hetland, R. D. and DiMarco, S. F. (2008). How does the character of oxygen demand control the structure of hypoxia on the Texas-Louisiana continental shelf? *J. Mar. Sys.*, 70(doi:10.1016/j.marsys.2007.03.002):49–62.

Hetland, R. D. and DiMarco, S. F. (2012). Skill assessment of a hydrodynamic model of circulation over the Texas- Louisiana continental shelf. *Ocean Modelling*,

43-44:64–76.

Horner-Devine, A. R., Hetland, R. D., and MacDonald, D. G. (2015). Mixing and transport in coastal river plumes. *Annu. Rev. Fluid Mech.*, 47:569–594.

Houghton, R. W. (1997). Lagrangian flow at the foot of a shelfbreak front using a dye tracer injected into the bottom boundary layer. *Geophys. Res. Lett.*, 24(16):2035–2038.

Houghton, R. W. and Visbeck, M. (1998). Upwelling and convergencein the Middle Atlantic Bight shelfbreak front. *Geophys. Res. Lett.*, 25(15):2765–2768.

Ivey, G. N., Winters, K. B., and Koseff, J. R. (2008). Density stratification, turbulence, but how much mixing? *Annu. Rev. Fluid Mech.*, 40:169–184.

Jochens, A. E., DiMarco, S. F., Nowlin, W. D., Reid, R. O., and Kennicutt, M. C. (2002). Northeastern Gulf of Mexico chemical oceanography and hydrography study: Synthesis report. Technical report, Minerals Management Service, New Orleans, LA.

Ko, D. S., Martin, P. J., Rowley, C. D., and Preller, R. H. (2008). A real- time coastal ocean prediction experiment for MREA04. *J. Mar. Syst.*, 69:17–28.

Lentz, S. J. and Chapman, D. C. (2004). The importance of nonlinear cross-shelf momentum flux during wind-driven coastal upwelling. *J. Phys. Oceanogr.*, 34:2444–2457.

Lentz, S. J. and Trowbridge, J. H. (1991). The bottom boundary layer vver the Northern California shelf. *J. Phys. Oceanogr.*, 21:1186–1201.

Lohrenz, S. E., Dagg, M. J., and Whitledge, T. E. (1990). Enhanced primary production at the plume/oceanic interface of the Mississippi River. *Cont. Shelf Res.*, 10:639–664.

MacCready, P. and Rhines, P. B. (1993). Slippery bottom boundary layers on a slope. *J. Phys. Oceanogr.*, 23:5–22.

Marta-Almeida, M., Hetland, R. D., and Zhang, X. (2013). Evaluation of model nesting performance on the Texas-Louisiana continental shelf. *J. Geophys. Res.*, 118(5):2476–2491, DOI: 10.1002/jgrc.20163.

Mattern, J. P., Fennel, K., and Dowd, M. (2013). Sensitivity and uncertainty analysis of model hypoxia estimates for the Texas-Louisiana shelf. *J. Geophys. Res.*, 118:1316–1332.

Meade, R. (1996). River-sediment inputs to major deltas. In Milliman, J. and Haq, B. U., editors, *Sea-leavel rise and coastal subsidence*, volume 2, pages 63–85. Springer Netherlands.

Middleton, J. F. and Ramsden, D. (1996). The evolution of the bottom boundary layer on the sloping continental shelf: A numerical study. *J. Geophys. Res.*, 101:18061–18077.

Milliman, J. D. and Meade, R. H. (1983). World-wide delivery of river sediment to the ocean. *Journal of Geology*, 91(1):1–21.

Murrell, M. C. and Lehrter, J. C. (2011). Sediment and lower water column oxygen consumption in the seasonally hypoxic region of the Louisiana continental shelf. *Estuaries and Coasts*, 34(5):912–924.

Nowlin, W. D., Jochens, A. E., Reid, R. O., and DiMarco, S. F. (1998). Texas-Louisiana shelf circulation and transport process study: synthesis report LATEX A, Vols. 1. and 2. OCS study MMS 98-0035 and MMS 98-0036. Technical report, U.S. Department of the Interior, Minerals Management Service, Gulf of Mexico OCS Regional Office., New Orleans.

Nowlin, W. D. N. D., Jochens, A. E., DiMarco, S. F., Reid, R. O., and Howard, M. K. (2005). Low-frequency circulation over the Texas-Louisiana continental shelf. In Sturges, W. and Lugo-Fernandez, A., editors, *Circulation in the Gulf of Mexico: Observations and Models*, pages 219–240. Washington D.C. American Geophysical

Union.

Pickart, R. S. (2000). Bottom boundary layer structure and detachment in the shelfbreak jet of the Middle Atlantic Bight. *J. Phys. Oceanogr.*, 30:2668–2686.

Rabalais, N., Turner, R., Sen Gupta, B., Boesch, D., Chapman, P., and Murrell, M. (2007). Hypoxia in the northern Gulf of Mexico: Does the science support the plan to reduce, mitigate, and control hypoxia? *Estuaries and Coasts*, 30(5):753–772.

Rabalais, N. N., Turner, R. E., Dortch, Q., Justić, D., Bierman, Jr., V. J., and Wiseman, Jr., W. J. (2002a). Nutruent-enhanced productivity in the northern Gulf of Mexico: past, present and future. *Hydrobiologia*, 475/476:39–63.

Rabalais, N. N., Turner, R. E., and Jr., W. J. W. (2002b). Gulf of Mexico hypoxia, A.K.A. "The Dead Zone". *Annual Review of Ecology and Systematics*, 33:235–263.

Rabalais, N. N., Wiseman, W. J., and Turner, R. E. (1994). Comparison of continuous records of near-bottom dissolved oxygen from the hypoxia zone along the Louisiana coast. *Estuaries*, 17(4):850–861.

Renaud, M. L. (1986). Hypoxia in Louisiana coastal waters during 1983: Implications for fisheries. *Fish. Bull.*, 84(1):19–26.

Rowe, G. T., Kaeki, M. E. C., Morse, J. W., Boland, G. S., and Briones, E. G. E. (2002). Sediment community metabolism associated with continental shelf hypoxia, northern Gulf of Mexico. *Estuaries*, 25(6):1097–1106.

Sherman, F., Imberger, J., and Corcos, G. (1978). Turbulence and mixing in stably stratified waters. *Annu. Rev. Fluid Mech.*, 10:267–288.

Simpson, J. H. (1981). The shelf-sea fronts: implications of their existence and behaviour. *Philo. Trans. Royal Soc. Series A*, 302:531–546.

Stacey, M. T., Rippeth, T., and Nash, J. D. (2011). Turbulence and stratification in estuaries and coastal seas. In Wolanski, E. and McLusky, D., editors, *Treatise on estuarine and coastal science*, volume 2, pages 9–36. Amsterdam: Elsevier.

Trowbridge, J. H. and Lentz, S. J. (1991). Asymmetric behavior of an oceanic boundary layer above a sloping bottom. *J. Phys. Oceanogr.*, 21:1171–1185.

Trowbridge, J. H. and Lentz, S. J. (1998). Dynamics of the bottom boundary layer on the Northern California shelf. *J. Phys. Oceanogr.*, 28:2075–2093.

Turner, R. E. and Rabalais, N. N. (1994). Coastal eutrophication near the Mississippi river delta. *Nature*, 368(14):619–621.

Wallcraft, A. J., Metzger, E. J., and Carroll, S. N. (2009). Software design description for the HYbrid Coordinate Ocean Model (HYCOM). Technical Report NRL/MR/7320–09-9166, Naval Research Lab., Stennis Space Center, MS. Oceanography Div.

Weiss, R. F. (1970). The solubility of nitrogen, oxygen, and argon in water and seawater. *Deep-Sea Res.*, 17:721–735.

Williams, P. J. L. and Jenkinson, N. W. (1982). A transportable microprocessor-controlled precise winkler titration suitable for field station and shipboard use. *Limnol. Oceanogr.*, 27(3):576–584.

Wiseman, Jr, W. J., Rabalais, N. N., Turner, R. E., Dinnel, S. P., and MacNaughton, A. (1997). Seasonal and interannual variability within the Louisiana coastal current: stratification and hypoxia. *J. Mar. Sys.*, 12:237–248.

Yankovsky, A. E. and Chapman, D. C. (1997). A simple theory for the fate of buoyant coastal discharges. *J. Phys. Oceanogr.*, 27:1386–1401.

Zhang, W. G., Wilkin, J. L., and Schofield, O. M. E. (2010). Simulation of water age and residence time in New York Bight. *J. Phys. Oceanogr.*, 40(5):965–982.

Zhang, X., DiMarco, S., Smith IV, D., Howard, M., Jochens, A., and Hetland, R. (2009). Near-resonant ocean response to sea breeze on a stratified continental shelf. *J. Phys. Oceanogr.*, 39(9):2137–2155.

Zhang, X., Hetland, R. D., Marta-Almeida, M., and DiMarco, S. F. (2012a). A nu-

merical investigation of the Mississippi and Atchafalaya freshwater transport, filling and flushing times on the Texas-Louisiana Shelf. *J. Geophys. Res.*, 117:C11009, 21 pp., doi:10.1029/2012JC008108.

Zhang, X., Marta-Almeida, M., and Hetland, R. (2012b). A high-resolution pre-operational forecast model of circulation on the Texas-Louisiana continental shelf and slope. *Journal of Operational Oceanography*, 5(1):19–34.

Zhang, Z. and Hetland, R. D. (2012). A numerical study on convergence of alongshore flows over the Texas-Louisiana shelf. *J. Geophys. Res.*, 117:C11010, 18 pp., doi:10.1029/2012JC008145.